2011

The Long-Rage Directional Behavior of the Nematode C. Elegans

Margherita Peliti

THE LONG-RANGE DIRECTIONAL BEHAVIOR OF THE NEMATODE *C.ELEGANS*

A Thesis Presented to the Faculty of

The Rockefeller University

in Partial Fulfillment of the Requirements for

the degree of Doctor of Philosophy

by

Margherita Peliti

June 2011

THE LONG-RANGE DIRECTIONAL BEHAVIOR OF THE NEMATODE *C.ELEGANS*

Margherita Peliti, Ph.D.

The Rockefeller University 2011

Like any mobile organism, *C. elegans* relies on sensory cues to find food. In the absence of such cues, animals might display defined search patterns or other stereotyped behavior. The motion of *C. elegans* has previously been characterized as a sinusoid whose direction can be modulated by gradual steering or by sharp turns, reversals and omega bends. However, such a fine-grained behavioral description does not by itself predict the long-range features of the animals' pattern of movement.

Using large (24 cm x 24 cm) Petri dishes, we characterized the movement pattern of *C. elegans* in the absence of stimuli. To collect trajectories over such a large surface, we devised an imaging setup employing an array of consumer flatbed scanners. We have confirmed quantitatively the results obtained with the scanner-array setup with a camera imaging setup, in a more stringently homogeneous environment.

Wild-type worms display striking behavior in the absence of food. The majority (~60%) of the animals' paths displays persistence in the direction of motion over length scales that are 50-100 times the body-length of *C. elegans*. The overall direction of movement differs from animal to animal, suggesting that the directed motion we observe might not be interpreted as a taxis to an external cue in the experimental environment.

Interestingly, animals appear to exhibit directionality at large scales despite non-directional motion at smaller scales. We quantified the extent of local directional persistence by computing the autocorrelation function of the velocities. Unexpectedly,

correlations in the direction of motion decay over time scales that are much faster than the scales over which directional persistence appears to be maintained.

We sought to establish quantitatively that the worm motion is, in fact, biased. To determine whether a null, random walk-like model of locomotion could account for directional behavior, we generated synthetic trajectories drawing from the same angle and step distributions of individual trajectories, and quantified the probabilities of obtaining larger net displacements than the experimental. Such a model fails to reproduce the experimental results. Moreover, the mean square displacements computed for the data display non-diffusive behavior, further demonstrating that the observed directional persistence cannot be explained by a simple random-walk model.

To corroborate the hypothesis of biased movement in a model-independent fashion, we employed a geometrical characterization of the trajectories. Isotropic, unbiased walks result in paths that display a random distribution of turning angles between consecutive segments. In contrast, parsing of the worm's trajectories yields different results depending on the segmentation scale adopted. In fact, increasing the segment size results in increasingly narrow turning angle distributions, centered around the zero. This suggests the emergence of directional coherence at long time scales.

In order to investigate whether directional persistence is attained by a sensory mechanism, we analyzed the paths displayed by animals with impaired sensory function. Animals mutant for *che-2*, which display disrupted ciliary morphology and pleiotropic behavioral defects, exhibited non-directional behavior. Surprisingly however, *daf-19* mutants, which lack sensory cilia altogether, displayed residual directionality, albeit at a lower penetrance (~20%) than the wild-type. This result suggests that directionality might implicate

sensory modalities that do not require ciliary function, such as AFD-mediated thermosensation or URX-mediated oxygen sensation. Alternatively, the behavior of *daf-19* mutants might imply that neural activity, but not sensory inputs, are required to achieve directed motion.

Mutations in *osm-9*, a TRPV channel implicated in several avoidance behaviors in the worm, did not result in an observable phenotype. In contrast, mutations in *tax-2*/*tax-4*, a cGMP-gated channel required to transduce a number of sensory stimuli, resulted in loss of directionality. However, specific mutations targeting the signal transduction pathways for thermotaxis, olfaction, phototaxis, and aerotaxis, upstream of TAX-4, did not disrupt directional behavior.

To get further insight into the nature of the stimulus directing the animals' behavior, if any, we performed rescue experiments of TAX-4 function in specific subsets of neurons. In agreement with the results obtained by genetic lesions in the signal transduction pathways for thermotaxis and odortaxis, no rescue of directional behavior was observed when expressing TAX-4 in the thermosensory neuron AFD, or in the olfactory neurons AWB and AWC. Partial rescue of wild-type behavior was obtained by expression of TAX-4 in a set of five cells, which comprised the oxygen-sensing AQR, PQR and URX neurons as well as the ASJ and ASK sensory neurons, which transduce chemical stimuli and responses to dauer pheromone.

To address the concern that the animals' motion might be directed to a chemosensory cue within the plate, we investigated the correlation between path directions displayed by animals that were assayed on a same plate. We did not observe a detectable correlation

between path headings, indicating that the worm is not chemotaxing to a plate-specific cue.

In conclusion, our results indicate that the motion of *C. elegans* cannot be assimilated to a random walk, and that directional persistence arises at long times despite local non-directional behavior. In addition, although we have not conclusively ruled out a sensory-based explanation, the genetic and phenomenological evidence gathered foreshadows the intriguing possibility that *C. elegans* might be achieving directional motion by relying solely on self-based information.

per Agostino

“We gotta go and never stop going till we get there.”

“Where we going, man?”

“I don't know but we gotta go.”

- Jack Kerouac, *On the Road*

ACKNOWLEDGEMENTS

First and foremost, I want to thank my thesis advisor, Shai Shaham. I came to his lab holding a few pages of something that only vaguely resembled this project, and to my surprise and delight Shai embraced it. He has given me scientific freedom throughout, and support that extended well beyond the laboratory. Shai has been a wonderful teacher, and I still learn from his stance, the originality of his scientific interests and his rigor in interpreting data and questioning motivations.

I want to thank Stanislas Leibler, who has been as involved in the project as an actual advisor. At times when labor takes over and stumps creativity, Stan has pushed me to think deeper and farther. His uncompromising approach to science is a constant inspiration.

Thanks to all the members of the Leibler and the Shaham lab, whom I could always turn to when I had questions to ask and ideas to bounce off. Special thanks must go to John Chuang, in the Leibler lab. John helped me at many points during the project, particularly in building the imaging setups and developing tracking algorithms. John was also my baymate of one year. The days spent tinkering with him, or discussing improbable contraptions, were endless fun. My thanks also go to Doeke Hekstra, whose thorough and original questioning does not cease to delight me. Thanks to Francis Corson for suggesting to me a clever way to compare my trajectories to randomized ones; and to Peter Insley for kind and useful comments on this manuscript. Thanks to our laboratory aide Sharon White, who helped me with media preparations.

Fred Cross and Cori Bargmann, as member and chair of my thesis committee, contributed to nurture this project. I am thankful to you both for your insights, and for the time you made for me, during meetings and outside. I am also extremely grateful to Cori, who provided me with all the TAX-4 transgenic strains utilized in this work.

I want to thank Aravi Samuel, for serving as my external committee, as well as the Dean's Office of the Rockefeller University, for the support and flexibility they accorded me.

Last, I am deeply grateful to my family and friends. I truly could not have done any of this without your love and support.

Table of Contents

List of Figures

List of Tables

Chapter 1. Introduction

Motivation

Mobile creatures run on batteries: they have to constantly locate new resources in order to insure their survival (Montague and Berns, 2002). Accordingly, we anticipate that an organism's ability at acquiring resources will play an important part in insuring its long-term success. It is then not unreasonable to hope that organisms might have evolved well-defined foraging strategies, and that those might be observed in laboratory studies.

The specific question which constitutes the focus of my thesis' work is whether there are any stereotypical features in the way *C. elegans* moves about in space when no obvious directional cues are present. Does *C. elegans* indeed perform a random walk in such an environment, as it has previously been suggested – even though animals are known to be able to maintain a fixed direction of motion under certain conditions, as they do, for example, when migrating towards a preferred temperature (Hedgecock and Russell, 1975)? If a well-defined searching strategy were to be observed, it could yield valuable insight on the nature of problems faced by the organism in its natural environment. Searching strategies can be analyzed in terms of their efficiency for a given distribution of resources (Bartumeus et al., 2008; Bénichou et al., 2005; Viswanathan et al., 1999), or an explanation can be sought in terms of the constraints imposed by the animal's physiology (Berg, 1988; Li et al., 2008). Finally, an in-depth analysis of the animals' pattern of motion could shed light on the locomotion algorithm implemented by

Caenorhabditis elegans, which could in turn help elucidate the nature of the computations performed by the animal's nervous system.

The objection has been raised that *C. elegans,* although it represents a wonderful model for the genetic and neural dissection of behavior, is not amenable to the interpretation of behavior in an ecological sense, because so little is known of its lifestyle - and because the environment of the laboratory is too far removed from its natural habitat. However, the same objection could be made to the study of the chemotactic behavior of *Escherichia coli*; and yet, as the elegant work of H.C. Berg demonstrates, there are several lessons to be learned by how this small, single-celled organism solves the chemotactic task in face of the daunting physical constraints that it is faced with.

E. coli: a random biased walk strategy for chemotaxis

E. coli cells move about by rotation of helical filaments, termed "flagella", which are located on the cell's surface. Flagella can move in a coordinated fashion, forming a bundle that rotates counterclockwise and propels the cells forward in bouts of smooth motion, which are called "runs". Run durations are Poisson-distributed, meaning that a run has a constant probability to be terminated at any given moment. Runs end when the bundle coordination is lost, with every flagellum rotating on its own in a clockwise direction. When that happens, the cell "tumbles", moving about erratically with little overall net displacement; eventually, the bundle reforms, and the cell swims off in a new run, pointing in a direction picked more or less at random (Berg and Anderson, 1973; Macnab, 1977).

E. coli climbs up gradients of attractive substances by suppressing tumbling during runs that carry the cell up the gradient, effectively lengthening the duration of those runs; instead, when the cell is swimming away from the source of the attractant, no modulation of tumbling frequency is observed. These observations have led to the conclusion that the cells' chemotactic strategy is a random biased walk (Berg and Brown, 1972).

It has been experimentally established (Macnab and Koshland, 1972) that bacteria detect variations of concentration over time, rather than differences in concentration at different points on the body – a result that is indeed expected, considering that at the bacterial scale the magnitude of statistical fluctuations should overwhelm spatial sensing. The presence of diffusive noise also entails that the cell will make better estimates of concentrations if it integrates the stimulus over time. However, physical and physiological constraints place an upper bound on the integration time, as the cell's direction of motion is reset by tumbling (or, during extended runs, by Brownian motion) on the timescale of the second. Remarkably, *E. coli* displays a ~1s integration time (Segall et al., 1986), an interval which appears to be just matched to the ~1s average run duration.

Persistent motion of *D. discoideum* in the absence of external stimuli

To our knowledge, few studies since those on *E. coli* chemotaxis have detailed the statistical and geometrical features of the paths of organisms in reproducible settings. An exception is provided by recent work characterizing the trajectories of *Dictyostelium* amoebae on agar substrates in the absence of chemotactic stimuli (Li et al., 2008). *D. discoideum* are single-celled eukaryotes that crawl by extending a temporary protrusion,

called a pseudopod, in the direction of motion. Pseudopods possess a typical lifetime of 1–2 min, after which a new pseudopod forms, leading the cell in a new direction.

If pseudopods were oriented at random the movement of the amoebae would be well described by a correlated random walk, that is to say, by a process that is diffusive at large timescales but displays oriented motion over timescales that are smaller than the correlation time. Instead, *Dictyostelium* cells were found to display persistence in the direction of motion over typical intervals of ~30 minutes, that is, more than ten times the organism's characteristic turning frequency. How, then, is this directional persistence accomplished?

An analysis of the autocorrelation function of turns reveals a significant anti-correlation between consecutive turning events. Thus, *Dictyostelium* moves forward in a zig-zag fashion, with each pseudopod turning away from the direction of the previous one. Perhaps more importantly, the distribution of turning amplitudes peaks strongly around the zero, and exhibits an exponential decay – thus indicating that most changes in directions reorient the cell by only a small amount with respect to its previous direction.

In fact, the directional changes in the motion of *Dictyostelium* are modeled by the authors as a sum of two terms: a first, slowly-diffusing angular term plus a second term composed of noisy, rapid oscillations (the "zig-zags") around the first one. To recover the observed behavior, the authors have to impose the timescale for the diffusion of the slow term, which they set as 8 minutes/1 rad^2, a value equal to the observed timescale of directional persistence. A physiological hypothesis is advanced for the mechanism that gives rise to the anticorrelation between turns; however, the authors do not provide an

explanation for the defining feature of the amoebae's paths, that is, the mostly straight, highly correlated motion underlying the angular oscillations.

Systematic search in the absence of cues: searching behavior of the ant *Cataglyphis*

A striking example of a stereotyped, adaptive pattern of movement is that displayed by the desert ant *Cataglyphis* when searching for its nesting site. Remarkably, work on this organism has been conducted in both the field and the laboratory, allowing the characterization of the full complexity of its natural behavior, while also permitting to investigate in simpler settings the working of the ants' navigational system (Merkle and Wehner, 2008; Wolf and Wehner, 2000).

Cataglyphis fortis inhabits an extremely uniform habitat, the salt flats of Tunisia and Algeria. In order to find their way back to their nest in such a featureless environment the ants have evolved sophisticated navigational tools. When homing, *Cataglyphis* navigates by continuosly updating a home vector which corresponds to its position relative to the nest. In order to do so, the ant utilizes directional information obtained from the sky polarization pattern; the distances traveled are instead stored in memory (Sommer and Wehner, 2004; Wehner, 2003).

This means of navigation, known as path integration, is intrinsically prone to the accumulation of errors (Cheung et al., 2007); therefore, ants can encounter a situation in which their home vector is reset to zero and yet the nest has not been located. In this situation, *Cataglyphis* is observed to perform a strikingly stereotypical search strategy, consisting of loops of increasing radius that start and end at the origin (*i.e.*, at the zero of

the home vector) and point each time in different azimuthal directions. It has been argued that this strategy is efficient, in that the cyclic returns to the origin ensure that the ant will search more heavily in those areas where the nest is more likely to be located (Wehner and Srinivasan, 1981). Remarkably, the searching pattern exhibited by the isopod crustacean *H. reaumuri*, which also inhabits a desertic environment, closely resembles the strategy of *Cataglyphis* (Hoffmann, 1983), suggesting that this strategy might have characters of generality.

Animal navigation – an overview

The question of whether animals might or not possess dead reckoning tools dates at least back to Darwin (Darwin, 1873). In fact, homing is a common enough behavior in the animal kingdom that path integration mechanisms have been observed in organisms as different as honeybees (Dacke and Srinivasan, 2008), spiders (Görner and Claas, 1985; Seyfarth et al., 1982), crustaceans (Hoffmann, 1983; Walls and Layne, 2009a), and mammals (Etienne et al., 1996; Kimchi and Terkel, 2002; Mittelstaedt and Mittelstaedt, 1980).

Distances travelled are typically estimated from optical flow (Collett et al., 2006; Esch et al., 2001) or from purely proprioceptive information on motor output, as is the case for *Cataglyphis* and the fiddler crab *Uca pugilator* (Walls and Layne, 2009b; Wittlinger et al., 2006). The directional cues that inform navigation are more varied (Gould, 1998), and comprise the sky polarization pattern (Heinze and Homberg, 2007; Heinze and Reppert, 2011; Rossel and Wehner, 1982; von Frisch, 1967), the earth's geomagnetic field (Lohmann et al., 2004; Walker, 1997; Wiltschko and Wiltschko, 2005), as well as

mechanical (Görner and Claas, 1985; Seyfarth et al., 1982), visual (Collett and Collett, 2002; Lipp et al., 2004) and olfactory (Wallraff, 1996) properties of the environment.

However, just as common, and arguably more robust, are navigational mechanisms that rely purely on external cues, presumably without contribution from idiothetic mechanisms to gauge the distances travelled; examples are the visual, landmark-based navigation of mammals (Papi, 1992), birds (Biro et al., 2007) and insects (Collett and Collett, 2002), or the tracking of pheromone trails by ants (Hölldobler and Wilson, 1990).

Recently, the exciting discovery that cells in the entorhinal cortex at the hippocampal interface code for relative spatial positions (Hafting et al., 2005), combined with the observation that head direction cells might provide the neural correlate of directional heading (Taube, 2007), promises to shed light on how the mammalian brain computes home vectors and implements map-like representations of space.

Models: extensions of the random walk process.

Just like the dance of honeybees (von Frisch, 1967), the stereotyped search of desert ants or the long-range migration of birds and butterflies are exceptional in that the behavior displays conspicuous, highly stereotyped features, which can be easily brought out from the underlying environment. In contrast, the spontaneous movement pattern of foraging animals or animals that are searching for food has only been poorly characterized (Firle et al., 1998; Kareiva and Shigesada, 1983; Samu et al., 2003) (but see Budick and Dickinson, 2006), possibly due to the difficulties presented by extrapolating the

movement's statistical and geometrical features from the intrinsic complexity of the landscape.

While experimental studies are scarce, there has been considerable effort in modeling the movement patterns of animals in the absence of a biasing external cue. Those theoretical studies roughly fall in two classes: one that addresses the problem of how to statistically or geometrically describe animals' locomotion patterns – and how to infer from data a particular model of motion (Benhamou, 2006; Benhamou and Bovet, 1992; Qian et al., 1991). The second class of studies investigates the efficiency of searching strategies given a defined distribution of (hidden) food targets (Bartumeus et al., 2005; Bénichou et al., 2005; Viswanathan et al., 1999).

Descriptive models for the animals' motion mostly deal with extensions of the pure random walk. A random walk is a process whereby a walker moves by steps of a fixed length l, choosing a random, independently distributed direction at every step. The question of where the walker ends up after n steps was first posed by Pearson, in 1905 (Pearson, 1905). The solution to the problem was obtained by Rayleigh, also in 1905 (Rayleigh, 1905): it states that the probability density function of finding the walker at a distance r from its starting point, $P(r)$, is a Gaussian at large values of n:

$$P(r) = \frac{2}{l^2 n} \exp\left(-\frac{r^2}{l^2 n} \right) dr \, .$$

The expected value of the net displacement, that is, its average across different realizations of the walk, is zero, as it should since the process is isotropic. In contrast, the mean square displacement r^2 scales with the number of steps. In fact, a random walk can be thought of as a discretization of Brownian motion (Brown, 1828), and thus results in

standard diffusive behavior: $r^2=2Dt$, with D the diffusion constant of the process (Einstein, 1905). Importantly, even though random walks are isotropic, the single process realization needs not be: in fact, the object's shape deviates from a spherical one, and its anisotropy has been analytically quantitated (Aronovitz and Nelson, 1986; Rudnick and Gaspari, 1986).

Relaxing the assumption of a fixed step length l does not affect the diffusive behavior of the walk, provided that the distribution of step length has a finite variance, *i.e.* that it decays fast enough: in fact, the central limit theorem ensures that the probability density function for r will still be Gaussianly distributed. More interesting is the case of correlated random walks, which exhibit local persistence in the direction of motion. Those processes can be traced back historically to the mean-reversion process considered by Ornstein and Uhlenbeck, in 1930 (Uhlenbeck and Ornstein, 1930). The mean-reversion process describes the behavior of the velocity of a particle which is subjected to collisions with the molecules of the surrounding fluid. Since the particle experiences a greater number of collisions in the direction in which it is moving, its acceleration includes a dissipation term that is proportional to the velocity itself. As a result, the velocity of the particle displays an exponentially decaying memory; therefore, at short times the particle's square displacements scale quadratically with time, as should be expected for uniform motion. At long times, the velocities correlations have decayed, and the diffusive scaling of a pure random walk is recovered, although with a larger, effective diffusion constant than would be observed for a non-correlated process.

The behavior of the mean squared displacements at all times can be analytically derived for both the Ornstein-Uhlenbeck process and discretizations of it. In general, the scaling

of the mean square displacements (MSD) can be computed if the functional form of the velocity autocorrelation $f(\tau) = \langle v(t)\, v(t+\tau) \rangle$ is known. For the mean-reversion process, *i.e.* if the autocorrelation function decays exponentially, the squared mean displacements at time t are equal to: $r^2 = 2D\tau\left(\frac{t}{\tau} - 1 + e^{-t/\tau}\right)$ (Uhlenbeck and Ornstein, 1930). It can be seen that the typical velocity correlation time τ dictates a crossover between the diffusive behavior that prevails at long times, and the ballistic behavior that predominates at timescales t that are smaller than τ.

In practice, when dealing with experimental data, *i.e.* with finite-size samples, it is not trivial to distinguish between the case of a correlated random walk and that of a walk that is correlated as well as biased towards a preferred direction, because in both cases the motion exhibits directional persistence. The existence of an overall bias might be revealed by an analysis of the paths for the whole population, unless however the preferred direction varied from path to path. Several theoretical studies in the ecological field (Benhamou, 2004; Codling and Hill, 2005; Hill and Hader, 1997; Kareiva and Shigesada, 1983; Marsh and Jones, 1988) have attempted to define specific models of biased motion, and to infer from those, *a posteriori*, parameters whose behavior would effectively discriminate between a local and a global persistence mechanism.

While the perspective of those studies is relevant to us, in that they approach the inverse problem of inferring a stochastic process from experimental path observations, the treatments proposed lack in generality, as the behavior of the parameters selected appears to depend on the details of the model. Nonetheless, this literature contains indications of features that might more robustly help discriminate between unbiased and biased models

of motion. In fact, a walk that is not biased has to satisfy three conditions: 1. step lengths and directions must not be cross-correlated; 2. turning angles and directions must likewise not be cross-correlated; and 3. turning angles must not be self-correlated (Benhamou, 2006). Therefore, if a significant correlation is observed in any of these three cases, the null hypothesis of isotropic movement can be rejected.

A biased mode of locomotion entails non-diffusive scaling of the mean square displacements at large times (*i.e.* "anomalous diffusion"). However, correlated, isotropic random walks might also display divergence from diffusive behavior due to statistical fluctuations of the scaling exponent, or to a cutoff at large timescales that is too close to the correlation time (Qian et al., 1991). On the other hand, anomalous diffusion does not, by itself, imply that the stochastic movement process is anisotropic. For instance, a distribution of step lengths that is slowly-decaying, such as the power-law length distribution that characterizes Lévy flights, will result in scaling exponents that are larger than unity.

Further complications might arise if the process is not stationary. In the case, for example, of a two-state alternance between ballistic and diffusive motion, the asymptotic behavior will still display diffusive features, provided that the ballistic bouts have finite variance (this is, after all, the movement strategy of *E. coli*). However, the crossover scale between the two regimes cannot be easily be estimated from data, since for non-stationary processes the velocity correlation function $\langle v(t)\, v(t+\tau)\rangle$ can no longer be defined as a function of the lagtime τ only. As a consequence, if non-diffusive behavior is observed at large times, it would not be trivial to determine whether that can be

interpreted as *bona fide* anomalous diffusion, or as an indication that the process is still in the correlated regime.

In isotropic environments, anomalous diffusion can arise if the walk displays non-local interactions, as in the case for instance of self-avoiding walks, *i.e.*, of walks that cannot self intersect (Flory, 1953). Recently, looser models of self-avoidance have been considered where the walker is repelled by a diffusing substance that is secreted along the track (Grima, 2005; Sengupta et al., 2009). These models appear to yield different asymptotic predictions depending on whether noise is or not included in the treatment. At intermediate time scales, however, both models predict ballistic or otherwise super-diffusive behavior.

Efficiency of searching strategies

Lévy walks, or flights, are processes characterized by a power-law distribution of step lengths: $P(l) = l^{-\mu}$, $1<\mu<=3$, where the value of the exponent μ affects the long-range behavior of the walk, *e.g.* the scaling ν of the mean square displacements $r^2 \sim N^{\nu}$: $1 <= \nu < 2$ for $1 < \mu <= 3$. Recent theoretical work has suggested that such processes might represent an efficient foraging strategy when the distribution of food targets is sparse and food targets are revisitable (Bartumeus et al., 2005; Levandowsky et al., 1988; Raposo et al., 2003; Viswanathan et al., 1999). A walk is considered efficient here when it maximizes the ratio of the number of hits to the total distance travelled. The higher efficiency of a Lévy walk compared to diffusion might be attributed to the fact that those processes cover more territory relatively to Brownian ones, and are therefore more likely to come across a new target (Berkolaiko and Havlin, 1998; Larralde et al., 1992).

However, in principle, the area explored by a Lévy forager that can sense a target within a radius R is in fact equal to that of a walker moving in a straight line by the same path length.

Whether or not the structure of actual animals' paths displays Lévy-like long, power-law tails has remained controversial (Boyer et al., 2008; Edwards et al., 2007; Viswanathan et al., 1999). It has otherwise been claimed that animals' searching behavior is better described by a behavioral alternance between a local, diffusive searching mode and a fast, ballistic relocation model (Kramer and McLaughlin, 2001; O'Brien et al., 1990). With the further assumption that animals cannot sense targets during the relocation phase, this two-state strategy has been found to be efficient in the case of destructive searches, that is, when targets are depleted upon encounter (Bénichou et al., 2006; Bénichou et al., 2005). "Efficient", in this latter case, is defined as minimizing the mean time it takes the searcher to find a target.

"Infotaxis": a strategy for searching without gradients

Movement patterns are commonly investigated from one of two standpoints: the chemotactic behavior towards a strong attractive signal, versus the searching behavior in the complete absence of stimuli. A more realistic scenario involves considering a "dilute limit" for the stimulus, *i.e.* a situation where the signal is just at the threshold of detection, resulting in intermittent, sparse sensing by the animal (Vergassola et al., 2007). Under these circumstances, the stimulus' source cannot be attained by standard chemotactic strategies, which rely on temporal or spatial comparisons of concentrations.

The problem that the animal is faced with is that of estimating the source location from the incomplete information conveyed by the location and timing of the detection events. This entails a trade-off between proceeding based on current information and pausing to accumulate more information; it is in fact a general problem of statistical decision theory, where it is known as the exploitation versus exploration trade-off (McNamara and Houston, 1980). Vergassola et al. approach this problem by adopting an information theoretical framework. In fact, the authors show that the search time is indeed a function of the entropy of the source distribution.

The searching algorithm proposed is one where, at each step, the direction taken maximizes the expected reduction of entropy, and where subsequent odor detection ("hits") result in an update of the estimated probability of the location of the source, $P(r)$. Such a strategy is shown to result in a faster search process than simple diffusion. The typical trajectories obtained when iterating the algorithm in the presence of simulated odor plumes display an alternance between phases of directed motion upwind and phases with meandering excursions crosswind and downwind. Interestingly, crosswind excursions are a recurring feature of insect flights in turbulent environment (Budick and Dickinson, 2006; Kennedy, 1983); it is suggestive to think that, beyond the specifics of their implementation, which may vary from organism to organism, those meandering bouts might represent a constitutive part of searching strategies in noisy, dilute environments.

C. elegans – general description and overview

C. elegans is a small (~1 mm) free-living soil nematode that is commonly found in human environments, on nutrient- and bacteria-rich substrates such as compost heaps and decaying fruit (Andrássy 1983; Hodgkin and Doniach 1997, Barrière and Félix 2005). Animals are hermaphrodites and reproduce by self-fertilization; in the laboratory, males are observed at a low frequency of about 0.2% and arise by X-chromosomal non-disjunction. The *C. elegans* genome is relatively small (1 million base pairs), with a predicted ~20000 protein-coding genes (Stein et al. 2003). Mutation rate in the laboratory has been estimated at ~2 mutations per genome per generation (Denver et al. 2004).

C. elegans is thought to feed primarily on bacteria, although it also requires exogenous cholesterol, which bacteria do not provide, to proceed through development (Kurzchalia and Ward). Bacteria are taken in together with liquid during contractions of the pharynx, the feeding organ of the animal (Fang-Yen et al. 2009). Pharyngeal pumping takes place continuously, both on and off food, whereas defecation only occurs if the worms are actively feeding (Liu and Thomas 1994, Avery and Horvitz 1990). The life cycle of *C. elegans* is of about 3 and 1/2 days when grown at 20°C on the standard food source (lawns of the *E. coli* strain OP50 on NGM agar), with non-mated hermaphrodites producing about 300 offspring.

On agar surfaces *C. elegans* lies on its side, and crawls by propagating forward dorsoventral waves. Off-food, the standard laboratory strain N2 is observed to move at a speed of about 0.2 mm/s, that is, of a body length over 5 seconds. Forward motion is

punctuated by stochastic changes in direction, called reversals and omega turns (Croll 1975, Wallace 1969). Reversals are episodes of backward motion, which typically last 1-2 seconds, and lead to reorientation of the animal by an angle variable between 40˚ to 90˚ with respect to its previous direction of motion (Gray et al. 2004). Omega turns are stereotypical movements which occur when the head of the animal comes close to touching its tail, and which result in sharp turns of ~180˚. The direction of an animal's movement can also be modulated by smoother, gradual turning, which takes place when the animal's head swings are biased in either the ventral or dorsal direction.

Animals crawling on the water meniscus that is formed on agar plates are subjected to surface tension forces. An estimate of the order of magnitude of such a force is obtained by multiplying the surface tension of water, which is approximately equal to 75 mN/m, by the perimeter of the worm, assumed to be of 2mm; this gives a value of 150 μN. For comparison, gravity forces on an aqueous cylindrical mass of 2mm with a radius of 200 μm are of the order of the μN. It would be therefore tempting to argue that gravity does not play a conspicuous role at the worm's scale.

Developmental adaptations to nutrient availability

The short life cycle and large brood size of *C. elegans* translate in a population doubling time of as little as half a day. This rapid growth pattern means that whatever resources are available to a population at any given moment will quickly be depleted. Accordingly, *C. elegans* has evolved several developmental responses to deal with conditions of food scarcity. Whereas under favorable conditions juvenile worms develop through four larval

stages to adulthood, in harsh environments development can be halted at one of two points during this progression.

The first developmentally-arrested state, or "diapause", occurs early in the first larval stage (L1) when embryos are hatched in the absence of food (Baugh and Sternberg 2006). Under conditions of starvation, crowding and/or elevated temperatures (Ailion and Thomas 2000) worms can also arrest by developing into an alternative, arrested third-stage larva, the so-called "dauer" larva, which is long-lived, stress resistant, and displays physiological and behavioral adaptations for dispersal (Riddle and Albert 1997).

In addition to the developmental arrests, starved *C. elegans* fourth-stage larvae can enter an adult reproductive diapause, a delay of reproduction that results in increased longevity and protection of germ stem cells. However, if starvation is experienced late in the fourth developmental stage or else during adulthood, animals will switch to facultative vivipary, with embryos hatching within a hermaphrodite's body and thereby causing its death (Angelo and Van Gilst 2009).

Population densities are signaled by levels of constitutively-secreted pheromones, a blend of sugar derivatives termed ascarosides (Golden and Riddle 1982; Jeong et al. 2005, Srinivasan et al. 2008, Butcher et al. 2007, Butcher et al. 2009). Different, but overlapping subsets of ascarosides act in synergy to repel hermaphrodites at high, dauer-inducing concentrations, while at the same time working as an attractive signal to males at low concentrations. Among the great number of previously identified dauer-defective mutants, *i.e.* mutants that are defective in dauer-larva formation, only one, *daf-22*, has been shown to lack pheromone activity (Golden and Riddle 1985). *daf-22* is putatively

involved in ascarosides biosynthesis; in the same biosynthetic pathway acts the gene *dhs-28*, which is also required for pheromone production (Butcher et al. 2009). However, long-term liquid cultures of both *daf-22* and *dhs-28* mutants still display significant dauer-forming activity (Butcher et al. 2009).

Sensory repertoire and neuroanatomy of *C. elegans*

Worms are highly sensitive to environmental signals and can respond to a wide range of stimuli, of the chemical, mechanical, electrical, and thermal variety. Because of the highly reproducible morphology and connectivity of the animal's nervous system, it has been possible to map sensory function to individual cell types (Hall and Russell 1991; Ward et al. 1975; White et al. 1986). Over 70 of the 302 neurons possessed by hermaphrodites of *C. elegans* are putative sensory neurons. Most of these neurons are located in the main sensory organs of the animal, the amphids and phasmids, which are situated respectively in the head and the tail of the animal (Fig. 1).

The amphids are the largest sensory organs ("sensilla") of the animal, and comprise each 12 sensory neurons and two glial cells, the socket and sheath cell. Amphidial neurons extend two processes from the cell body: an axonal process towards the nerve ring, the main circumferential bundle of axons in the worm; and a dendritic process towards the nose, which terminates in a ciliated ending.

Eight neurons in the amphid (ADF, ADL, ASE, ASG, ASH, ASI, ASJ, ASK) terminate in a single or double cilium that is exposed to the external environment through a pore formed by the socket (see Table 1) (Ward et al. 1975; Ware et al. 1975). Those neurons

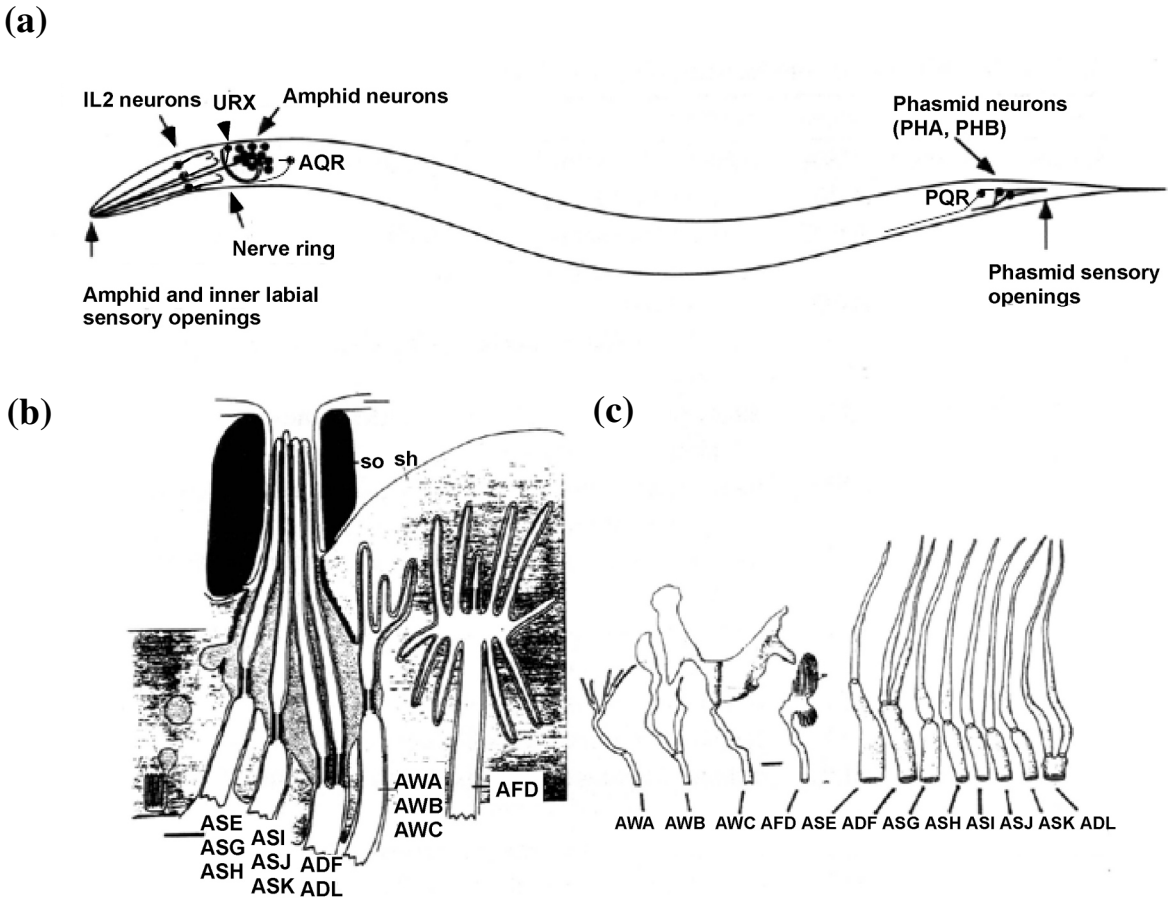

Fig. 1. Chemosensory organs of *C. elegans*. **(a)** Schematic of the position of the chemosensory organs in the animal. **(b)** Schematic of the amphid at the nose tip, showing the amphid pore and the neurons' ciliated endings. so: socket cell; sh: sheath cell. **(c)** Reconstruction of the ciliary structures of individual amphid neurons. Adapted from (Bargmann, 2006).

Table 1. Sensory neurons of *C. elegans* and corresponding known function.

Stimuli	**Neurons**
Volatile compounds	AWA, AWC, AWB (avoidance)
Soluble compounds	ASE, ASG, ASI, ASJ
Temperature	AFD, AWC?
Dauer pheromone, food	ADF, ASG, ASI, ASJ, ASK
Oxygen	AQR, PQR, URX, BAG
Internal (regulation of reversals frequency)	AWC, ASI, ASK
Noxious (touch, chemical, osmotic)	ASH, ASK, ADL, PHA, PHB
Light	ASH, ASJ, ASK, AWB
Electric field	ASH, ASJ, ASK
Chemicals, touch (putative)	Inner and outer labial neurons

sense mainly water-soluble chemicals (Bargmann et al. 1990; Bargmann and Horvitz 1991a,b; Kaplan and Horvitz 1993; Troemel et al. 1995). The ciliated endings of three neurons, AWA, AWB and AWC, possess a wing-like structure that is enwrapped by the amphid sheath cell ("wing" cells). Those cells detect volatile odorants (Bargmann et al. 1993). The shape of the AFD neuron, which detects thermal stimuli (Mori and Ohshima 1995), is more complex. In addition to a ciliated ending, this neuron displays numerous microvillar projections, which are also enclosed in the amphid sheath cell.

The structure of the phasmids is very much similar to that of the amphids: phasmids contain each a socket and a sheath cell, as well as two exposed ciliated sensory neurons, PHA and PHB, which have a role in sensation of soluble repellents (Hilliard et al. 2002). The head comprises additional sensory neurons, which are located in sensory organs called the cephalic, inner labial and outer labial sensilla. Inner labial sensilla have a six-fold symmetry, and contain each two putative chemosensory neurons as well as one mechanosensory neuron. Outer labial sensilla, in contrast, only possess one neuron each, with a dendritic ending that is embedded in the cuticle of the animal; those neurons have a mechanosensory function (Hart 1995; Kaplan and Driscoll 1997). Cephalic sensilla comprise one mechanosensory neuron, CEP. Finally, three neuronal types in the head are not associated with any sensillum; those are the URX, URY and BAG neurons; among those, only the BAG neuron is ciliated. URX and BAG mediate attraction to preferred levels of oxygen (Gray et al. 2004, Cheung et al. 2005, Zimmer et al. 2009); in addition to that, the BAG neuron has a role in acute CO_2 avoidance (Hallem and Sternberg 2008). The function of the URY neuron is unknown.

Responses to water-soluble attractants such as salt ions, cyclic nucleotides and amino acids are mostly mediated by the amphidial ASE ciliated neuron (Ward 1973). However, ablating the ASE pair with a laser microbeam does not completely abolish chemotaxis. This residual chemotactic response is weak, and appears to be distributed among several other exposed amphidial neurons (including ADF, ASG, ASI, ASK, and ASJ) (Bargmann and Horvitz, 1991b). Soluble repellents are sensed by the ASK, ASH and ADL neurons, as well as by PHA and PHB in the phasmids. *C. elegans* also avoids solutions of high osmolarity, a behavior that requires the ASH neuron (Bargmann et al., 1990).

Odorants are mainly sensed by the winged neurons AWA, AWB and AWC. The AWB neuron mediates responses to repulsive compounds, whereas AWA and AWC mediate attraction to non-overlapping sets of compounds (Bargmann et al., 1993). While nematodes are typically sensitive to millimolar concentrations of soluble compounds, the detection threshold for odorants has been estimated to be in the picomolar range (Bargmann and Mori, 1997).

C. elegans displays an extraordinary sensitivity to temperature. When placed in radial or linear gradients, nematodes are observed to migrate to their cultivation temperature (Hedgecock and Russell, 1975). Within 3°C of this temperature *C. elegans* is observed to track isotherms, straying by as little as 0.05°C on standard gradients with typical slopes of ~1°C/cm. Animals will occasionally fall off a given isotherm, and will then resume tracking on a different isotherm (Hedgecock and Russell, 1975; Ryu and Samuel, 2002). The amphidial AFD sensory neuron is required for wild-type thermotaxis; worms in which this cell is ablated display either a cryophilic phenotype or an athermotactic one

(Mori and Ohshima, 1995). More recent reports suggest a role for the olfactory neuron AWC in the animals' response to temperature (Biron et al., 2008).

Dauer signaling, and in general sensation of pheromones and of antagonizing food cues, is under the control of signaling from the ASI, ASJ, ASG and ADF neurons. Specifically, ASI, ADF and ASG share a role in inhibiting entry into dauer (Bargmann and Horvitz, 1991a), whereas ASJ is required for recovery from the dauer stage (*ibid.*). ASK-ablated worms do not display a developmental phenotype; however, the cell has been shown to respond to pheromones by calcium-imaging studies (Macosko et al., 2009).

C. elegans prefers levels of oxygen lower than the atmospheric (21%), and will aerotax to concentrations intermediate between 4% and 12% in linear oxygen gradients (Dusenbery, 1980b; Gray et al., 2004). This behavioral response requires the URX, AQR, PQR and BAG neurons (Chang et al., 2006; Cheung et al., 2005; Dusenbery, 1980b; Gray et al., 2004). AQR and PQR have not been mentioned previously; they are ciliated sensory neurons whose endings are in contact with the fluid that fills the animal's pseudocoelomic body cavity, which suggests that the function of these neurons might be in monitoring internal oxygen concentrations (Cheung et al., 2005; Coates and de Bono, 2002; Gray et al., 2004).

Remarkably, the behavior of *C. elegans* in linear oxygen gradients is determined by a naturally-occurring polymorphism at the gene *npr-1*. In fact, the *npr-1* allele that is carried by the standard laboratory strain, N2, results in aerotaxis to preferred concentrations of oxygen that are of about 14%. In contrast, strains that carry the *npr-*

1(215F) version of the allele display a preference for lower oxygen concentrations and a marked avoidance of concentrations close to the atmospheric (Gray et al., 2004). This same polymorphism appears to affect a variety of *C. elegans* behaviors, among which is the striking aggregation pattern displayed by *npr-1(215F)* or other low-activity alleles of *npr-1* on food (de Bono and Bargmann, 1998; Hodgkin and Doniach, 1997). In fact, natural isolates that carry the N2 allele of *npr-1* are observed to move at a low speed on a bacterial lawn, and disperse upon it. In contrast, wild strains carrying the *npr-1(215F)* allele are found to move at higher speed on bacteria, and to aggregate together at the edges of the lawn.

Taxis behavior is also observed when nematodes are placed in an electric field (Gabel et al., 2007; Sukul and Croll, 1978). Animals display oriented motion towards the negative pole of electric fields in the range of a few V/cm, and are able to track fields that rotate at frequencies below 14˚/s. By laser-ablation and calcium-imaging studies, the main sensory contributors to this behavior have been identified in the ASJ, ASK and ASH neurons (Gabel et al., 2007).

C. elegans displays an avoidance response to UV light as well as to frequencies in the high range of the visible spectrum. Animals respond to light being shined on their head by initiating a reversal; conversely, if light is directed to the tail of a worm during backward motion, the animal switches to forward motion (Ward et al., 2008). The question of how *C. elegans*, in spite of its lacking dedicated sensory structures, might be capable of transducing photo stimuli has been baffling the field since the advent of GFP transgenic techniques (Chalfie et al., 1994) resulted in daily observation of the behavior by hosts of researchers. Photo-avoidance behavior in *C. elegans* has been recently shown

to require the taste receptor homolog *lite-1* upstream of a signaling transduction pathway that is also utilized in odor signal transduction (Edwards et al., 2008; Liu et al., 2010). The head-avoidance response has been shown to require the function of the ASJ, ASK, ASH and AWB neurons (Ward et al., 2008).

Mutants with impaired sensory function. 1. Ciliary morphology

The sensory mutations isolated in *C. elegans* in early screens for defective chemotaxis (*che-*) or defective avoidance of solutions of high osmolarity (*osm-*) have led to the identification of a number of genes whose loss-of-function results in abnormal ciliary morphology (Culotti and Russell, 1978; Dusenbery et al., 1975; Ward, 1973). Additional cilia-defective mutants have been identified in dye-filling screens – a method for indirectly assaying the morphological integrity of ciliary structures (Perkins et al., 1986; Starich et al., 1995). When wild-type worms are soaked in fluorescent dyes such as FITC and DiI several neurons stain with the dye and become then visible under epi-fluorescence. Although the mechanism of dye uptake has not been elucidated, dye-filling defects are tightly associated with abnormal ciliary ultrastructure. Strikingly, virtually all mutants with defective cilia structures display a *che-* or an *osm-* phenotype (Lewis and Hodgkin, 1977), therefore suggesting that cilia play an essential role in mediating behavioral responses to environmental signals.

Several of these mutations have mapped to intraflagellar transport (IFT) genes, a battery of genes involved in intracellular transport of ciliary precursors to the neuronal dendritic (Scholey et al., 2004). Mutants in this class of genes, such as *che-2* or *osm-6*, display cilia that are severely shortened or missing (Perkins et al., 1986). These mutants exhibit

impaired sensory perception of chemical, electrical, and mechanical stimuli, as well as abnormal regulation of the dauer developmental decision (Albert et al., 1981; Culotti and Russell, 1978; Gabel et al., 2007; Lewis and Hodgkin, 1977). Surprisingly, given that the thermosensory AFD neuron is also ciliated, thermotaxis is spared by this class of mutations. An analysis of the cell ultrastructure by electron microscopy reveals that its microvillar protrusions appear wild-type in ciliary mutants (Perkins et al. 1986), suggesting a role for this structure in mediating thermotactic behavior. .

IFT genes are under the transcriptional control of the RFX-type transcription factor, *daf-19* (Swoboda et al., 2000). *daf-19* mutants display a complete absence of cilia and, accordingly, more severe behavioral defects than mutations in any of its target genes. Loss of *daf-19* function, however, does not disrupt neuronal fate specification, as sensory neurons in *daf-19* animals still express cell-type specific markers. Remarkably, *daf-19* function can be rescued cell-autonomously, resulting in single, fully-functional ciliated neurons that can direct behavioral responses to external stimuli (Senti et al., 2009).

Interestingly, while other ciliary mutants exhibit a dauer-defective phenotype, *daf-19* mutants enter dauer constitutively; for this reason, the strain is usually propagated as a double mutant with either a nuclear hormone receptor *daf-12* mutant or a *daf-16/FoxO* insulin-signaling mutant. Beyond its transcriptional role, *daf-19* is also important for synaptic maintenance in all nonciliated neurons. These separate roles have been shown to depend on the function of different isoforms of the gene (Senti and Swoboda, 2008).

Mutants with impaired sensory function. 2. Sensory transduction channels

Despite the variety of stimuli sensed by the worm, most sensory pathways seem to converge downstream at the level of the neuronal sensory transduction channels. Indeed, most non-mechanical inputs lead to cell depolarization via the opening of either of two signal transduction channels – a cyclic-GMP channel encoded by the genes *tax-2* and *tax-4* (Coburn and Bargmann, 1996; Komatsu et al., 1996), or a TRPV channel encoded by *osm-9* and *ocr-2* (Colbert et al., 1997; Tobin et al., 2002).

Loss of *tax-4* or *tax-2* function results in pleiotropic behavioral defects. Mutations in *tax-4* or *tax-2* result in defects in ASE chemotaxis to water-soluble compounds, AWC chemotaxis to volatile odors, AWB avoidance of volatile repellents, and AFD thermotaxis as well as in ASJ-mediated responses to light; additionally, *tax-4* mutants are also defective in aerotaxis (Gray et al., 2004; Komatsu et al., 1996; Ward et al., 2008). *tax-2* and *tax-4* are co-expressed in all of those neurons, as well as in a number of other sensory neurons (ASG, ASI and ASK in the amphids, as well as the oxygen-sensing PQR, AQR, URX and BAG) (Coburn and Bargmann 1996); as expected from their predicted role in sensory transduction, TAX-2 and TAX-4 are found to localize primarily to the neurons' ciliated sensory endings (Coburn and Bargmann, 1996; Komatsu et al., 1996). *tax-2* and *tax-4* are predicted to work as a heterodimeric channel, with *tax-4* coding for the channel's alpha subunit whereas *tax-2* encodes the channel's beta subunit (Komatsu et al., 1999).

Amphidial neurons that do not require *tax-4/tax-2* for their function signal through a different channel, a TRPV channel encoded by the *osm-9* and *ocr-2* genes. A notable

exception to this is constituted by the ASK-mediated chemotaxis to the aminoacid lysine, which has been shown to require a deg/Enac channel (Wang et al., 2008). Mutations in *osm-9* and *ocr-2* affect AWA- and ASH- mediated sensory responses, as well as phasmidial-mediated avoidance behaviors; the behavioral effects due to the loss of *osm-9*/*ocr-2* function in other amphidial cells have not been characterized (Colbert et al., 1997; Tobin et al., 2002). Beyond its role in sensory signal transduction, *osm-9* also regulates olfactory plasticity in the AWC neuron (Colbert and Bargmann, 1995).

Mutants with impaired sensory function. 3. Guanylate cyclases

The *C. elegans* genome codes for 27 predicted guanylate cyclases that might function as sources of cGMP upstream of TAX-4 signaling (Ortiz et al., 2006). Distinct sets of guanylate cyclases appear to be involved in the animals' perception of oxygen, temperature, and chemical compounds. The *odr-1* guanylate cyclase is expressed in the ASI, ASJ, ASK, AWB and AWC neurons, and is required for AWB- and AWC-mediated olfaction, as well as for phototransduction (L'Etoile and Bargmann, 2000; Liu et al., 2010). A different guanylate cyclase, *daf-11*, is expressed in the same neurons as *odr-1*. *daf-11* mutants also display defective AWB- and AWC- mediated olfactory responses; in addition to that, mutations in this gene disrupt normal dauer formation and recovery (Birnby et al., 2000; Vowels and Thomas, 1994)

The AFD thermosensory neuron expresses four guanylate cyclases (Ortiz et al., 2006). A triple mutant for three of those genes, *gcy-8*, *gcy-18*, and *gcy-23* has been shown to display severe defects in thermotaxis behavior (Inada et al., 2006). The oxygen-sensing AQR, PQR and URX neurons co-express a different set of guanylate cyclases, *gcy-32*

and *gcy-34* through *gcy-37* (Chang et al., 2006); mutations in either *gcy-35* or *gcy-36* result in defective sensory responses to oxygen (Gray et al., 2004; Zimmer et al., 2009).

Behavioral adaptations to nutrient availability

On shorter timescales than those of development, fluctuations in the availability of resources can be dealt with effectively by rapid, reversible behavioral responses. *C. elegans* responds to the presence or the absence of food, or to starvation-induced stress, by modulating a number of behaviors. Here, I will briefly outline those responses that pertain the most to the study of the animals' locomotory behavior.

1. A biased-random walk model for chemotaxis

Because most chemosensory stimuli are sensed by a single neuronal type, *C. elegans* cannot rely on head-tail comparisons to estimate compound concentrations (Ward, 1973). Furthermore, since the animal lies on its side during locomotion, chemicals are effectively sensed at only one point in the body; in fact, ablation of a left or right neuron possessing bilateral symmetry does not abolish chemotactic behavior (Bargmann and Horvitz, 1991b).

So what sensing mechanism do the animals employ to climb up gradient of attractants? It is unlikely that animals might be responding to absolute concentration levels, since *C. elegans* chemotaxis has been observed in gradients that differ 1000-fold in absolute concentration (Ward, 1973). Early studies with immobilized animals suggest that *C. elegans* responds to positive or negative changes in concentration over time (Dusenbery,

1980a). If the animal experiences a drop in concentration it initiates a backing response, whereas if concentrations rise the frequency of reversals is suppressed.

These observations have been confirmed by quantitative analysis of the behavior of freely moving animals in gradients of the soluble attractants ammonium chloride and biotin (Pierce-Shimomura et al., 1999). The animals' instantaneous speed and turning rate, as measured in plates containing different, uniform concentrations of the attractants, appears to only weakly depend on concentration. Instead, in the presence of a spatial gradient, animals are found to display a correlation between the rate of sharp turns and the rate of change in concentration *dC/dt* experienced along the track. Central to this observation is the segmentation of the animals' paths into "runs" and "pirouettes"; runs being bouts of continuous forward motion, and pirouettes being episodes of sharp turning, generated by clusters of reversals and/or omega bends, which effectively work to reset the animal's direction of motion. The authors also observe that the value of *dC/dt* before a pirouette, *i.e.* the concentration change experienced by an animal along its track, is on average negative for up to ~15 s before the turn is initiated.

In conclusion, it appears that *C. elegans* performs chemotaxis to soluble compounds by modulating the frequency of pirouettes as a function of changes in concentration. This strategy, reminiscent of the biased random walk strategy of E. coli, is not only specific to chemotaxis, as it is also employed in thermotaxis towards a preferred temperature (Ryu and Samuel, 2002).

2. Evidence for an additional mechanism at work in chemotaxis

Does the random biased walk offer a complete account of the chemotactic strategy of *C. elegans?* Indirect evidence for a different mechanism comes from Ward's seminal study of nematode chemotaxis (Ward, 1973), and specifically from the observation of the behavior of *vab-10* mutants. Because of a defect in development, *vab-10* animals have the head bent an angle with the body. The head entrains the animal along, resulting in a loopy pattern of movement. Surprisingly, in attractant gradients, *vab-10* mutants still attain the gradient's peak. The mutants' paths, however, differ markedly from those of the wild-type, displaying a continuous spiraling pattern towards the source of attractant. This observation suggests that the animals might be pointing directly towards the attractant source during movement, and argues for a spatial comparison mechanism for chemotaxis.

In fact, direct steering towards the source of attractant has been also reported to occur in the wild-type in the presence of sodium chloride gradients or of gradients of the AWC-sensed diacetyl or isoamyl-alcohol odorants (Iino and Yoshida, 2009). This strategy appears to be employed in parallel to the random biased walk strategy for chemotaxis; the extent to which each one contributes to the animals' performance is, however, unclear.

3. A two-state behavioral alternance on food

Turning frequency is not only regulated in response to drops and increases of concentrations of attractants, but can be also modulated according to the behavioral state and the feeding history of the animal. On a relatively constant environment of a plate seeded with bacteria, animals are observed to alternate between two locomotory states: a

"dwelling" state, characterized by suppression of sharp turns, frequent shallow turns, and low speed; and a "roaming" state, in which speed is increased and turns are suppressed, which in effect relocates the animals to a different location on the lawn (Fujiwara et al., 2002). The dwelling state is occupied by wild-type animals about 80% of the time, although the statistics of the transitions between states has not been characterized. Remarkably, the basic features of this behavioral alternance – a state with low angular velocity and high speed, and viceversa – have been observed elsewhere across phyla (Herbers, 1981; Sokolowski, 1980), suggesting that this phenomenon might represent a more general, heuristic solution to the problem of the exploitation of a resource patch.

Interestingly, the behavioral balance between roaming and dwelling states is affected by the perceived quality of the bacterial food source: animals on poor quality foods display extended bouts of roaming behavior (Shtonda and Avery, 2006). Mutations that disrupt sensory perception, such as those affecting ciliary function or sensory signal transduction, also affect this behavioral balance: the amount of time spent in the roaming state is reduced in *che-2* and *tax-4* mutants, and as a result their tracks remain confined to a small area of the lawn even after long observation times. Importanty, this result also suggests that dwelling does not to require sensory perception (Ben Arous et al., 2009).

4. Neuronal control of behavioral states transitions off-food

Dwelling is not observed off food (Gray et al. 2005; Hills et al., 2004; Wakabayashi et al., 2004). Instead, when worms are first transferred to a bacteria-free plate, a different pattern of locomotion is observed: the animals' speed increases about 10-fold, accompanied by a parallel increase in the frequency of sharp turns. This behavior, which

has been referred to as “area-restricted search”, “pivoting”, or “local search”, is transient, as turning is suppressed to a baseline frequency of about 1 turn/5 minutes in the following 20-30 minutes of starvation.

Insight into the neuronal control of wild-type turning frequencies in the distinct behavioral states comes once again from laser-ablation studies. ASI-ablated animals display an increased frequency of both shallow turns and omega bends at all times after removal from food. As opposed to that, AWC-ablated animals exhibit a suppression of all turns in the first 15 minutes off-food, a phenotype that is also similar to that observed in animals lacking ASK.

Downstream of the sensory neuronal layer, regulation of turning frequency has been mapped to the AIZ, AIB and AIY interneurons. AIY and AIB are direct synaptic partners of AWC, and AIY directs its input on to AIZ. Killing AIZ reduces reversals during feeding, whereas killing AIB results in fewer turns after removal from food. AIY ablations result in an increased rate of turns at longer time scales, disrupting the normal locomotion pattern of animals in conditions of starvation. Interestingly, while a direct connection exists between the sensory AWC and ASI neurons and the AIY interneuron, none of the interneurons identified in this study constitutes a primary target of ASK input. Going further downstream, a second layer of interneurons and motor neurons is found to encode more fine-grained features of locomotion, such as the frequency of reversals and of omega turns, and the amplitude of the sinusoidal movement (Gray et al., 2005).

Chapter 2. Materials and methods

Off-food locomotory assay

To minimize growth of contaminants all assays were performed on NGM plates lacking peptone. Assay plates (240mm x 240mm polystyrene culture plates; Nunc, Corning) were poured 7 to 14 days before an experiment and subsequently kept at 4°C in air-tight boxes. After an assay, plates were soaked in a sodium hypochlorite solution, washed, and recycled.

Assays were carried out on 1-day-old adults by selecting L4 larvae on the day before the experiment. In order to exclude interactions among animals, worms were assayed individually unless indicated. Bacteria were removed by transferring twice the animals with an eyelash pick to individual unseeded NGM plates, where they were let to crawl for ~10' before being transferred to the assay plate. Plates were sealed by wrapping them in Parafilm (Cole-Parmer) just before imaging.

Imaging setups

1. A fixed-camera setup for imaging of *C. elegans* over large surfaces (with John Chuang)

The setup is depicted in Figure 2. Animals were illuminated with transmitted light generated by a 24"x 24" edge-lit LED light source for minimal heating ("LitePad", Rosco). Images were acquired with a consumer Digital Rebel 300D Canon camera

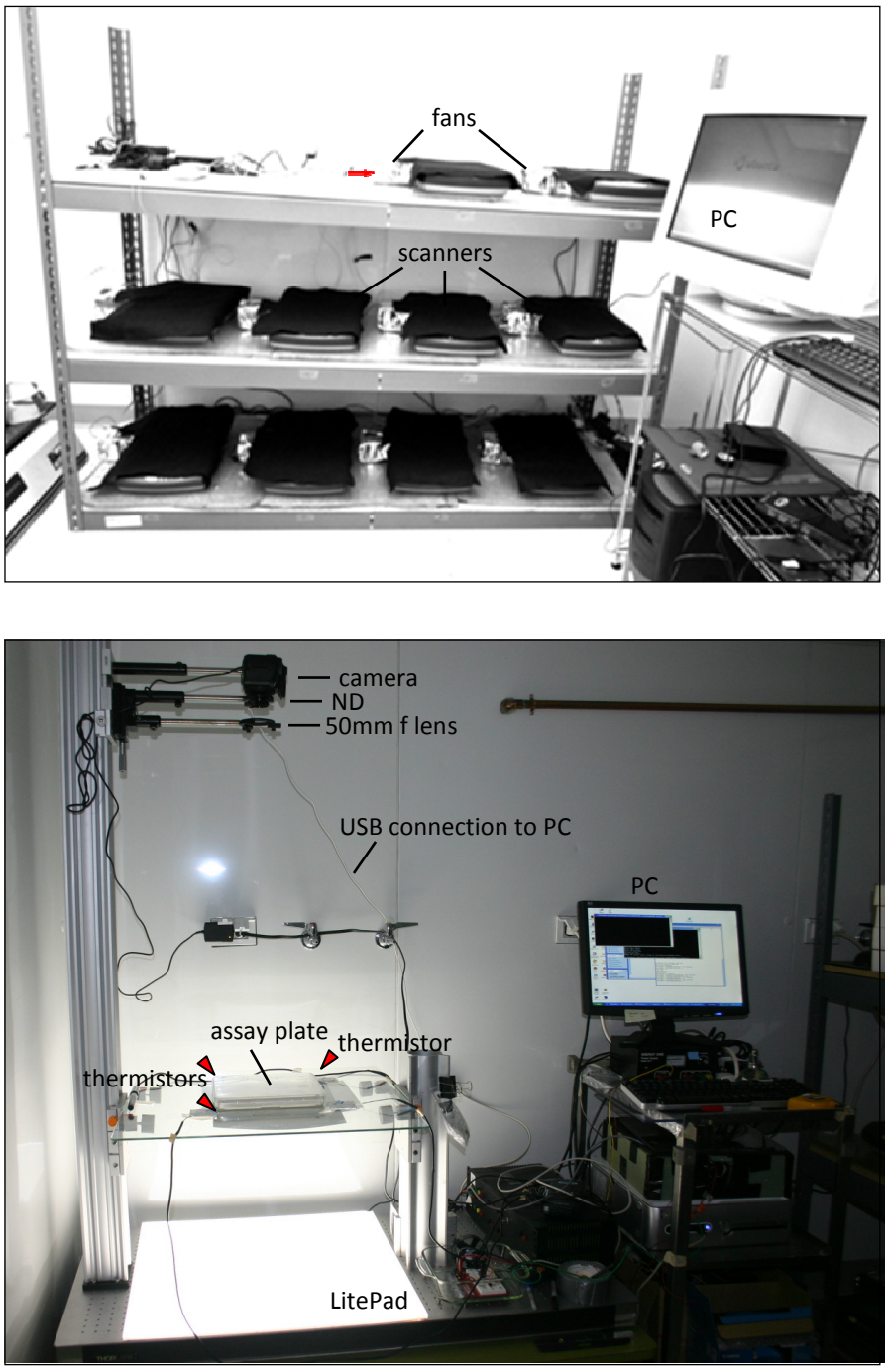

Fig. 2. Imaging setups. **(a)** Scanner-array setup. 10 flatbed scanners are connected via USB connections to a PC running Linux. The arrow indicates the direction of airflow within the scanner body. **(b)** Camera imaging setup. Light source: LED Lite-Pad (Rosco). ND: Neutral density filter. Temperature was monitored at the three corners of the plate indicated by arrowheads.

custom-mounted with a 50mm focal length lens (Beseler, 50mm f/3.5 Beslar Enlarging Lens) and a neutral density filter (Hoya, NDX4). In order to image the full plate surface of 240mm x 240mm the camera sensor (6.3 megapixels) was placed at a working distance of 3 ft. from the glass stage holding the plates, resulting in a resolution of ~10 pixels/mm. To enhance contrast, we further equipped the stage with two light control films (Vikuiti^{TM}, 3M), which we placed at a right angle from each other. The camera was controlled by custom time-lapse software developed with Microsoft Visual C++ using the Canon SDK (EDSDK 2.5) (John S. Chuang), and images were acquired at a frame rate of 1 image/1.5 seconds. All experiments were performed in a temperature- and humidity-controlled room (T = 22.0 +/- 0.2 °C, humidity: 54% +/- 2%). The typical temperature difference at different points on the stage in contact with of the edges of the plate was estimated by measurements with a thermistor ("Stainless Steel Temperature Probe", Vernier) to be within 0.1°C.

Images were collected as JPEGS for 80' and subsequently binarized with a custom Image-Pro Plus macro script (Media Cybernetics). Background subtraction was performed by taking the absolute difference between a given frame and a frame at a later time-point. The resulting image was then low-pass filtered and thresholded. Finally, the animals' positional information was extracted by tracking the binarized image sequences with custom MATLAB code (MathWorks) adapted from the Parallel Worm Tracker (Ramot et al., 2008).

2. Parallel Automated Imaging with an Array of Scanners

In order to run simultaneous time-lapse experiments we devised an imaging setup comprising an array of consumer scanners (Michel et al., 2008). In our setup 10 flatbed scanners (EPSON Perfection 2400 Photo) are connected to a single PC running Linux (Ubuntu 8.04) and interfaced using the SANE application programming interface (http://www.sane-project.org/). Scanners are directed via a Perl script to acquire images at a resolution of 300 dpi, *i.e.*, about 0.4 pixels/cm, which results in a frame rate of 1 image/20 seconds. Heat dissipation from the internal cold-cathode fluorescent lamp causes the scanners' surface to heat to temperatures that are noxious to *C. elegans*. We therefore modified the scanners to allow for fan-driven airflow across the scanners' body, thus reducing the temperature difference across opposite sides of each scanner, relative to the fan, to ~1°C.

Image sequences collected with this setup are segmented in ImageJ (http://rsbweb.nih.gov/ij/) and tracked with the ImageJ MTrack2 plugin, developed by N. Stuurman (http://valelab.ucsf.edu/~nico/Ijplugins/Mtrack2.html).

Strains and culture methods

The Shaham laboratory copy of the N2 Bristol strain was used as a wild-type reference. Mutant strains used in this work, listed below, were obtained from the Caenorhabditis Genetics Center (CGC) unless noted.

CB1033 *che-2(e1033),*

CF1108 *daf-19(m86); daf-16(mu86)* (laboratory copy)

CX10 *osm-9(ky10),*

PR691 *tax-2(p691),*

PR678 *tax-4(p678),*

CX2065 *odr-1(n1936),*

IK597 *gcy-8(oy44); gcy-18(nj38); gcy-23(nj37),*

CX6803 *gcy-31(ok296); gcy-33(232); gcy-35(769)* (a gift of C.I. Bargmann).

All TAX-4-expressing strains, listed below, were a gift of C.I. Bargmann.

CX6750 *tax-4(ks28)*; *kyEx747* (*tax-4*::TAX-4::GFP (50 ng/µl) + coel::GFP (30 ng/µl))

CX6704 *tax-4(ks28)*; *kyEx733* (*gcy-8*::TAX-4::GFP (50 ng/µl) + coel::GFP (30 ng/µl))

CX7535 *tax-4(ks28)*; *kyEx936* (*odr-3*::TAX-4::GFP (50 ng/µl) + *elt-2*::GFP (15 ng/µl))

CX8016 *tax-4(ks28)*; *kyEx1205* (*str-1*::TAX-4::GFP (50 ng/µl) + *elt-2*::GFP (15 ng/µl))

CX11121 *tax-4(p678)*; *kyEx2936* (*srh-11*::TAX-4::GFP (50 ng/µl) + *sra-9*::TAX-4::GFP (50 ng/µl) + *gcy-36*::TAX-4::GFP (2 ng/µl) + *elt-2*::GFP)

CX10544 *tax-4(p678)*; *kyEx2603* (*srh-11*::TAX-4::GFP (50 ng/µl) + *gcy-36*::TAX-4::GFP (2ng/µl) + *elt-2*::GFP (7ng/µl))

CX10549 *tax-4(p678)*; *kyEx2608* (*sra-9*::TAX-4::GFP (50 ng/µl) + *gcy-36*::TAX-4::GFP (2ng/µl) + *elt-2*::GFP (7ng/µl))

CX11113 *tax-4(p678)*; *kyEx2928* (*gcy-36*::TAX-4::GFP (2ng/µl) + *elt-2*::GFP (7ng/µl))

CX11112 *tax-4(p678)*; *kyEx2925* (*srh-11*::TAX-4::GFP (50 ng/µl) + *sra-9*::TAX-4::GFP (50 ng/µl) + *elt-2*::GFP (10 ng/µl))

daf-19;daf-16;tax-4 triple mutants were obtained by crossing *tax-4(p678)* males into *daf-19;daf-16* hermaphrodites and selecting for dye-filling defective tax-4 homozygous adults that grew to adulthood.

Nematodes were cultured on standard nematode growth medium (NGM) agar plates (Sulston and Hodgkin, 1988) seeded with the *E. coli* strain OP50. Nematodes cultures were maintained at 20°C.

Thermotaxis Assay

A linear thermal gradient from 18°C to 26°C was established across an aluminium surface using two Peltier feedback devices. Staged adult animals cultivated on OP50 at 25°C were washed in S-basal medium and transferred to the centre of a 10 cm square Petri dish containing 12 ml of NGM agar. This dish was placed onto the aluminium surface, with a thin layer of glycerol between the dish and aluminium slab to ensure adequate heat conductance. Animals were allowed to disperse for a period of 45 min, fixed with chloroform, and counted across 6 bins, from cold to hot. The centre third of the assay plate, including equal areas across all six bins, was removed from the analysis as some animals did not disperse. 50 to a few hundred worms participated in each assay.

Dye-filling Assay

For dye-filling assays, animals were rinsed off a plate with M9 medium (Sulston and Hodgkin, 1988) and spun down briefly in a picofuge. The supernatant was removed, and

a M9 wash was repeated twice. A stock concentration of the lipophilic dye DiI (5mg/ml) was added to the resuspended animals to a 1:500 dilution. Animals were then incubated in the dark at 20°C for 45' in DiI (5mg/ml), and recovered in the dark for ~2 hours at room temperature.

Electron Microscopy

Animals were recovered from the assay plate using an eyelash within minutes of the end of an acquisition, and transferred to a seeded plate. Animals were then stained, embedded in resin, and serially sectioned using standard methods (Lundquist et al., 2001). Photographs were taken with an FEI Tecnai G2 Spirit BioTwin transmission electron microscope equipped with a Gatan 4K × 4K digital camera.

Chapter 3. Off-food trajectories of wild-type *C. elegans*

Introduction

In this section we present our characterization of the behavior of individual *C. elegans* off food. In doing so, we sought to expand from the standard in the field, and developed imaging setups to collect animals' paths over surfaces of 22 cm x 22 cm. This experimental design allows us to characterize the animals' unperturbed locomotion at timescales comparable with that of starvation, and reveals behavioral features that are hindered from observation on the commonly employed 9 cm assay plates.

Trajectories of individual N2 animals off food were obtained with two distinct setups – a camera-based setup, characterized by more stringently controlled temperature and lighting conditions, as well as by a faster acquisition rate (1 frame/1.5 seconds); and a scanner-array setup, which presents lighting and temperature inhomogeneities and subjects the animals to mechanical vibrations, but which nonetheless provides the advantage of allowing parallel acquisition of 10 image sequences at a time. In what follows, the datasets obtained with the two setups will be compared point by point.

The initial characterization of wild-type behavior was carried out with a single scanner, in a set of proof-of-principle experiments performed in the Leibler laboratory. The camera imaging setup was subsequently developed with John Chuang, with the rationale of controlling for possible artifacts that might result from the unique environment of the scanners setup. Importantly, beyond validating the results obtained with the scanner-

array setup, the higher time resolution that characterizes the camera dataset allows, in principle, to address the question of how the long-range properties of the animals' motion are engendered from a simple set of stereotyped locomotory rules.

In this section we also present statistical and geometrical methods aimed at characterizing the stochastic motion of *C. elegans*. The purpose of this analysis is at least twofold: first, we seek a quantitative description of the animals' paths, that is, one that will allow us to compare paths obtained in different conditions and under different perturbations. Second, we want to answer the basic question of whether the animals exhibit a search strategy that is any different than a simple random walk. We would also like to propose, although this goes beyond the scope of this thesis, that an accurate phenomenological description of the locomotion algorithm of *C. elegans* could direct the design of new experiments to address the question of how such algorithm is implemented at the level of the nervous system.

The off food trajectories of the wild-type display long-range directional behavior

On both the camera and the scanner-array setup, animals were started on the center of agar plates measuring 22 cm x 22 cm and followed for 80 minutes or until they reached the edge of the plate, whichever was the shortest. We collected n=44 trajectories for the camera setup and n=250 trajectories for the scanners-array setup. Six such trajectories, as obtained with the camera setup, are shown in Figure 3. Despite great individual variability in the pattern of motion, the animals' paths display a striking behavior: the typical trajectory follows a more-or-less directed course towards the edge of the plate, over length scales that approximate 10 cm, that is to say ~100 times the nematodes' body

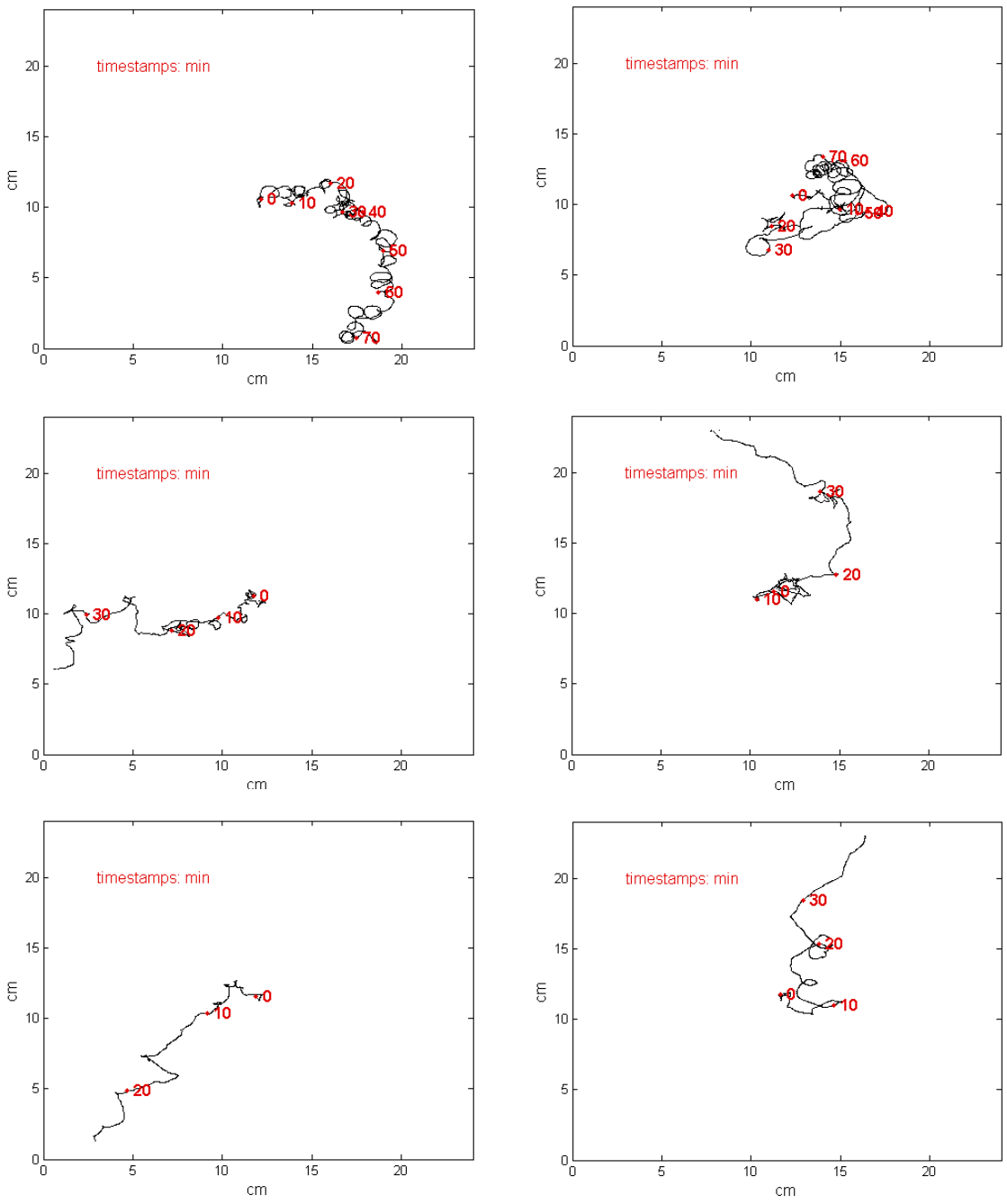

Fig. 3. Trajectories of the wild-type on the camera setup. Individual animals were started from the center of the plate, and images collected at a rate of 1 frame/1.5 s for 80'. Sequences were analyzed for the whole movie duration, or until animals reached the edge of the plate. Red dots on the trajectory indicate the position of the animal at 10 minutes intervals.

length. Remarkably, persistence in the direction of motion seems to be achieved in spite of local changes in direction, which are visible as kinks and loops in the trajectory. Paths collected with the scanner-array setup display analogous directional features, despite the differences in the experimental setup. For comparison, a subset of those trajectories is shown in Figure 4. Within the same day, both directional and non-directional behavior was observed on either setup, suggesting that directionality does not arise as a behavioral response to the day-to-day fluctuations of an environmental variable, nor does it correlate with the growth conditions of the parent plate.

The simplest explanation for directional persistence is that the animals are migrating towards, or in avoidance to, a fixed external cue, as they do in standard chemotaxis or thermotaxis paradigms. We reasoned that, if this was indeed the case, the distribution of individual directions with respect to the setup would reveal a preference for or actively avoid a given sector of the setup. We therefore analyzed the distribution of the paths' directions, as measured coarsely by the end-to-end vectors of each trajectory. However, no particular bias was observed in the distribution of the end-of-end vectors on either setup (Fig. 5), even when trajectories scored as non-directional were discarded from the analysis.

Assuming that individual animals' trajectories cannot result from an isotropic model of locomotion, this result suggests that one of two further assumptions has to be made: either the external cue varies from assay to assay, or the external cue is in fact constant across assays, but it is employed by the animals simply as a reference to maintain an individually-selected direction. Alternatively, we must assume a memory-based or other self-based mechanism to explain the animals' directional persistence.

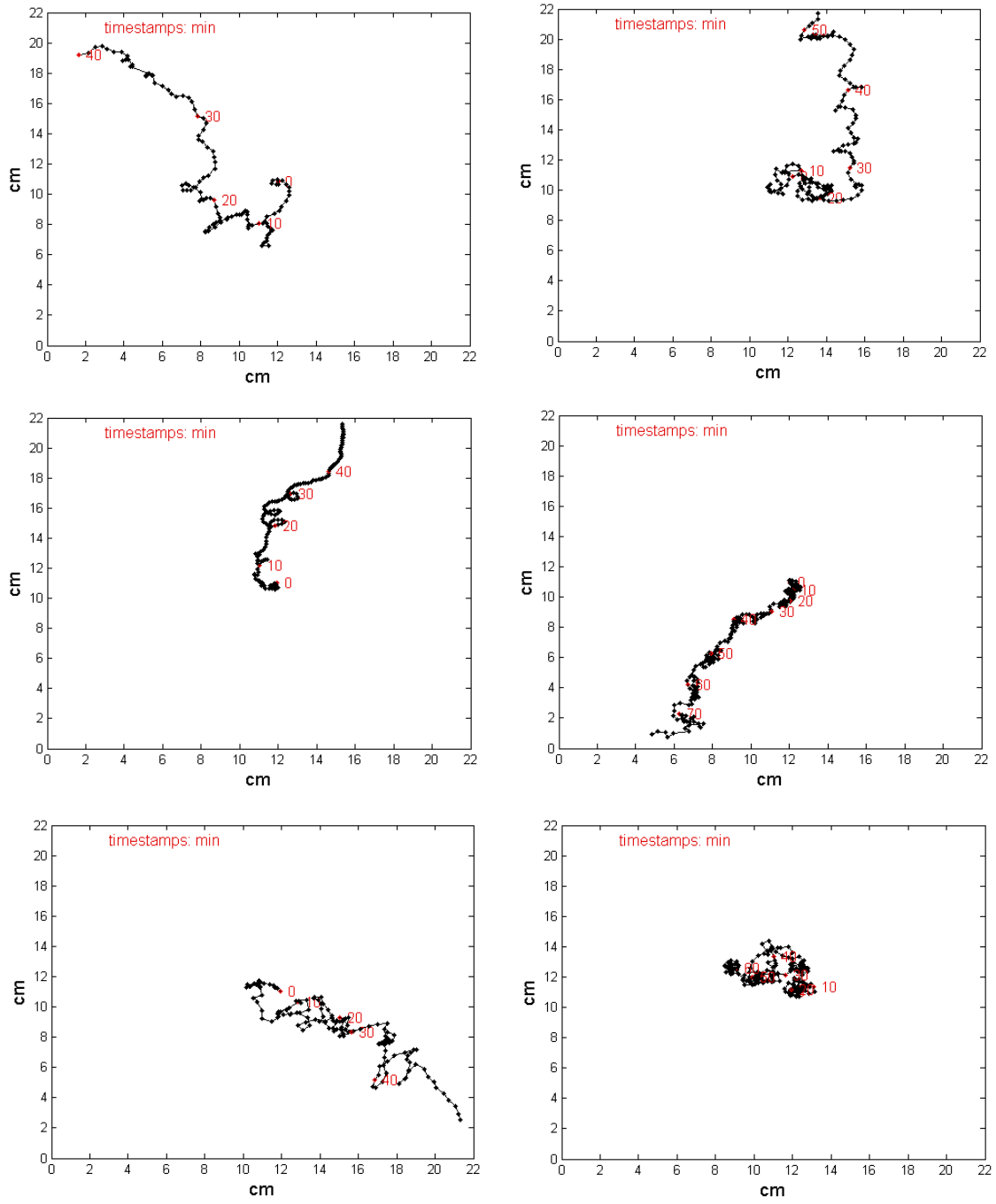

Fig. 4. Trajectories of the wild-type on the scanner-array setup. Individual animals were started from the center of the plate, and images collected at a rate of 1 frame/20 seconds for 90'. Sequences were analyzed for the whole movie duration, or until animals reached the edge of the plate. Red dots on the trajectory indicate the position of the animal at 10 minutes intervals.

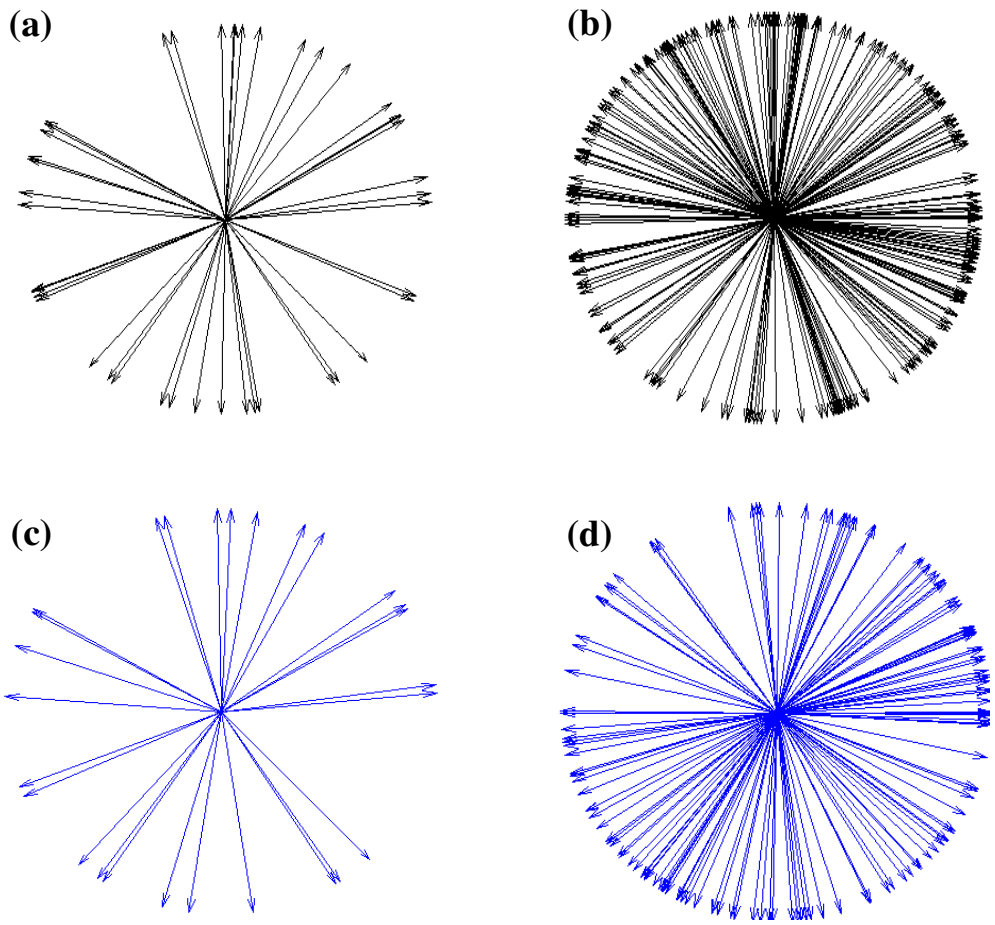

Fig. 5. Population distributions of the end-to-end directions. **(a)** Distribution of end-to-end direction vectors, camera setup. *n*=44 **(b)** Distribution of end-to-end direction vectors, scanners setup. *n*=250 **(c)** Distribution of end-to-end direction vectors, directional trajectories only. Camera setup, *n*=29 **(d)** Distribution of end-to-end direction vectors, directional trajectories only. Scanners setup, *n*=142.

Statistical analysis of individual trajectories

In a first effort to characterize and classify the behavior of the animals' trajectories we analyzed the basic features of each path: speed, direction of the frame-to-frame velocities, and turning angles. Our trajectory data yields, for each animal path, a positional vector $\vec{r}(t) = \{\mathrm{x(t)}, \mathrm{y(t)}\}$, where x and y are the coordinates of the centroid of the worm at the instant t. From now on, we will refer to the vectorial difference between consecutive positions, $\vec{v}(t) = \vec{r}(t+1) - \vec{r}(t)$, indifferently as ('frame-to-frame') displacements or velocity vectors. Speed refers to the module of the velocity vector. Direction, θ, is defined as the angle between the velocity vector and the reference frame of the setup. Turning angles, α, are computed as differences between consecutive directions: $\alpha = \theta(t+1) - \theta(t)$, $-\pi \leq \alpha < \pi$. A turning angle is therefore equal to zero when consecutive directions lie parallel to each other. The individual and population results for the two setups employed will be detailed below.

We compared different distributions by means of the Kolmogorov-Smirnov test. The Kolmogorov-Smirnov statistic D of two samples S_1 and S_2 is defined as the maximum difference, in module, of the respective cumulative distributions C_{S1}, C_{S2} at a point x: $D = \max_{\mathrm{x}} \left| C_{S1}(x) - C_{S2}(x) \right|$. In the case of the null hypothesis (samples drawn from the same distribution), the distribution of the Kolmogorov-Smirnov statistic itself can be calculated; therefore, the significance of any observed nonzero value of D can be computed (von Mises, 1964). The Kolmogorov-Smirnov test possesses the additional property of being invariant under reparametrizations of x; for example, the same significance is obtained using x as using $\log x$.

1. Speed distributions

On the camera setup, at a sampling rate of ~1.5 seconds, the animals' speed is found to fluctuate between 0 (*i.e.*, velocities values lesser than our sensitivity threshold of 0.05mm/s) and ~0.5 mm/s. The resulting speed distribution, as is obtained by pooling together all the individual contributions for a total of n=44 assays, averages 0.2 mm/s (+/- 0.1 mm/s, standard deviation), in agreement with the previously established result for the speed of N2 animals off food. The individual speed profile is somewhat variable from animal to animal. Mean average speeds, however, are in most cases equal to 0.2 mm/s (we observed only a few outliers where <v> = 0.1 mm/s or <v> = 0.3 mm/s) (Figure 6).

On the scanner-array setup, the distribution of instantaneous speed across the population appears flatter and shifted to lesser values compared to the camera one. Velocities larger than 0.3 mm/s are seldom observed, and the average velocity across the whole population equals 0.1 mm/s (+/- 0.1 mm/s, standard deviation) (Fig. 6). These differences are likely owed to the sparser sampling rate of the setup, which results in averaging of the velocity over both larger time intervals (20 seconds) and intervening changes in direction. To investigate whether this measure could constitute a good predictor of a track's "directedness", we plotted the value of the average speed for each path versus the corresponding "effective" speed, computed as the ratio of the net displacement to the total time. These two quantities appear positively correlated, in that small values of the average speed (<v> < 0.1 mm/s) are associated with small net displacements, and *viceversa*[1].

[1] A small value of the average speed could correspond to a slow-moving worm, as well as to a worm that exhibits frequent changes in direction.

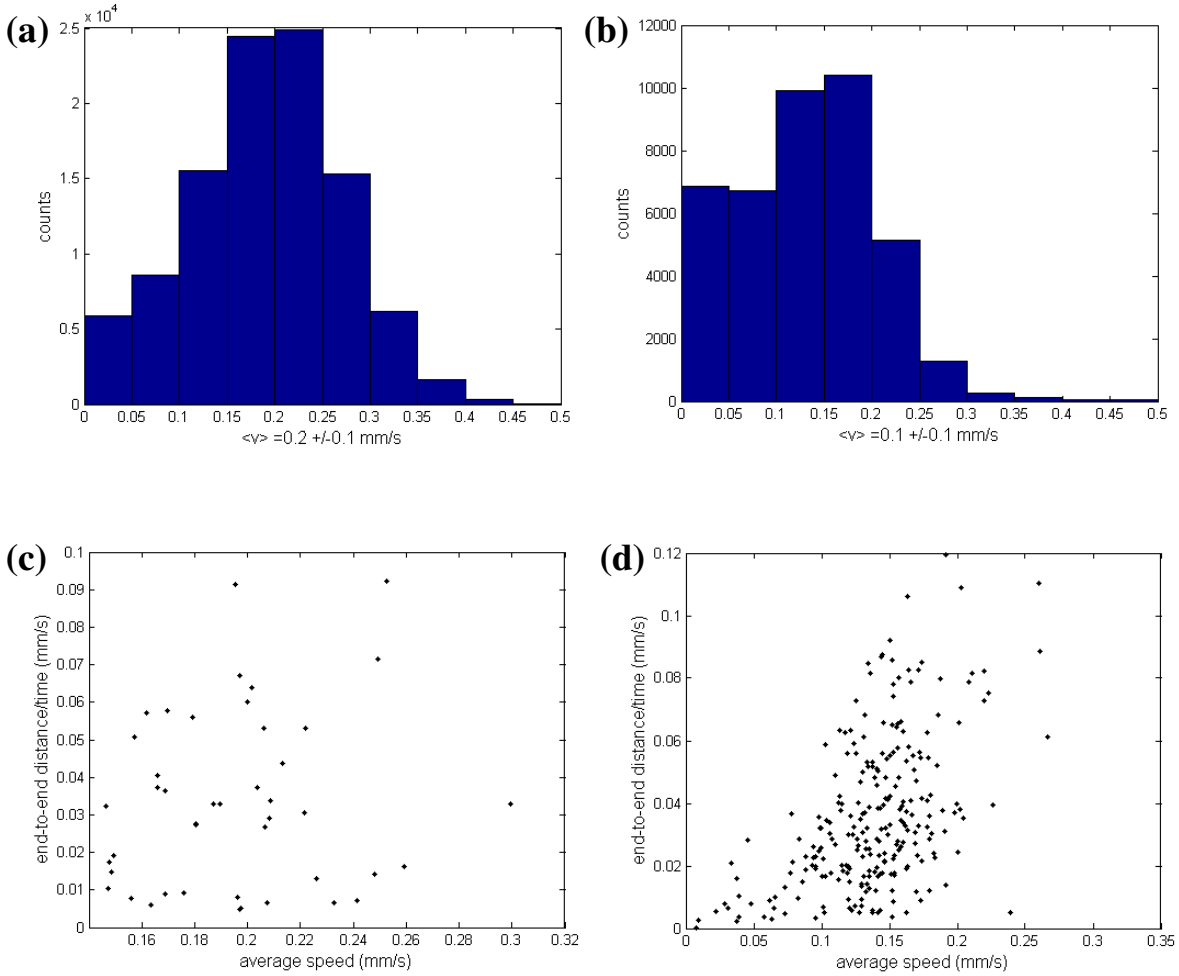

Fig. 6. Population distributions of speed and net displacement. **(a)** Histogram of the instantaneous (frame-to-frame) speed for *n*=44 movies, camera setup **(b)** Histogram of the instantaneous (frame-to-frame) speed for *n*=250 movies, scanners setup **(c)** Bidimensional plot of the average speed per trajectory against the trajectory's net displacement over time. Camera setup, *n*=44 **(d)** Bidimensional plot of the average speed per trajectory against the trajectory's net displacement over time. Scanners setup, *n*=250.

However, ~80% of the distribution is comprised within a narrow, intermediate range of speed values (0.1mm/s <= <v> <= 0.2 mm/s); in this range, no obvious correlation between average speed and effective speed can be observed, suggesting that an animal's instantaneous velocity is not a general indicator of the long-range properties of the path.

2. Headings

Histograms of the angles of individual displacement vectors, with respect to the camera setup, appear to display significant divergence from random for the great majority of trajectories (89% $p < 0.05$, Kolmogorov-Smirnov test), reflecting the individual paths' preferred direction (Fig. 7). Trajectories collected with the scanners exhibit the same qualitative profile, in that the paths' preferred direction is evident in the distribution of the velocities profile (Fig. 8). However, with this setup only ~40% of trajectories display a significant divergence from uniform at the same significance level, perhaps because of the smaller size of a typical scanner acquisition (~100 points per trajectory, versus the ~1000 points/trajectory of camera paths).

A biased distribution of directions, like the one we observe, would argue against an unbiased random-walk mechanism for locomotion, unless that was characterized by long-range correlations. This suggests two alternative scenarios for the observed behavior: 1. the animals' motion is in fact biased, perhaps in response to an external cue; 2. the animals' motion is random, but appears biased because of directional correlations on a scale that is of the order of the total observation time. In order to address the first

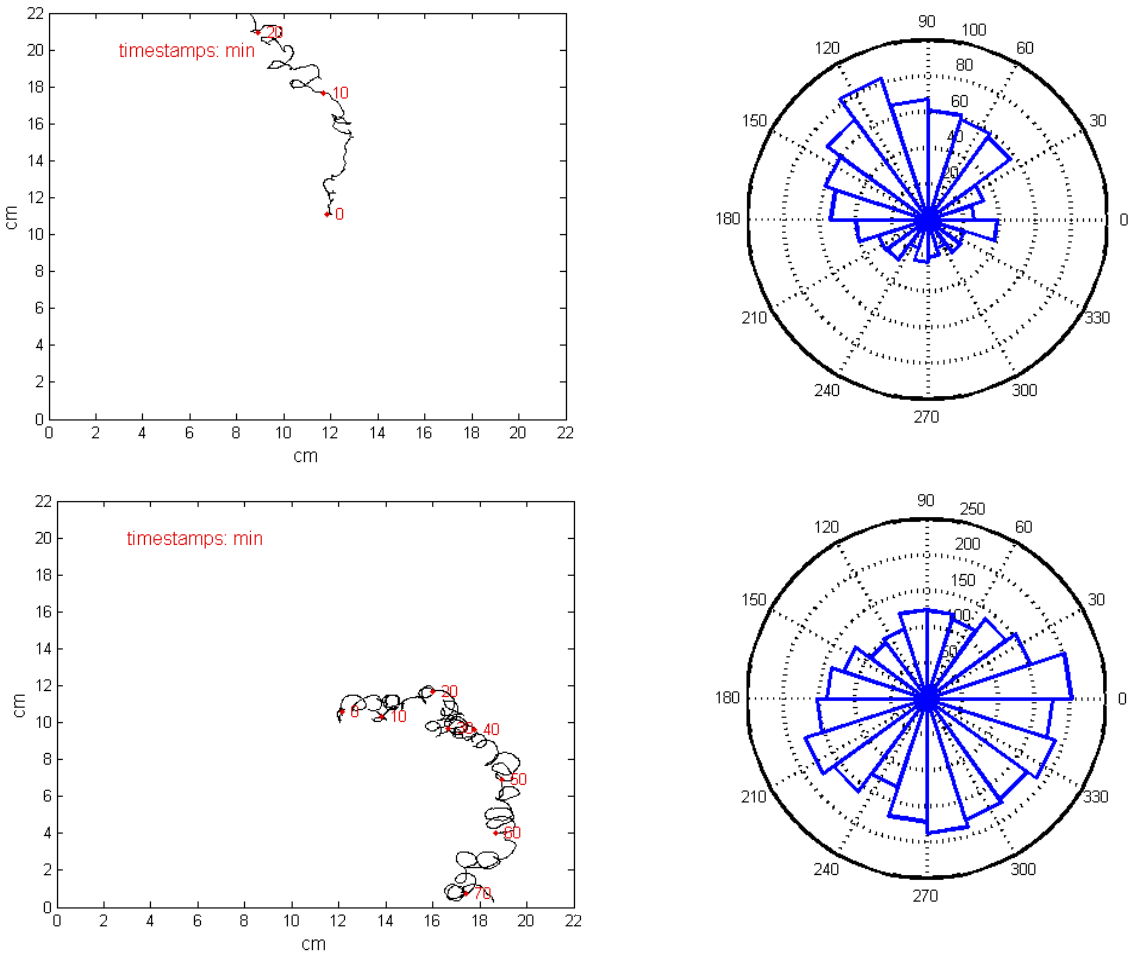

Fig. 7. Distribution of instantaneous directions, camera setup. **(a), (c)** Representative trajectories obtained with the camera setup. **(b), (d)** Histograms of corresponding instantaneous directions, relative to the setup. P-values are equal to: **(b)** $3 \cdot 10^{-21}$, **(d)** $1 \cdot 10^{-11}$ (two-sample Kolmogorov-Smirnov test against a same-sized sample drawn from a uniform distribution).

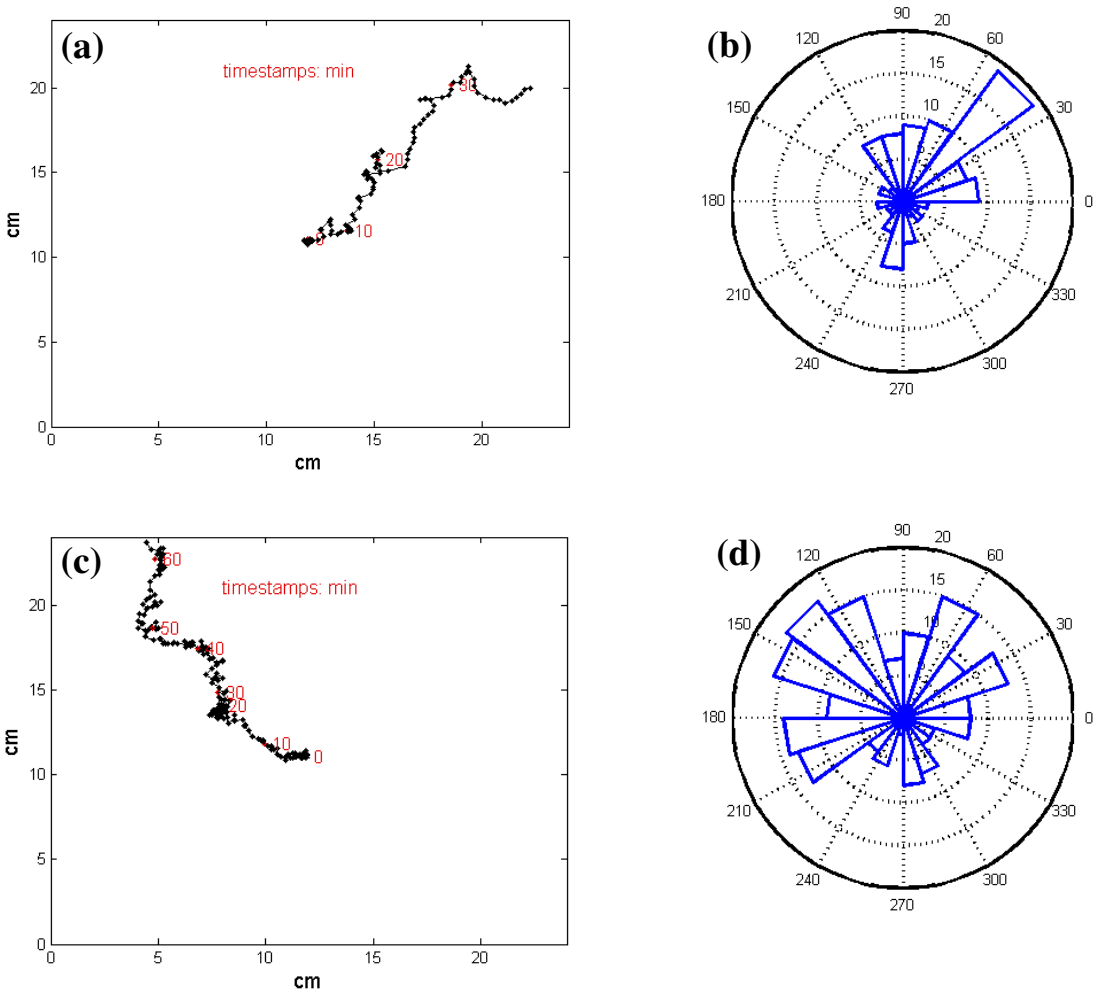

Fig. 8. Distribution of instantaneous directions, scanners setup. **(a), (c)** Representative trajectories obtained with the camera setup. **(b), (d)** Histograms of corresponding instantaneous directions, relative to the setup. P-values are equal to: **(b)** 0.07, **(d)** 0.0002 (two-sample Kolmogorov-Smirnov test against a same-sized sample drawn from a uniform distribution).

hypothesis, we pooled the totality of the instantaneous directions collected with the camera setup.

In contrast to the distribution profile displayed by individual paths, the distribution for the whole population does not reveal a preference towards a particular sector of the setup (Fig. 9), suggesting that the setup displays no consistent bias across repetitions of the experiment. We obtain an analogous result when pooling the frame-to-frame directions for the whole scanners dataset: the vectors appear flatly distributed relative to the setup (Fig. 9). Interestingly, although both distributions display a flat angular profile, they are found to diverge significantly from uniform by the Kolmogorov-Smirnov test ($p = 3 \cdot 10^{-4}$, scanners dataset; $p = 0.005$, camera dataset).

3. Turning angles

We next turned to the analysis of another variable characterizing the animals' motion: the turning angle α, defined as the difference between consecutive directions. On the camera setup, for a given trajectory, histograms of directional changes display a strong peak around zero, with 80%-90% of the distribution comprised of turning angles smaller than $\pi/6$ in module (Fig. 10). This result is consistent with the classic description of the locomotory behavior of *C. elegans* as consisting mainly of forward motion interrupted by occasional changes in direction (Croll, 1975).

The same analysis performed on the scanners dataset yields a slightly different picture: because of the sparser sampling rate, we observe distributions with a larger spread in the distributions of turning angles (Fig. 10). Moreover, those distributions, in the case of

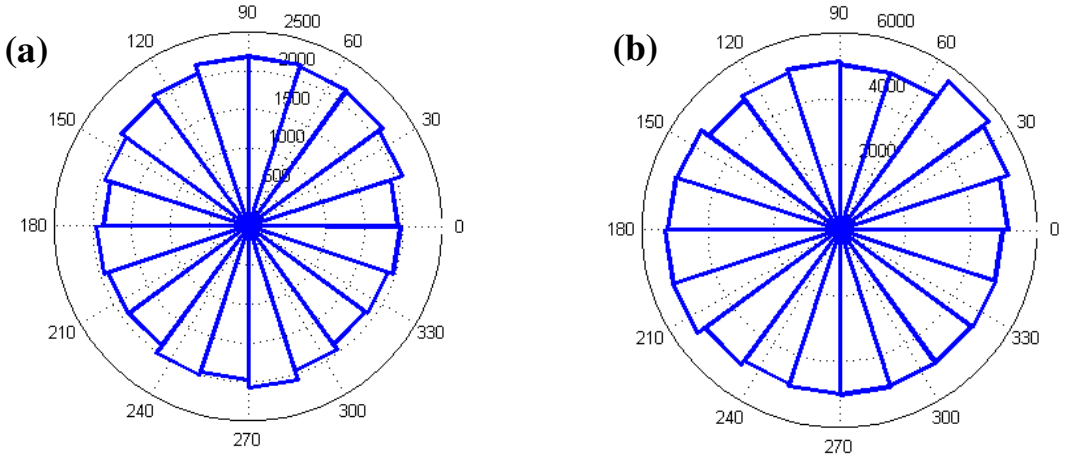

Fig. 9. Population distribution of directions. **(a)** Distribution of instantaneous directions for the whole dataset, scanner-array setup (250 trajectories). P-value of the sample against a same-sized sample drawn from a uniform distribution (Kolmogorov-Smirnov test): $3 \cdot 10^{-4}$. **(b)** Distribution of instantaneous directions for the whole dataset, camera setup (44 trajectories). P-value of the sample against a same-sized sample drawn from a uniform distribution, Kolmogorov-Smirnov test: 0.005.

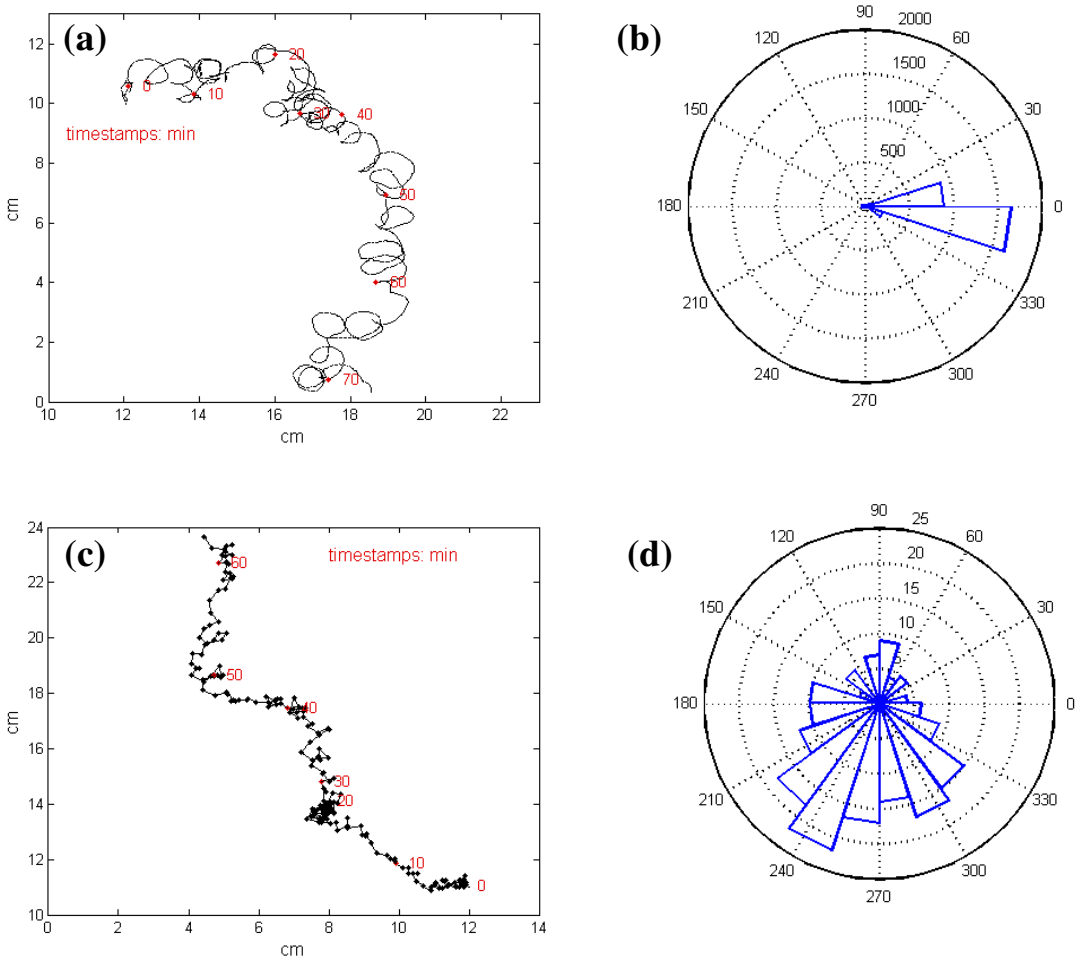

Fig. 10. Distribution of instantaneous turning angles of individual trajectories. **(a)** Representative trajectory obtained with the camera setup **(b)** Histogram of the turning angles, *i.e.* the angles between consecutive velocity vectors, for the trajectory in **(a)**. P-value: $6 \cdot 10^{-192}$ (against a same-sized sample drawn from a uniform distribution, Kolmogorov-Smirnov test) **(c)** Representative trajectory obtained with the camera setup **(d)** Histogram of the turning angles, *i.e.* the angles between consecutive velocity vectors, for the trajectory in **(c)**. P-value: $2 \cdot 10^{-5}$ (against a same-sized sample drawn from a uniform distribution, Kolmogorov-Smirnov test).

locally convoluted trajectories, are no longer centered around zero, reflecting again the coarse-graining of the path induced by the diminished acquisition rate.

4. Coarse-grained turning angles

The distinct profile observed for the distributions of turning angles on the two setups suggests the intriguing possibility that the animals' behavior might display different features at different scales. We sought to address this question by analyzing the behavior of trajectories artificially sampled at increasingly diminishing rates ("coarse-grained"). Coarse-grained trajectories are constructed from data $\vec{r}(t) = \{x(t), y(t)\}$ by retaining one point every *m,* for growing values of the sampling parameter *m*. By this procedure, we obtain a new family of paths: $\vec{r}_m(t') = \{x_m(t'), y_m(t')\}$, with $x_m(t') = x(mt)$, $y_m(t') = y(mt)$, $t = 1,...,n/m$, where *n* is the number of steps. In order to minimize the dependence of the results on the choice of the initial condition, we considered, for each value of *m,* all the trajectories obtained by starting the path at points comprised between 1 and *m*-1.

Figure 11 shows the skewed profile of turning angles of a directional, but convoluted trajectory, acquired at the scanners' sampling rate. Coarse-graining of the path results first in symmetrization of the turning angle distribution (*m* = 2, corresponding to a sampling rate of 40 s), and eventually in the collapse of the distribution around zero (*m* = 4 and *m* = 8, corresponding to a sampling rate of 80 s and of 160 s, respectively). This behavior seems to constitute a general feature of directional trajectories: at increasing

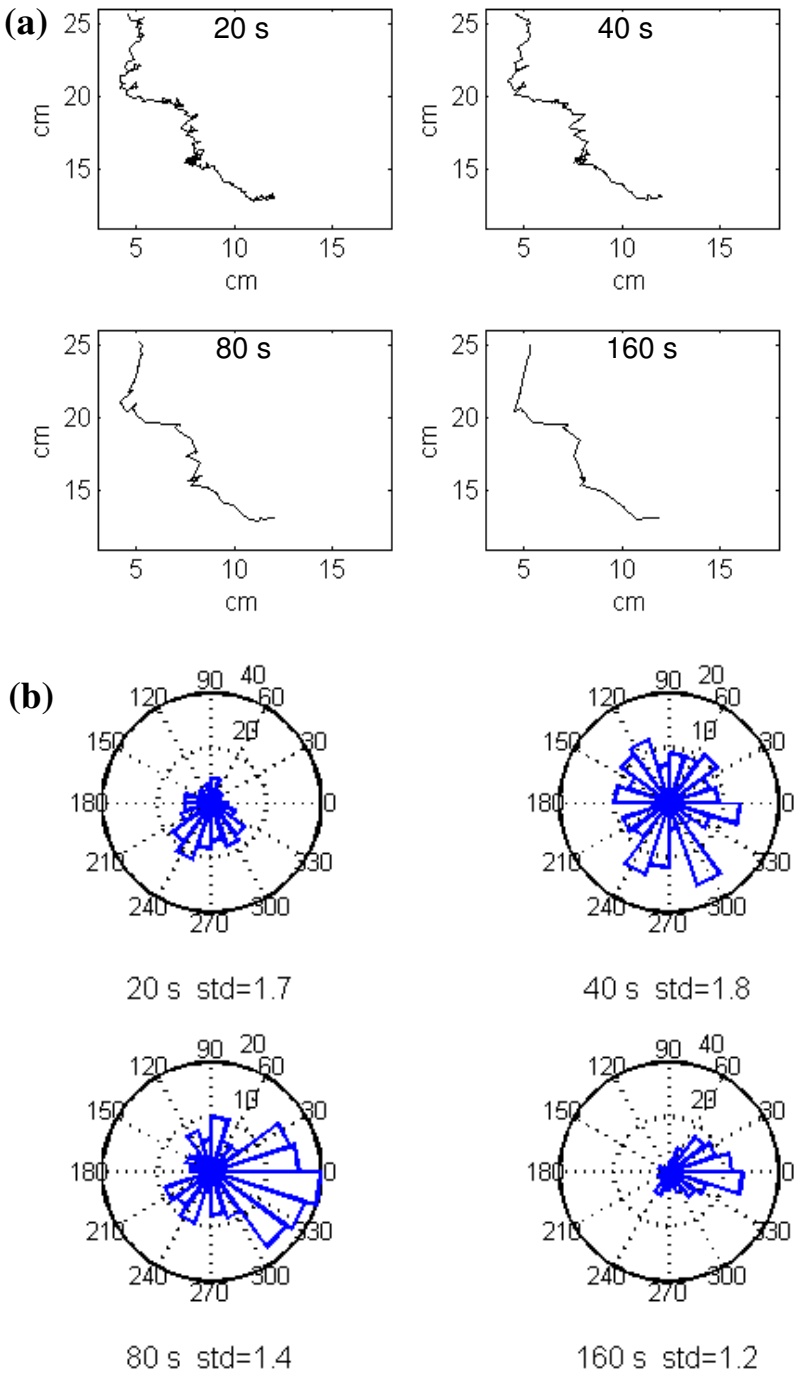

Fig. 11. Turning angles distribution upon coarse-graining (directional path, scanners setup). **(a)** Representative directional trajectory, sampled at 20 s, 40 s, 80 s and 160 s, respectively **(b)** Distribution of the angles between coarse-grained trajectory segments, obtained by sub-sampling the path 1 point every 20 s, 40 s, 80 s and 160s, respectively. See text for details. P-values *vs.* uniform, Kolmogorov-Smirnov test: 2 · 10-5 (20 s), 0.9 (40 s), 0.3 (80 s), 0.007 (160 s).

scales of coarse-graining we observe a fanning out of the turning angles distribution, whereas, at larger scales, that distribution displays a narrow, zero-centered profile. Directional paths acquired with the camera setup display analogous features, as shown in Fig. 12.

A distribution peak around zero simply indicates that different portions of the trajectories possess a similar orientation, and indeed this phenomenon is not observed for non-directional trajectories (Fig. 13 and Fig. 14, scanners and camera setup, respectively). More interesting is the result that the distribution flattens out at intermediate scales. This might indicate that the animals' local directional bias is "forgotten" on a relatively short time, and therefore suggests the intriguing possibility that long-range directional behavior might arise by a different mechanism than a step-by-step correlation between directions.

Scaling analysis

The distinct profiles of the turning angles distributions observed for different values of the coarse-graining scale prompted us to seek a description of the data that would account for the different degree of directionality exhibited by the paths at different scales. In thinking about possible methods to quantify the extent of convolution displayed by our trajectories, we were reminded of Mandelbrot's classic illustration of how to define the length of a coastline (Mandelbrot, 1967).

If the problem of measuring a coastline is approached by walking a yardstick of size δ along its length, it will be observed that the total length $L = N(\delta)\ \delta$, where $N(\delta)$ is the number of yardsticks of size δ that fit along the curve, increases without limit as δ is

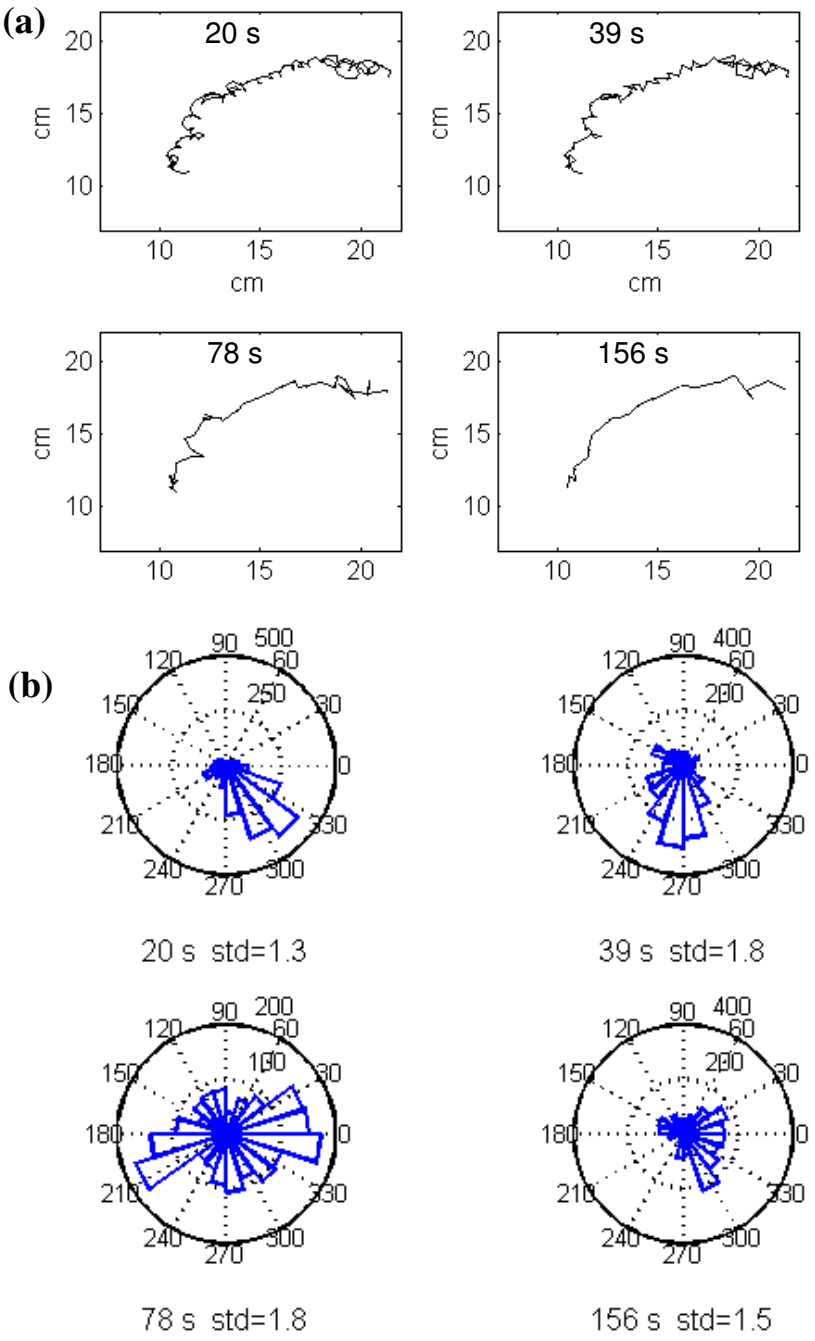

Fig. 12. Turning angles distribution upon coarse-graining (directional path, camera setup). **(a)** Representative directional trajectory, sampled at 20 s, ~40 s, ~80 s and ~160 s, respectively **(b)** Distribution of the angles between coarse-grained trajectory segments, obtained by sub-sampling the path 1 point every 20 s, ~40 s, ~80 s and ~160s, respectively. See text for details. P-values *vs.* uniform, Kolmogorov-Smirnov test: 10^{-133} (20 s), 10^{-77} (39 s), 10^{-12} (78 s), 10^{-19} (156 s).

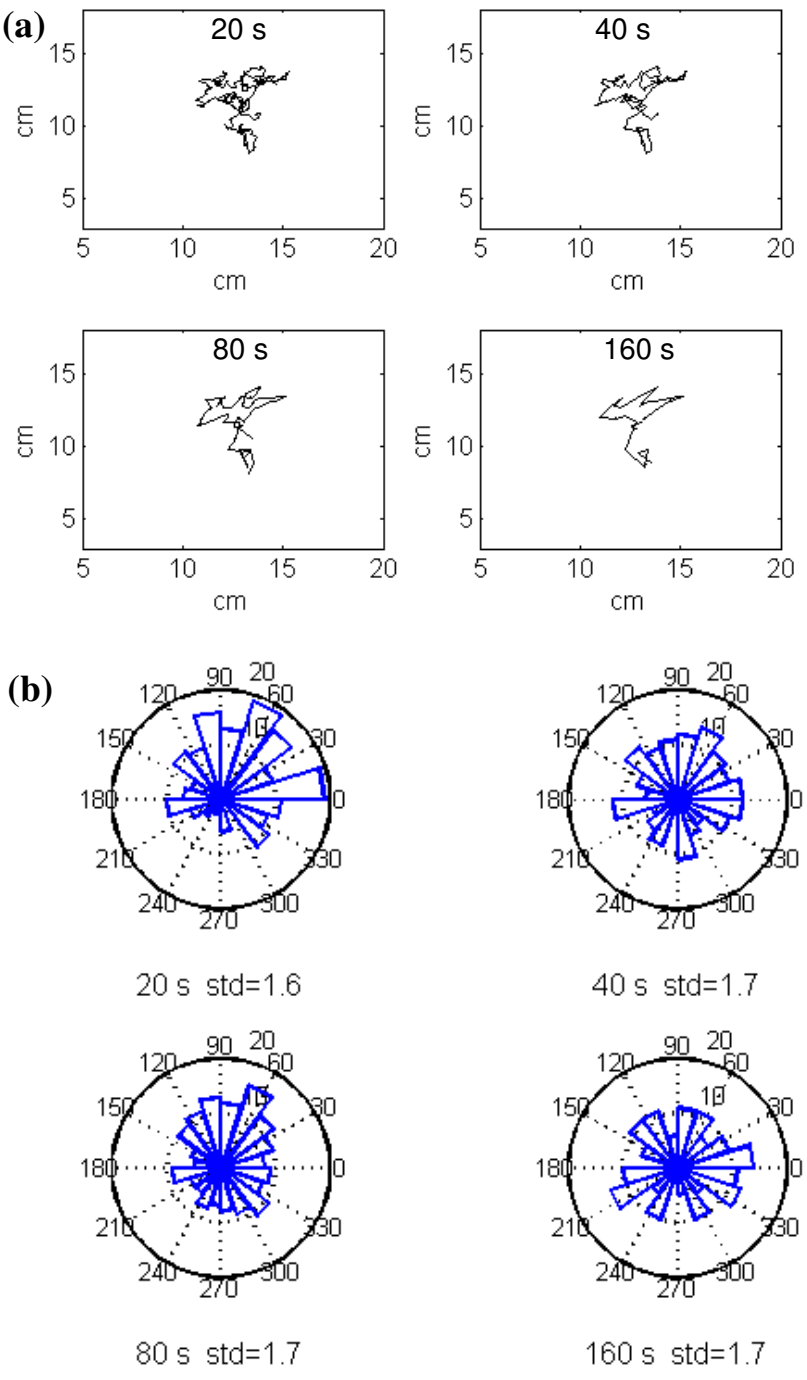

Fig. 13. Turning angles distribution upon coarse-graining (non-directional path, scanners setup). **(a)** Representative non-directional trajectory, sampled at 20 s, 40 s, 80 s and 160 s, respectively **(b)** Distribution of the angles between coarse-grained trajectory segments, obtained by sub-sampling the path 1 point every 20 s, 40 s, 80 s and 160s, respectively. See text for details. P-values *vs.* uniform, Kolmogorov-Smirnov test: 0.09 (20 s), 0.1 (40 s), 0.4 (80 s), 0.6 (160 s).

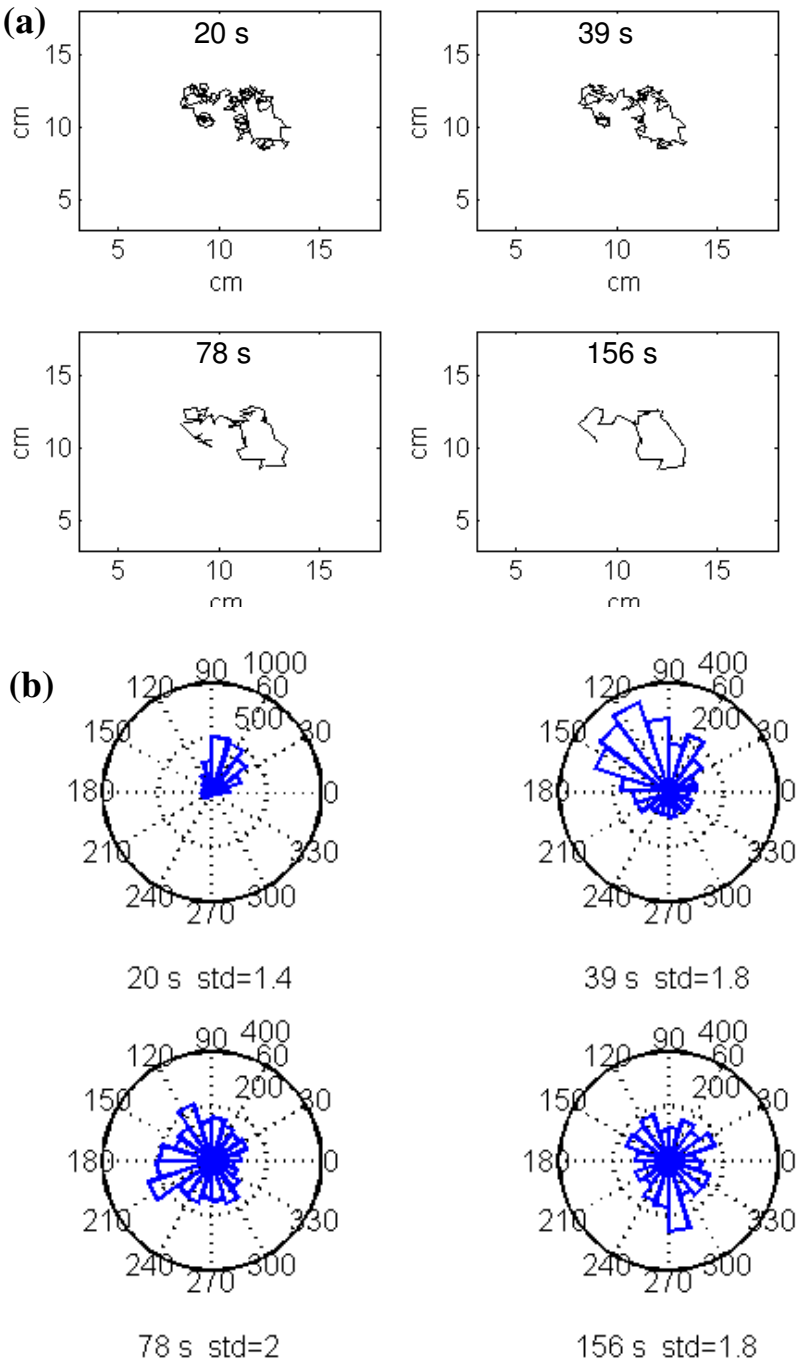

Fig. 14. Turning angles distribution upon coarse-graining (non-directional path, camera setup). **(a)** Representative non-directional trajectory, camera setup, sampled at ~20 s, ~40 s, 8~0 s and ~160 s, respectively **(b)** Distribution of the angles between coarse-grained trajectory segments, obtained by sub-sampling the path 1 point every ~20 s, ~40 s, ~80 s and ~160s, respectively. See text for details. P-values *vs.* uniform, Kolmogorov-Smirnov test: 10^{-173} (20 s), 10^{-76} (39 s), 10^{-6} (78 s), 0.04 (156 s).

decreased and more and more fine-grained features are taken into account (Fig. 15). Remarkably, however, the functional relation between the length of the curve, measured at a scale δ, and δ itself is a general property of the curve, and it is not affected by the adoption of a different measuring method. This relation can be expressed as $L \sim \delta^{1-D}$, where D is the fractal dimension of the curve (Mandelbrot, 1967). A curve's scaling properties yield, therefore, a better characterization than its ill-defined total length. Specifically, the slope of a log-log plot of the length versus the measurement scale provides an estimate of the curve's fractal dimension, a quantity that informs on the degree of space-filling of the trajectory. In particular, a straight line should have slope zero, since measurements of its length are not affected by the observation scale selected; whereas self-similar curves, a category which includes the random walk process, display same slope at all scales.

In analogy with this method, we investigated the scaling behavior of our experimental trajectories (Fig. 15). To that end, we sampled the trajectories in time by retaining one point every δ. We then defined the coarse-grained length of the path at the scale m by measuring the length of the broken line connecting the selected points. In order to minimize the dependence of the results on the choice of the initial condition, we averaged, for each value of δ, the coarse-grained lengths of all the trajectories obtained by varying the first sampled point between 1 and δ-1. Lastly, we normalized the coarse-grained length by taking its ratio to the total length of the curve, and plotted its behavior on a log-log plot against the coarse-graining scale δ.

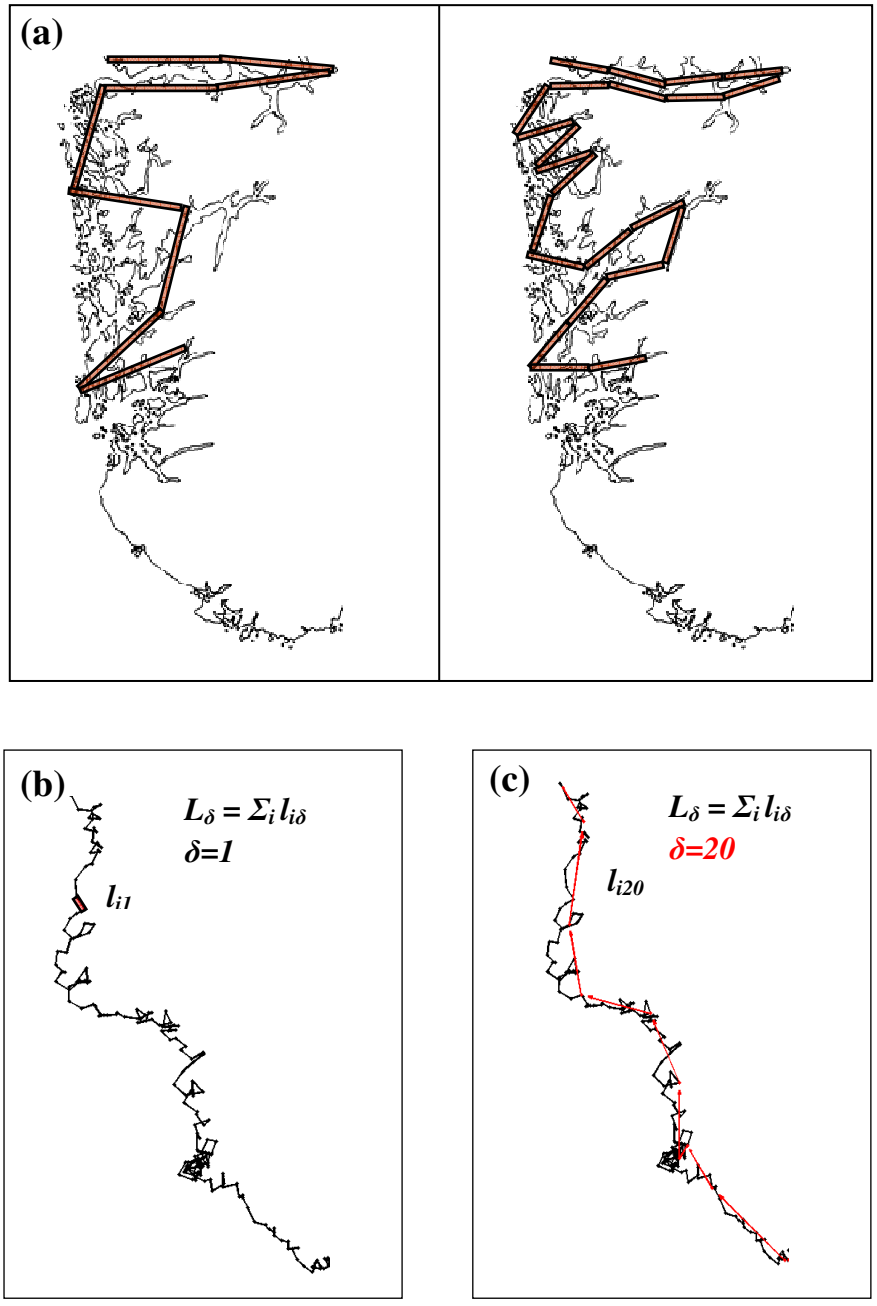

Fig. 15. Scaling analysis of coarse-grained path lengths. **(a)** Measurement of a coastline by the yardstick method (Mandelbrot, 1967). As the size of the yardstick decreases, more and more features are taken into account, and the length of the coastline increases. **(b)** The total length of a path, L_1, is defined as the sum of segments l_{i1} connecting the animal's position at all points. **(c)** The coarse-grained length of a path at a given scale δ, L_δ , is defined by sampling the path one point every δ and summing the segments $l_{i\delta}$ connecting such points.

The results obtained for a set of representative trajectories obtained with the scanners setup are shown in Figure 16. The scaling behavior of the paths' coarse-grained lengths is plotted, by comparison, together with that of a correlated random walk of same size; details on the random walk model and simulations are provided in the next section ("Quantifying directionality: synthetic trajectories"). Directional trajectories exhibit a markedly different behavior than that of a random walk. The slope of the plot flattens out at long times, reflecting the grossly linear behavior of the path once its fine-grained features have been sampled out. Indeed, the scaling behavior exhibited by distinct directional paths appears to only differ at small times, suggesting again that convoluted local behavior does not affect directionality at longer time scales. This result extends our observations on the distributions of coarse-grained turning angles, and provides an immediate visualization of the long-range coherence of a path.

Velocity Autocorrelation Function

As mentioned previously, the locomotion pattern of *C. elegans* is mostly constituted of forward motion, with occasional sharp changes in direction. We expect this to result, locally at least, in persistence in the animals' direction of motion, which would constitute a trivial explanation for the observed long-range bias in the animals' trajectories. Therefore, we sought to determine the timescale of the local directional bias by computing the autocorrelation function of the velocities for each individual trajectory. We define the velocity correlation function $f(\tau)$ for a given lag τ in the standard way, as the average, along the whole path, of the scalar product between the direction at frame i and the direction at frame $i+\tau$, minus a term representing the average velocity squared;

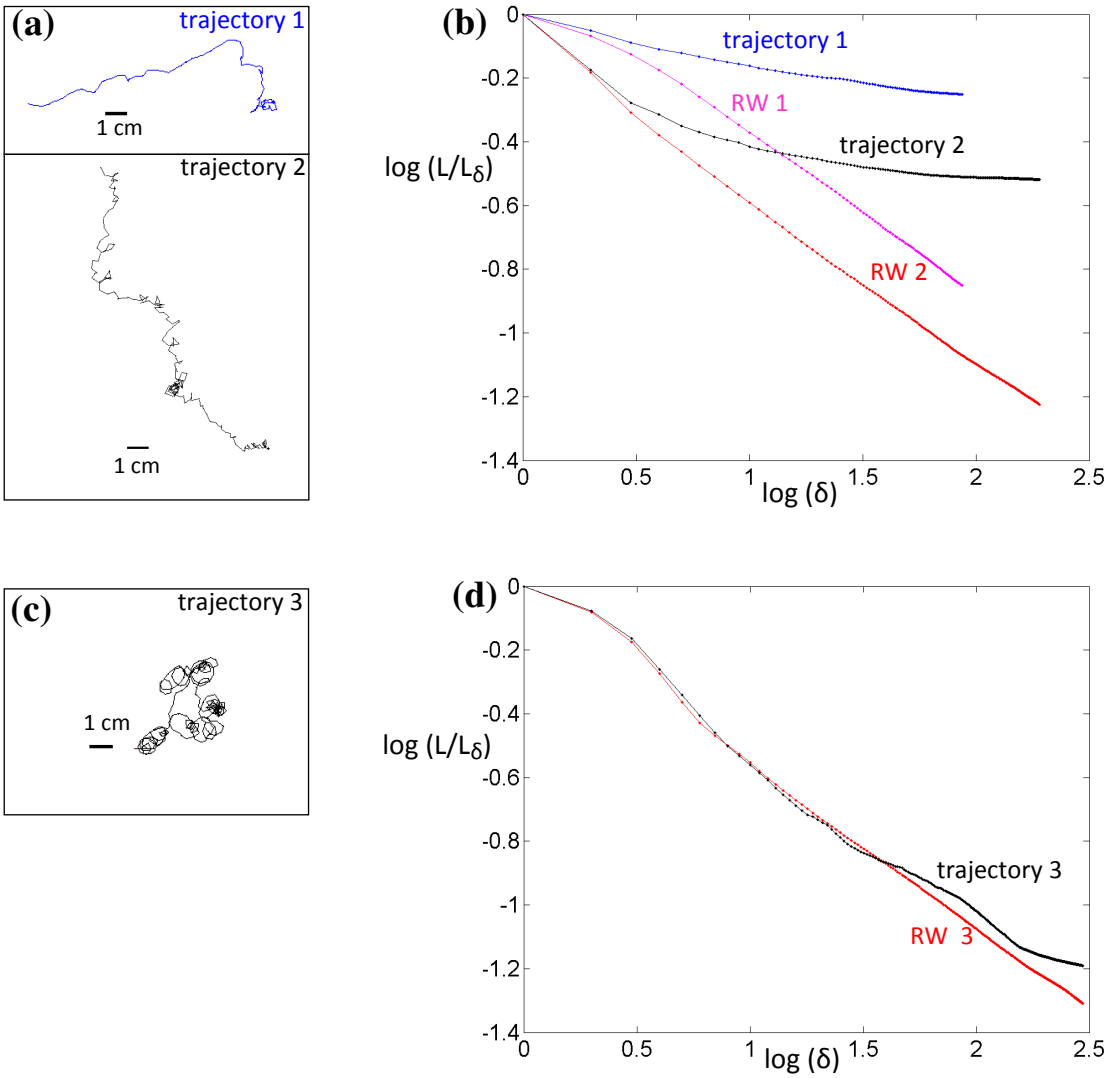

Fig. 16. Scaling behavior of coarse-grained lengths. **(a)** Directional trajectories, scanners setup. Top: "smooth" trajectory; bottom: "convoluted" trajectory. **(b)** Log-log plot of the scaling behavior of the coarse-grained normalized length versus the coarse-graining scale. Blue curve: scaling behavior for trajectory #1. Magenta curve: scaling behavior of a realization of a corresponding (correlated) random walk (RW 1). Black curve: scaling behavior for trajectory #2. Red curve: scaling behavior of a realization of a corresponding (correlated) random walk (RW 2). **(c)** Non-directional trajectory, scanners setup. **(d)** Log-log plot of the scaling behavior of the coarse-grained normalized length versus the coarse-graining scale. Black curve: scaling behavior for the trajectory in **(c)**. Red curve: scaling behavior of a realization of a corresponding (correlated) random walk (RW 3).

that is, $f(\tau) = \left(\frac{1}{n-\tau-1}\right)\sum_{i=1:n-\tau-1}\vec{u}(i+\tau)\cdot\vec{u}(i) - \left(\left(\frac{1}{n-1}\right)\sum_{i=1:n-1}\vec{u}(i)\right)^2$, where $\vec{u}(i) = \frac{\vec{x}(i+1)-\vec{x}(i)}{\left|\vec{x}(i+1)-\vec{x}(i)\right|}$ is the unitary velocity vector, obtained by subtracting the positional vector at time point *i* from the positional vector at the following time point.

We estimate the statistical error on *f(τ)* by sampling with replacement from the distribution of the dot products of $\vec{u}(i)$, $\vec{u}(i+\tau)$. A typical result for paths acquired with the camera setup is shown in Fig.17: the velocity correlation function displays an initial rapid decay followed by a regime in which its values oscillate around the zero. These oscillations suggest that the animals' looping and reversing behavior might be performed at a stereotypical frequency.

In fact, the autocorrelation signal, analyzed in the frequency domain, displays a peak for frequencies of ~ 0.005-0.01 Hz (shown Fig. 18 for one of the trajectories considered). Smoothing the path with a cubic spline interpolant results in a trajectory that is basically devoid of loops; interestingly, the velocity self-correlation of the smoothed path still oscillates at a similar frequency, indicating that the periodicity of the signal stems from the timing of loops or reversals initiation, rather than loop execution.

Surprisingly, the autocorrelation functions of directional paths display similar features as those of non-directional ones (Fig.17). This suggests that measures derived from this function, *e.g.* the timescale of the decay, will fail to accurately predict a path's long-range behavior. Indeed, if it is right to define the correlation time, for a given trajectory, as the time point where the autocorrelation function first decays to zero, it is found that more of

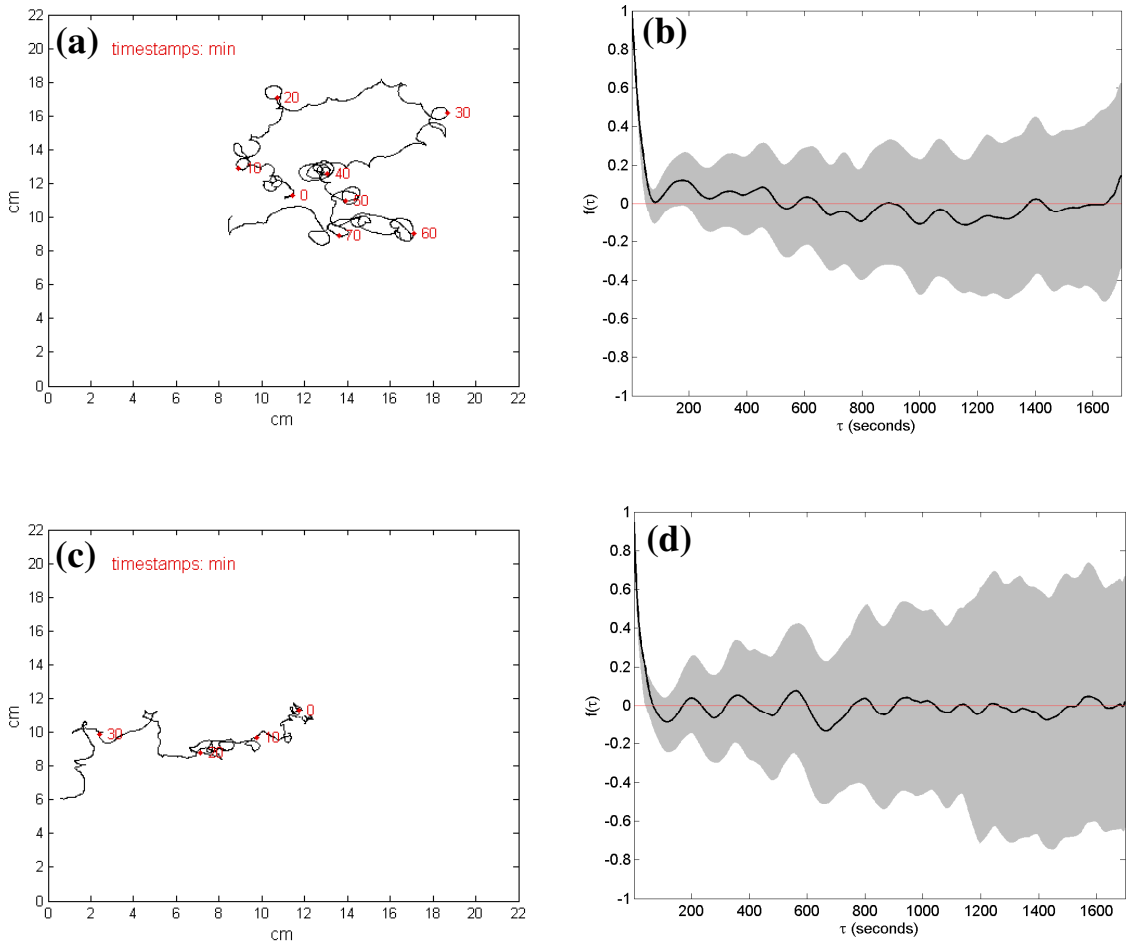

Fig. 17. Autocorrelation function of the velocities. **(a)** Non-directional trajectory, camera setup. **(b)** Corresponding autocorrelation of the velocities $f(\tau)$ as a function of the lag time τ. The signal was smoothed over a sliding time window of 50 points. Gray shading: autocorrelation +/- standard deviation, computed by sampling with replacement from the data. **(c)** Directional trajectory, camera setup. **(d)** Corresponding autocorrelation of the velocities. The signal was smoothed over a sliding time window of 50 points; the untreated signal is shown in Fig. 18. Gray shading: autocorrelation +/- standard deviation, computed as in **(b)**.

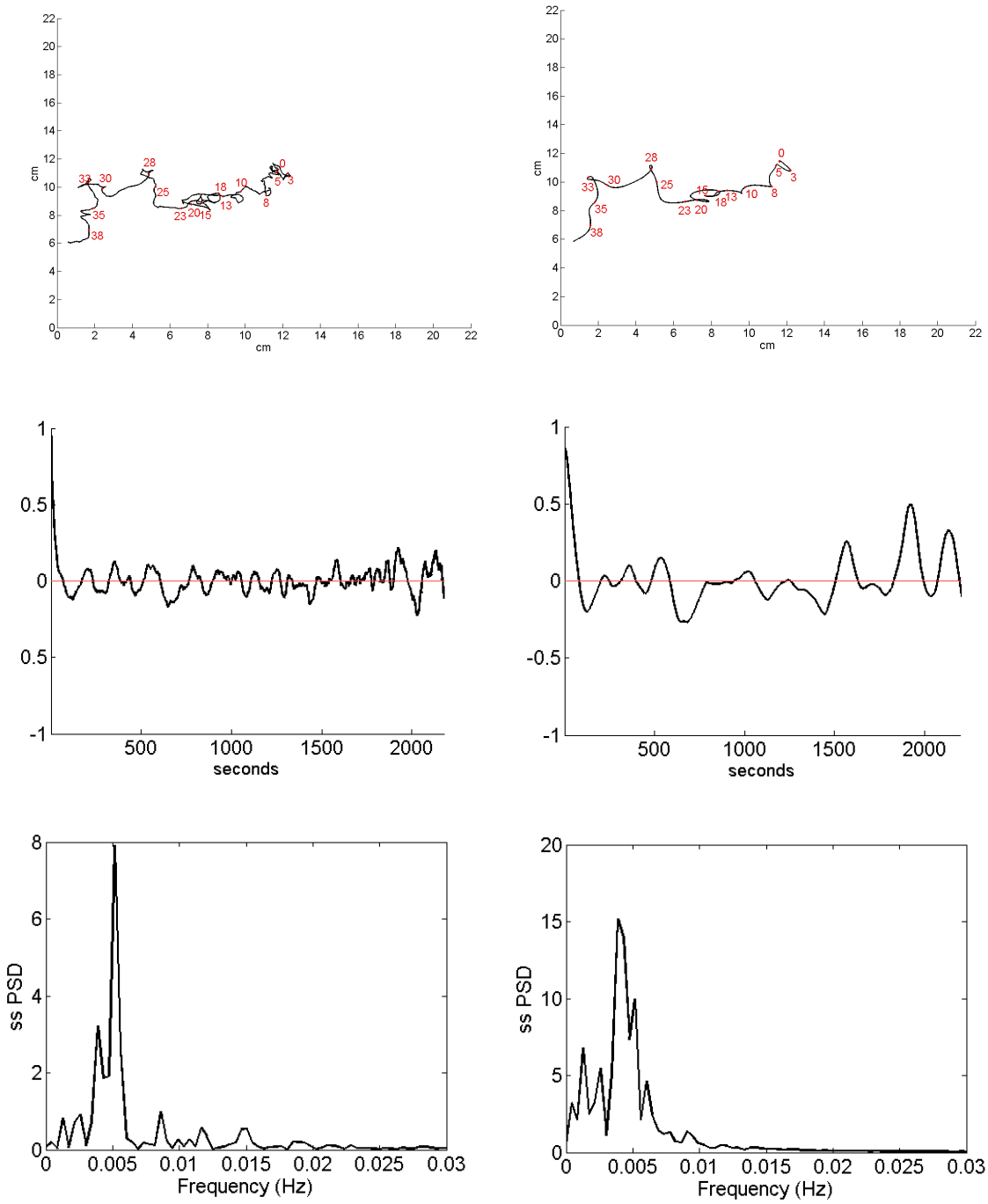

Fig. 18. Power spectral density of the velocity autocorrelation signal. **(a)** Camera trajectory. Timestamps, in red, are in minutes. **(b)** Camera trajectory, interpolated by a cubic spline. **(c)** Velocity self-correlation for the path in **(a)**. **(d)** Velocity self-correlation for the path in **(b)**. **(e)** Single-sided power spectral density plot for the signal in **(b)**. **(f)** Single-sided power spectral density plot for the signal in **(c)**.

80% of the paths acquired with the camera setup reset their direction of motion within 1-2 minutes; whereas directional persistence appears, at least qualitatively, to be maintained on scales of almost an order of magnitude larger. This observation hints at the same conclusion inferred from the behavior of the distributions of coarse-grained angles: both results seem to imply that directionality cannot be explained as a by-product of local persistence in the direction of motion.

Quantifying directionality: synthetic trajectories

In order to address the question of whether the animals' directed behavior could be accounted for by a random-walk model of locomotion, we compared the experimental trajectories to simulated, random trajectories ("synthetic trajectories"), which we built starting from individual experimental distributions of turning angles and speed. As a criterion of directionality, we adopted the probability of obtaining a larger or equal value than the experimental net displacement from random (Fig.19). We normalize this quantity by the number of steps in the path, so that the quantity computed corresponds to the effective speed of the animal over the total observation time.

By replacing, in our measure, the net displacement with the maximum distance between any two points of the path, we would obtain a parameter that is commonly utilized to define measures of a path's straightness, that is, the maximum linear distance covered by the path, d, divided by the path's total length L, d/L (Katz and George, 1985). However, the net displacement possesses the advantage over d/L of being a quantity whose behavior is well characterized for random walk processes.

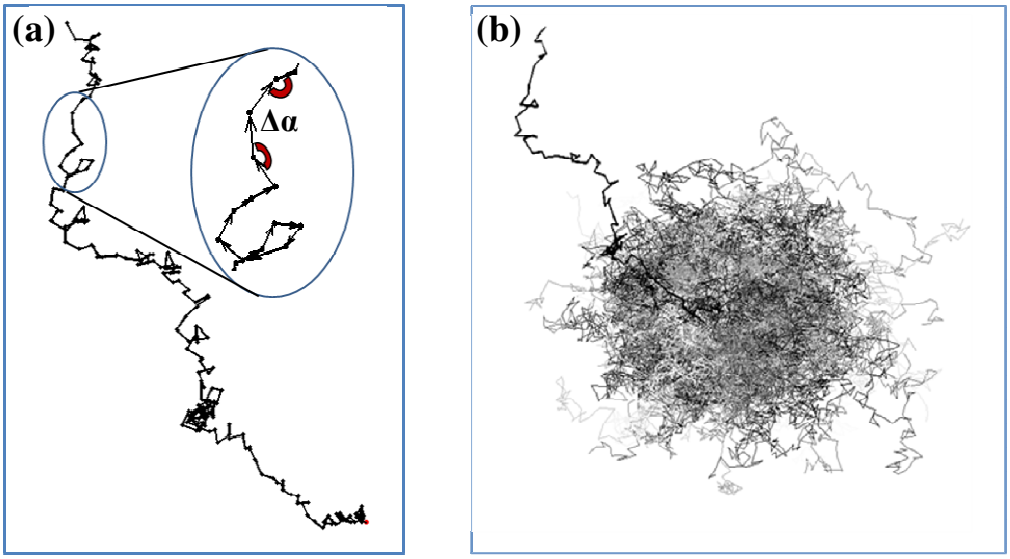

Fig. 19. Comparison of the data to a null model of random walk: synthetic trajectories. **(a)** Definition of turning angles Δα. Synthetic trajectories are built from data by drawing at each point from the distribution of speed and turning angles for a given path. We then compute the probability of obtaining, from an ensemble of synthetic paths, a larger net displacement than observed experimentally. **(b)** Visual depiction of the output of a set of simulations. Black: experimental trajectory. Gray: corresponding synthetic trajectories.

Computing the directionality index

The details of our simulations are as follows: histograms of the module and direction of the frame-to-frame displacements are computed for each trajectory. From those histograms, we obtain the distribution frequencies for both of those variables. We then generate synthetic frame-to-frame displacements by drawing random, independent pairs of values for the module of the displacement and its direction, respectively, at frequencies specified by the computed histograms. Finally, the resulting synthetic trajectory is constructed by adding together a number of displacements equal to the number of steps of the original trajectory.

To compute the likelihood of obtaining, from this specific model of stochastic motion, trajectories that travel as far in an interval T as the experimental one, we generated 50000 synthetic trajectories for each experimental trajectory. Remarkably, the distribution of the X- and Y- component of the synthetic end-to-end vector ($X = \sum_{i=1}^{n} v_x(i)$, $Y = \sum_{i=1}^{n} v_y(i)$, where $v_x(i)$ and $v_y(i)$ are the x- and y-component, respectively, of the synthetic velocity at the timepoint i), follows a Gaussian distribution, indicating that we are in the conditions of applicability of the central limit theorem, even though the directions of our null model are not randomly distributed (Fig. 20).

Because the distribution of the end-to-end vectors is known and is Gaussian, we can derive an explicit expression for the probability distribution of the synthetic net displacements. In fact, the normalized square of the net displacement, $d^2 = \frac{X^2}{\sigma_X{}^2} + \frac{Y^2}{\sigma_Y{}^2}$, is equal to the sum of the squares of two independently-distributed Gaussian variables,

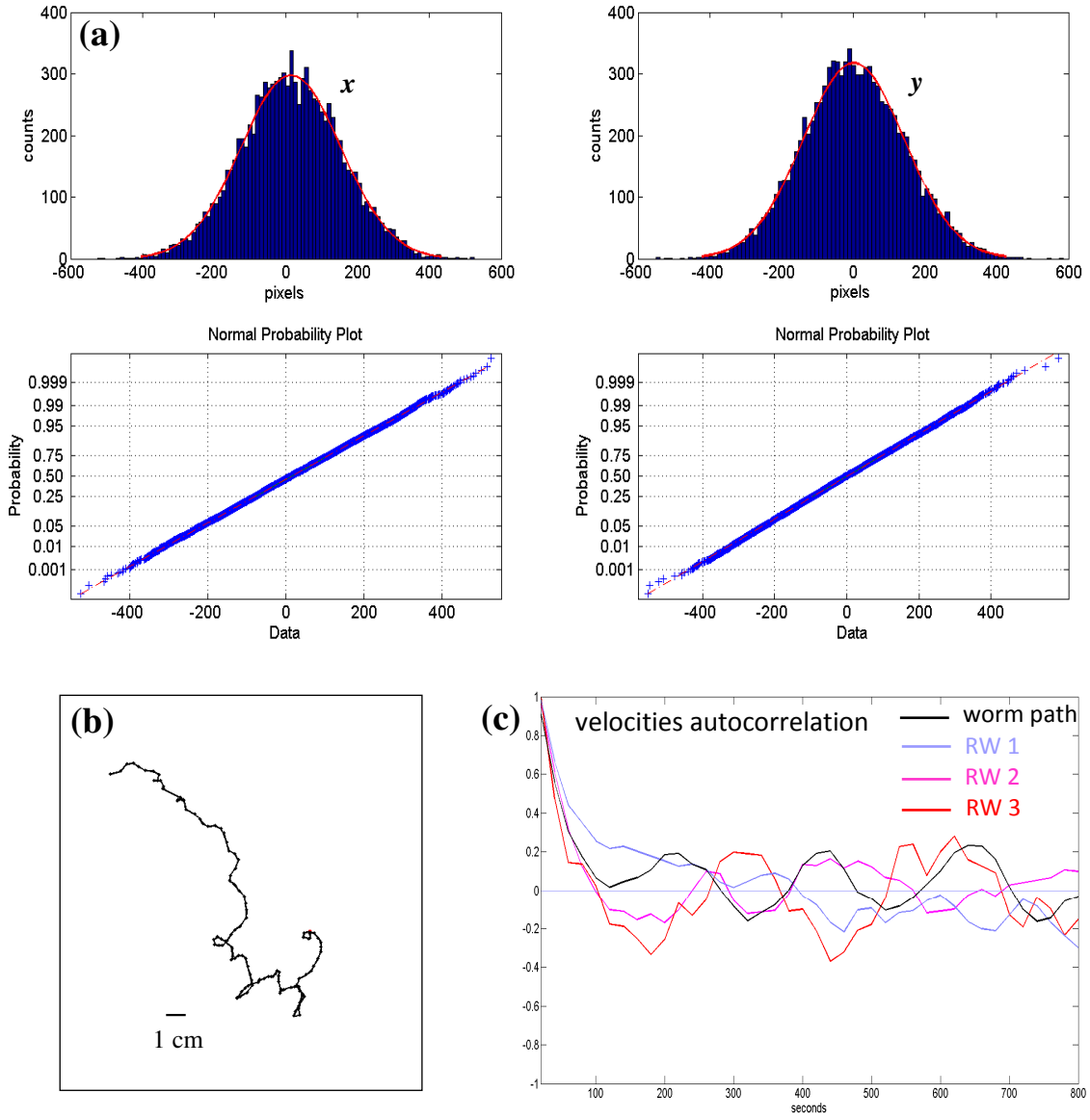

Fig. 20. Distribution of the synthetic end-to-end vectors, and autocorrelation function of synthetic velocities. **(a) top:** Distribution of the x- and y- components of the end-to-end synthetic vectors. **(a) bottom:** Normal probability plot of the x- and y- components, respectively, of the end-to-end synthetic vectors. The red line joins the first and third quartile of the data. A linear plot indicates a Gaussian probability distribution. **(b)** Sample trajectory, scanner-array setup. **(c)** Black curve: autocorrelation function of the velocities for the trajectory in **(b)**. Blue, red and magenta curves: autocorrelation function of the velocities for three corresponding synthetic trajectories.

and its probability density function is therefore a chi-square with two degrees of freedom (Abramowitz and Stegun, 1972). The chi-square cumulative distribution, evaluated for $d^2 = \tilde{d}^2$, where $\tilde{d}$ is the experimental net displacement for a given trajectory (normalized by its standard deviation), returns then the probability of observing from random a net displacement that is smaller than the experimental one.

The directionality index p is then simply derived from this quantity: $p = 1 - \chi^2(\tilde{d})$. In fact, by its definition, the directionality index corresponds to the p-value of rejecting the null hypothesis of our model of random walk. To compute it, it is necessary that the variances on X and Y be known; to that end, we make use of estimates of σ_x^2 and σ_y^2 obtained by fitting the distributions of X and Y to two Gaussians (the two variances are in fact the same, because of the rotational invariance of the null model). The analytical expression for p provides a consistency check for its value as computed, empirically, from the number of outliers obtained from simulation, and therefore a check for the validity of the algorithm.

Application to data

Here we expose the results of our analysis for the datasets obtained with both setups. Briefly, our directionality index corresponds to the probability of obtaining from random a larger effective speed (net displacement over number of steps) than the experimental value. This index is in fact equal to the p-value of rejecting the null model for the trajectory considered. Because the distributions span several order of magnitude, indices are displayed on a log scale, and ranked on the x axis from the smallest (*i.e.* more

directional) to the highest (less directional: an index of 1 means that any random trajectory will fare better than the experimental one).

The distribution of indices, or p-values, obtained for data is plotted for reference together with the distribution of p-values computed for a same-sized sample of synthetic trajectories. A coarse quantification of the overall directionality displayed by the whole population can be obtained by computing the percentage of p-values that are lower than an arbitrary threshold, which we fix at 0.05. This measure, however, fails to take into account the magnitude of the significant p-values. Alternatively, a population measure of directionality can be defined as the distance between the distribution of p-values for the data and that obtained from a sample of random walks. To measure the distance between the two distributions we make use of the previously described Kolmogorov-Smirnov statistics.

The results for the trajectory dataset obtained with the scanners setup are shown in Fig. 21. We estimate the variance on the dataset by sampling, with replacement, from the data. The variance on the random walk distribution is obtained by computing it over n random samples. The data shows a striking divergence from the null model ($pKS = 10^{-42}$), with probabilities of obtaining the most directional paths from the null model as small as 10^{-11}. 56% of the trajectories display directionality indices lower than our 0.05 threshold, versus the 5% that would be expected from random. Remarkably, synthetic trajectories retain some of the local directional persistence of the original path, as shown (Fig. 20) by the behavior of the autocorrelation function for an experimental trajectory and for three of its corresponding synthetic trajectories.

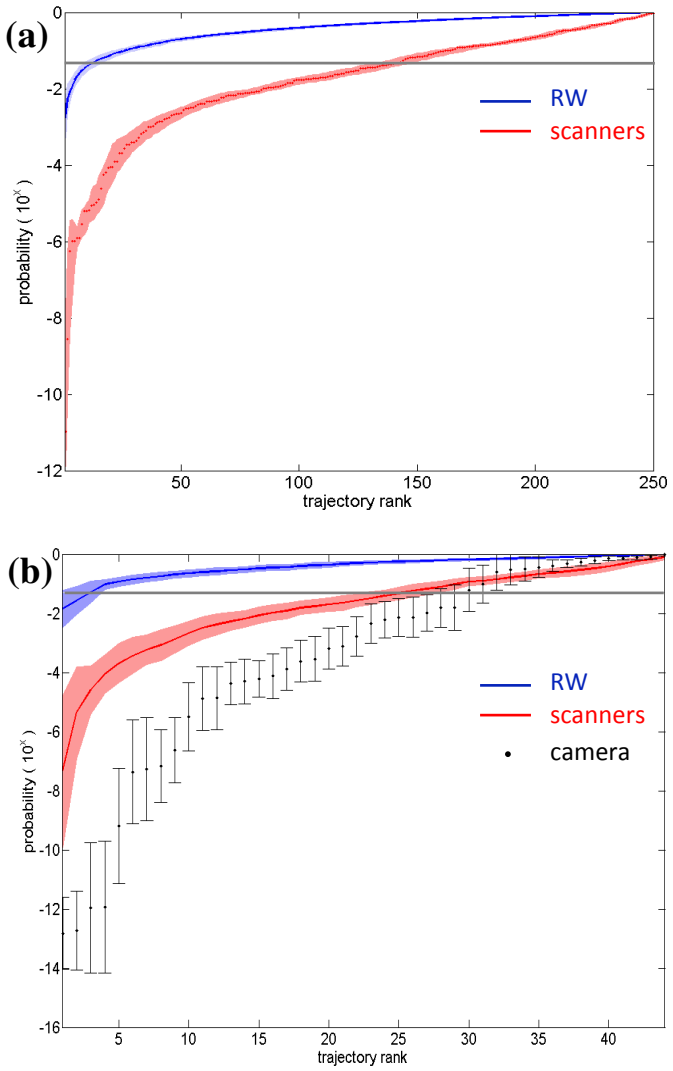

Fig. 21. Synthetic trajectories: results (1). **(a)** Directionality indices, scanners dataset. For a given path, the index equals the probability of obtaining from the null model a larger net displacement than the experimental. On the y axis, in log scale: directionality indices of individual paths. On the x axis: trajectory rank of paths sorted from the most to the least directional. Red dots: data. Red shading: one standard deviation (std) above and below the average, computed by re-sampling with replacement from the data. Blue curve: indices for the null model. Blue shading: one std above and below the null model average. P-value (Kolmogorov-Smirnov test): 10^{-42}. Gray line: p=0.05. 56% < 0.05 (n = 250). **(b)** Directionality indices, camera setup. Black dots: indices for the camera dataset. Error bar: one standard deviation. Red curve: average indices of a set of random subsamples of scanner trajectories. Red shading: one std above and below the scanner samples average. Blue curve: indices for the null model. Blue shading: one std above and below the null model average. P-value against the null model: $p = 10^{-9}$. P-value against the scanners average: $p = 0.01$. 65% < 0.05 ($n = 44$).

We reasoned that sampling of the paths at the estimated correlation time, and comparing the resulting trajectories to the null model, would provide a more accurate measure of directionality. Repeating the analysis on these "decorrelated" paths yields the same basic result: the behavior of the wild-type displays a highly significant divergence from that of our model of random walk (29% $p < 0.05$, $pKS = 10^{-11}$). The data obtained in the more homogeneous environment of the camera setup displays, reassuringly, the same directional behavior, as estimated by our directionality criterion. Figure 22 shows the distributions of directionality indices for both datasets, where the camera dataset was artificially sampled at the same temporal resolution as the scanners'. When considering the camera trajectories at their original resolution, the divergence from the null model is even more marked (Figure 21). This constitutes further evidence of a process with longer directional persistence than would be obtained from the null model.

As it is the case for the scanners dataset, repeating the analysis on trajectories sampled at the "decorrelation" time still results in significant directional behavior (29% $p < 0.05$, $pKS = 10^{-4}$) (Fig. 22). Remarkably, the distributions of directionality indices computed on re-sampled paths display a strikingly similar behavior ($pKS = 0.9$). This sampling procedure will therefore be employed throughout the next chapter.

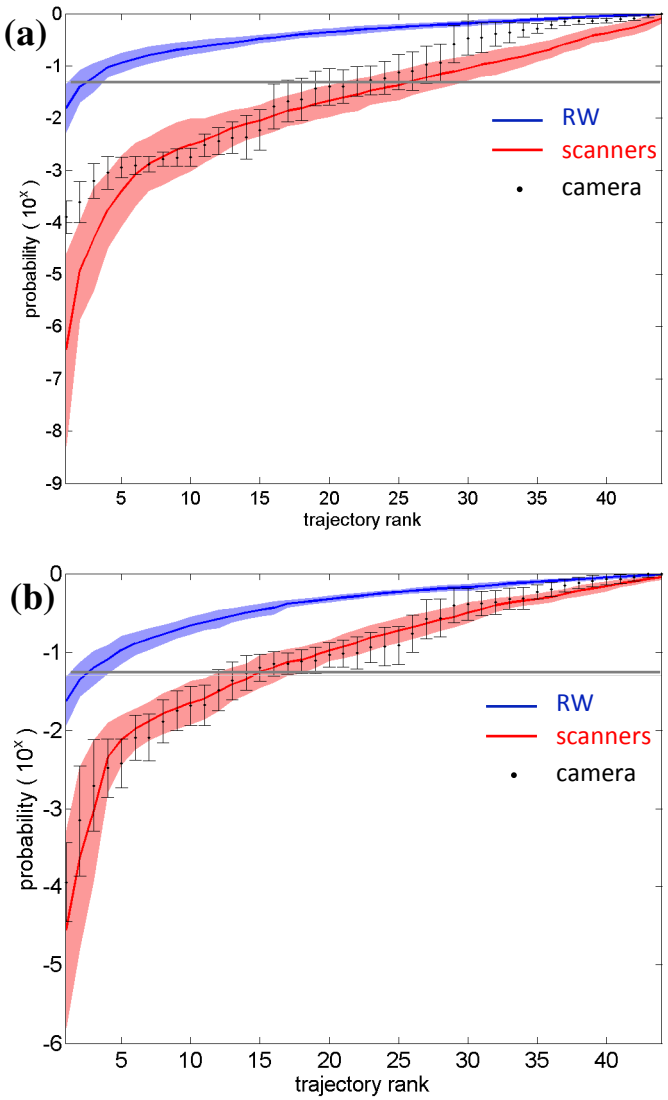

Fig. 22. Synthetic trajectories: results (2). **(a)** Directionality indices, camera setup. Paths were sub-sampled at the scanners' sampling rate (1 frame/20 seconds). Black dots: indices for the sub-sampled camera population. Error bars computed by re-sampling with replacement. Red curve: average directionality indices of a set of random subsamples of scanner paths. Red shading: one standard deviation (std) above and below the scanners subsamples average. Blue curve: indices for the null model. Blue shading: one std above and below the null model average. P-value against the null model: $p = 10^{-6}$. P-value against the scanners average: $p = 0.4$. 47% < 0.05 ($n = 44$). **(b)** Directionality indices of "decorrelated" paths, *i.e.* paths sub-sampled at their individual correlation time. Black dots, black error bars: camera data. Red curve: average indices for the scanners dataset. Blue curve: indices for the null model. Shadings: average +/- one std. P-value against the null model, camera data: $p = 10^{-4}$. P-value against the null model, scanners data: $p = 10^{-11}$ (29% p < 0.05). P-value against the scanners average, camera data: $p = 0.9$. 29% p < 0.05 ($n = 44$).

Mean squared displacements

Computation of the scaling exponent

The analysis method presented above suffers from several drawbacks. First of all, the net displacement is obtaining by measuring a single point of a trajectory starting from the origin, and therefore possesses noisy statistics. Because of this, we can only make an argument based on the behavior of its distribution across the whole population. Secondly, the expected value of the net displacement is well defined only over an ensemble of realizations of the random walk; for the single trajectory, the behavior of the displacement along the main axis of the walk can only be characterized relative to the displacement along the orthogonal axis (Rudnick and Gaspari, 1986). For this reason, our definition of directionality is constructed by reference to a null model of isotropic locomotion. However, this entails that the results obtained by this method are not model-independent; specifically, the behavior of the net displacement at long times is affected by the local properties of the walk, *i.e.* the existence of local directional persistence, or of correlations between the module and the direction of the velocity.

A more convenient quantity to distinguish between diffusive and directed motion is provided by the scaling exponent v of the mean squared displacements (MSD) with time. The mean square displacements ρ are defined as the average, over the trajectory, of the distance between a point at time t and a point an interval τ apart: $\rho(\tau) = \left\langle \left| \vec{r}(t+\tau) - \vec{r}(t) \right|^2 \right\rangle$. The behavior of the scaling exponent v of the MSD with τ, $\rho(\tau) \sim \tau^{v}$, has been well characterized for many isotropic models of stochastic motion. It is a well known result that for purely diffusive motion $v = 1$, due to the central limit

theorem, whereas naturally $\nu = 2$ for directed motion. Intermediate scaling exponents, as discussed in the Introduction, are to be expected asymptotically only for stochastic processes that display long-range or non-local correlations in the direction of motion.

We computed the mean square displacements for an individual path as an average over overlapping segments of the trajectory: $\rho(j) = \frac{1}{n-j}\sum_{i=1}^{n-j}(\vec{r}(i+j)-\vec{r}(i))^2$, where $\vec{r}(i)$ is the position of the animal at the instant $i\Delta T$. From this, we derive the scaling exponent by linear regression of the logarithm of the MSD against the logarithm of the lag time j. In order to take into account the larger statistical error associated with larger values of the lag time, we performed a weighted fit. To compute the weights, we consider that the error associated to the MSD at a given lag time j is proportional to the square root of n-j, where n is the total number of velocity vectors in the path. In doing so, we are assuming that the MSD calculated for overlapping lags are independent. Accordingly, we associate to each computed value of the log of the MSD, $\rho(j)$, a weight $w(j) = \frac{\rho(j)}{n-j}$.

Because the animals' motion displays some degree of local persistence, we expect that the scaling of the MSD at short times will display non-diffusive properties. In order to avoid a bias in our estimate of ν due to the contribution of correlated timescales, we introduce two cutoffs, t_1 and t_2, and fit the behavior of the plot at small times, $\tau < t_1$, as well as its "asymptotic" behavior at times $\tau > t_2$. We choose the first cutoff to be equal to the correlation time.

The choice of the second cutoff is more delicate, as we want to exclude from the fit the contribution of timescales that are too close to the crossover, but pushing the cutoff to

larger timescales results in diminished accuracy of the fit. To get insight into the dependency of the fit from an arbitrary choice of this parameter, we computed the scaling exponent for three distinct values of the cutoff, corresponding to two, three and five times the correlation time. These choices results in typical differences on our estimate of v of +/-0.1, which is in fact of the order of the estimated statistical error on the data, and thus does not affect our conclusions. We chose to fix the second cutoff at three times the correlation time.

Since the scaling exponents are estimated from finite size samples, they must be considered as random variables themselves. This entails that non-diffusive values of the scaling exponent might simply arise as a consequence of statistical fluctuations. In order to estimate the range of variation of v due to fluctuations, we computed the scaling exponents of the MSDs for an ensemble (N = 1000) of synthetic trajectories. From those we can evaluate the spread of the distribution around the expected, asymptotic value of 1. Similarly, we estimate the variance of the scaling exponent for the data by sampling with replacement from the distribution of the square displacements, and subsequently fitting the behavior of the recomputed MSDs.

Results

Shown in Figure (Fig. 23) is the characteristic behavior of a directional trajectory obtained with the camera setup. Directional trajectories obtained with the scanners display analogous behavior. We observe a divergence from diffusive scaling at both short times and times larger than our estimated correlation time. The scaling exponent at large times deviates by more than one standard deviation from the average scaling of a

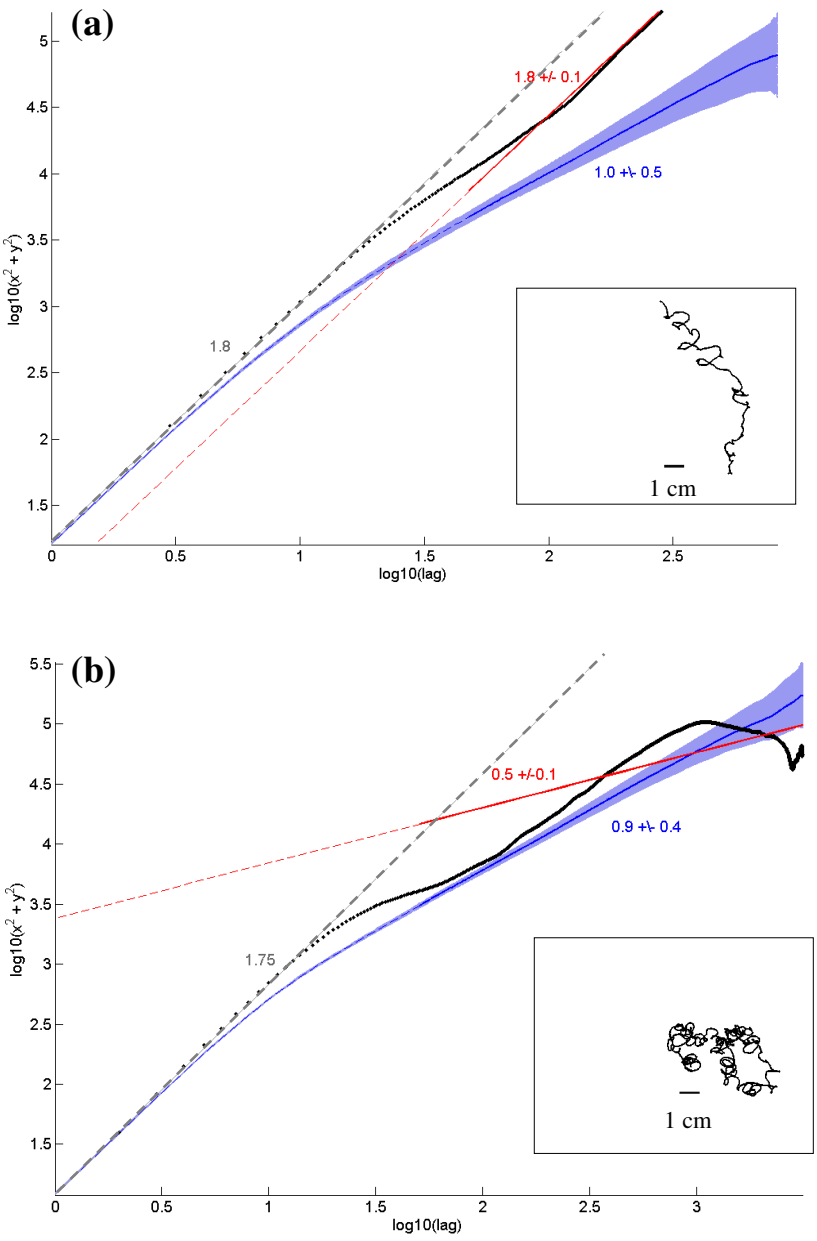

Fig. 23. Scaling of the mean square displacements with time for individual trajectories. **(a), (b)** Scaling of the mean square displacements for the trajectories shown in inset. Gray line: fit to times shorter than the correlation time. Red line: asymptotic fit (see text for details). Standard deviation computed by re-sampling of the data. Blue line: asymptotic fit to the null model. Blue shading: average mean square displacements for the null model +/- one standard deviation.

distribution of corresponding synthetic trajectories. This divergence is not displayed by the MSD of non-directional trajectories (Fig. 23). Interestingly, the behavior at intermediate timescales appears closer to diffusive than both the initial and the asymptotic behavior. This, in agreement with the results obtained by previously described methods, suggests again that the non-diffusive behavior observed at long timescales might not derive from local persistence in the direction of motion.

The behavior of the whole population can be examined by comparing the distribution of the scaling exponents for the totality of the dataset to the scaling exponents obtained from ensembles of corresponding synthetic trajectories. The distribution of scaling exponents for both setups is significantly shifted to larger values than that obtained from simulations of our model of correlated random walk (Fig. 24. Camera data: $< v > = 1.3$ +/-0.12 corresponding random walks: $< v > = 1.0$ +/-0.2. scanners data: $< v > = 1.3$+/-0.3; corresponding random walks: $< v > = 1.0$+/-0.3), again indicating that the worm's trajectories display a directional persistence that cannot be accounted for by this specific model of random walk.

Comparison to the random biased walk model

We sought to determine whether the directional bias displayed by the data could be explained in terms of the random biased walk model of *C. elegans* chemotaxis (Pierce-Shimomura et al., 1999). The basic prediction of the model is that the animal's direction in the instants preceding a turn will be anticorrelated with the sign of the concentration change of the attractant; in other words, turns are more likely to happen when the animal is climbing down the gradient. In order to test this hypothesis, we segmented

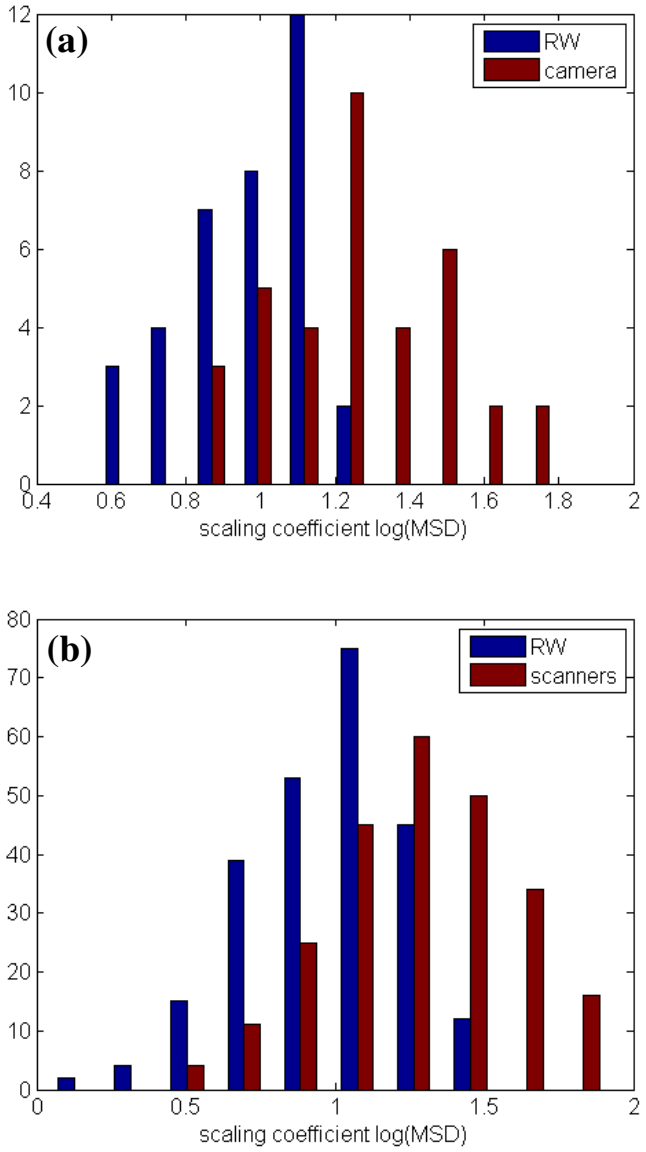

Fig. 24. Population distributions of the scaling exponents of the mean square displacements **(a)** Red: histogram of the scaling exponents v of the mean square displacements (MSD) for the camera dataset, computed by linear regression of the log of the MSD at long times. $\langle v \rangle$ = 1.3+/-0.2. Blue: histogram of the scaling exponents of the MSD of a same-sized set of synthetic trajectories. $\langle v \rangle$ = 1.0+/-0.2. P-value (Kolmogorov-Smirnov test): 10^{-7}. **(b)** Red: histogram of the scaling exponents v of the mean square displacements (MSD) for the scanners dataset, computed by linear regression of the log of the MSD at long times. $\langle v \rangle$ = 1.3+/-0.3. Blue: histogram of the scaling exponents of the MSD of a same-sized set of synthetic trajectories. $\langle v \rangle$ = 1.0+/-0.3. P-value (Kolmogorov-Smirnov test): 10^{-22}.

the trajectories obtained with the camera setup into “runs” and “turns”. Turns are defined by first identifying sharp changes in direction, as instances when the cosine of the turning angle between consecutive velocity vectors is smaller than a threshold value (which we set at 0.75). The segmentation procedure appears robust with respect to the choice of the threshold, since, at the acquisition rate of the camera setup, most sharp turns are larger than this cutoff. Sharp changes in direction are then assigned to a same turn if the time interval that separates them is smaller than a second threshold, set at 4.5 seconds. This clustering is motivated by the observation that, in *C. elegans*, reversals and omega bends are coupled to each other, and should therefore be considered as a single re-orientation event. The typical output of our segmentation algorithm is shown in Figure 25. In order to estimate concentration changes along the animal’s path, we posit the presence of a gradient whose direction we assume to be aligned with the average direction of the path (case 1), or to coincide in direction with the closest axis connecting the center of the plate to one of its edges (case 2). We then compute the sign of the concentration change *dC/dt* experienced by the animal at a given time-point as the sign of the cosine between the animal’s instantaneous direction and the direction of the gradient. Figure 25 shows, for two directional trajectories, a plot of the sign of *dC/dt* in the two cases considered, averaged over ~7 seconds before each turn, a time interval over which *dC/dt* displays negative values in chemotaxis assays (Pierce-Shimomura et al., 1999). The general result across the dataset is that in neither case is a correlation between turning events and negative sign of *dC/dt* observed, suggesting that the long-term directional persistence we observe might be achieved by a mechanism other than the modulation of turning frequency with direction.

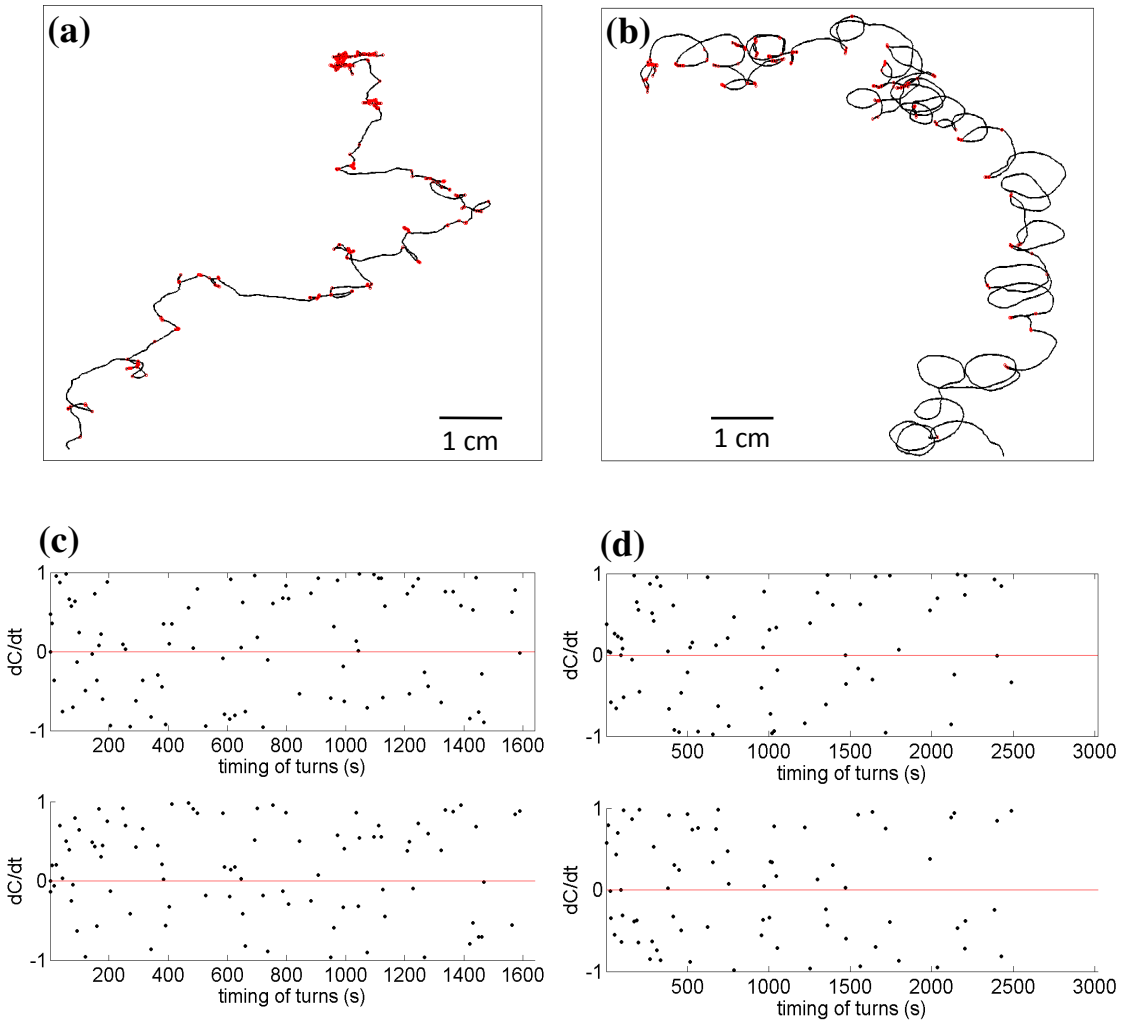

Fig. 25. Comparison to the random biased walk model. **(a), (b)** Directional trajectories. Sharp turns are marked by red dots. **(c), (d)** Scatter plot of the putative concentration change *dC/dt* experienced along the track in the instants preceding a turn, for every turn of the path shown in **(a)**. *dC/dt* was computed by assuming (top) a gradient aligned with the end-to-end vector of the path; (bottom) a gradient aligned with the closest axis connecting the center of the plate to one of its edges.

Redefining the null model: "mirror" trajectories

Both the scaling behavior of the mean square displacements and the results obtained for the net displacements of synthetic trajectories indicate that the directional bias displayed by the animals' trajectories cannot be accounted for by our model of random walk. However, as argued in more detail in Chapter 5, the model relies on a set of simplifying assumptions, such as that of the process being stationary, which, if relaxed, might alter the conclusions of our analysis.

To account for this possibility we redefined our null model so to preserve the exact local structure of the path. This approach has been suggested to us by Francis Corson. The model is defined as following: first, the trajectory is segmented into turns and intervening runs, as described in the previous section. Then, we construct a set of "mirror" trajectories, by flipping (with probability 1/2) the whole portion of the trajectory that is associated with a turn, for every single turn, and reassembling the different segments of the track (runs and turns) so that the directions at the ends of the segments coincide (Fig. 26). This procedure effectively reverses the direction change produced by the turn, while preserving local directional correlations as well as the temporal distribution of turns. We then compute, for the camera dataset, the probabilities of obtaining, from sets of synthetic "mirror" trajectories, equal or larger net displacements than those observed experimentally. Finally, we compare those probabilities to those that would be obtained for a set of realizations of the null model. The results of this analysis are presented in Figure 26. The data still displays significant divergence from the null model (40% $p < 0.05$, $pKS = 10^{-5}$), further strengthening our conclusion that local directional persistence does not account for the long-range directional bias we observe.

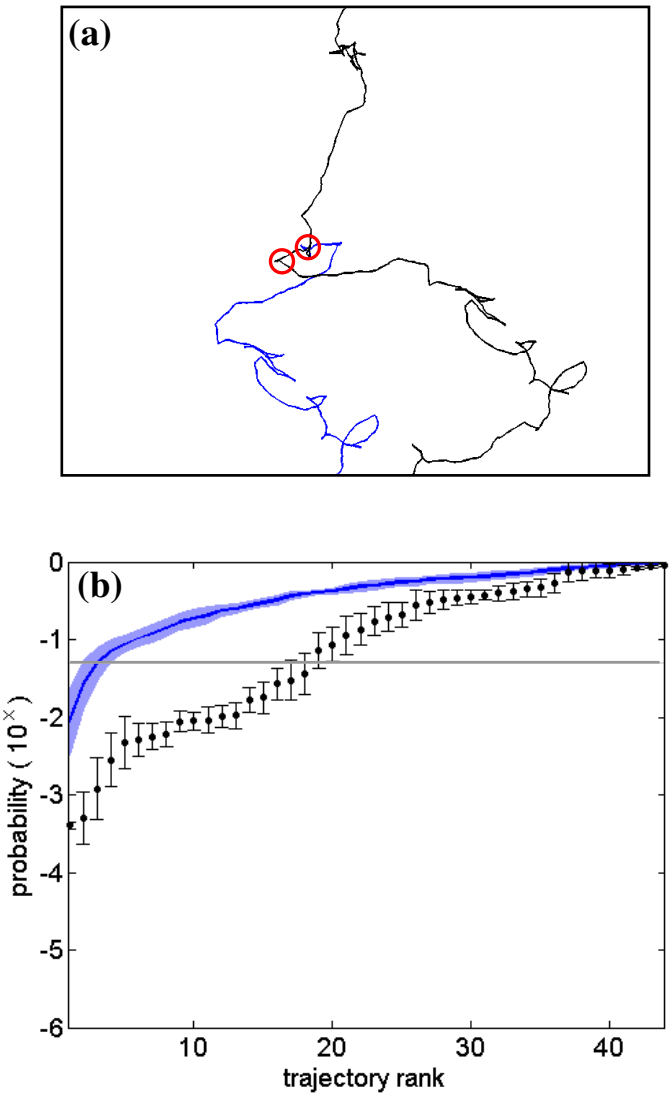

Fig. 26. "Mirror" trajectories. **(a)** Illustration of the "mirror" trajectory algorithm. The blue trajectory is obtained from the black one by reversing, with respect to the trajectory itself, the two episodes of turning highlighted in red. **(b)** Black dots, black error bars: camera data. Blue curve: directionality indices for the null model. Blue shading: average null model +/- one standard deviation. P-value against the null model, camera data: $p = 10^{-5}$. 40% $p < 0.05$ ($n = 44$).

Chapter 4. Role of sensory perception

In this chapter we address the question of the contribution of sensory perception to the animals' distinct mode of locomotion. Because the cellular basis of most of the animal's sensory capabilities is known, it is possible, to a certain extent, to target the function of a cell of interest, and to infer from that the nature of the external cue biasing the animals' motion, if any. We would like again to stress, however, that a requirement for sensory perception does not necessarily imply the presence of a biasing cue, as, in *C. elegans,* sensory function has been shown to be necessary for wild-type locomotory behavior even in homogeneous (Fujiwara et al., 2002) or featureless (Gray et al., 2005) environments.

While behavioral assays on the wild-type could be designed to address the hypothesis of an external biasing cue, we thought it practical to approach the question - with two exceptions that will be discussed below - by characterizing the behavior of specific mutants with impaired sensory function. Whereas a surgical approach, *i.e.*, laser-ablation of individual neurons, allows a specificity that is not afforded by genetic lesions (which generally affect more than a single cell), it requires nonetheless an initial lead on the identity of the neurons involved. A candidate-gene approach also presents the additional advantage, over laser-ablation studies, of a much greater number of animals that can be analyzed in a given day, which is of the essence when studying a phenotype that is defined in terms of its a distribution over a whole population. For the same reason all the results presented in this chapter were obtained from data collected with the scanners setup.

Table 1, in the Introduction, summarizes the known sensory repertoire of the worm and its cellular basis, which are reviewed in more detail in the same chapter. Briefly, *C. elegans* displays tactic, avoidance or escape behaviors in response to external cues such as chemical and mechanical stimuli, temperature, light and electric field; in addition to those, hermaphrodites are also repelled by their own constitutively-secreted dauer pheromone. We sought to characterize the behavior of mutants with impaired sensory function at three increasing levels of specificity: first, we analyzed the behavior of animals with general developmental defects, which result in impaired sensory function of all ciliated sensory neurons. Second, we investigated the behavioral effects of mutations in the cyclic-nucleotide gated channel *tax-4* and *tax-2*, as well as of mutations in the TRPV channel *osm-9*. These mutations are known to affect non-overlapping subsets of sensory modalities. Mutations in *tax-4*/*tax-2* resulted in the strongest behavioral phenotype, which prompted us to investigate the role of specific sensory modalities (*i.e.* chemosensation, thermosensation, oxygen sensation and sensation of light) by targeting the signal transduction machinery upstream of *tax-4*. At the same time, we sought to investigate the neural basis of the animals' directionality by performing cell-specific rescue of TAX-4 function.

Mutations that affect sensory morphology result in impaired directional behavior

Mutations that affect proper cilia formation disrupt nearly all sensory modalities, with the exception of thermosensation and of body mechanosensation (Culotti and Russell, 1978; Lewis and Hodgkin, 1977; Albert et al., 1981). Cilia might or might not be dispensable for aerotaxis, as one of the main neurons directing the aggregation phenotype of *npr-1,*

which is itself dependent on proper oxygen sensation, is the unciliated neuron URX (Coates and de Bono, 2002); however, aggregation and aerotaxis behaviors have also implicated the ciliated AQR and PQR neurons. The nematodes' response to light is known to require ciliated amphidial neurons, but experimental evidence pointing to a specific requirement for cilia has not yet been established (Liu et al., 2010; Ward et al., 2008).

The ciliary mutant *che-2* displays non-directional, confined tracks

Several genetic lesions specifically affect ciliary morphology and function (Culotti and Russell, 1978; Lewis and Hodgkin, 1977; Perkins et al., 1986). We have chosen to focus on the reference allele of the gene *che-2, e1033,* whose behavior has been characterized in many behavioral paradigms (see, for instance, Gray et al., 2005; Fujiwara et al., 2002). Chemotaxis of *che-2* mutant animals is not completely abolished, but displays indices that are a fraction than those of the wild-type (Bargmann et al., 1993).

We acquired a dataset of $n = 41$ trajectories of *che-2* mutants, which we assayed in the same conditions as the wild-type. For each trajectory in the dataset, we quantified directionality by computing the p-value of the animal's net displacement with reference to an ensemble of $N = 10000$ runs of synthetic trajectories, a method described in the previous chapter. The probabilities for the whole data set, plotted on a logarithmic scale, and ranked from the smallest (*i.e.* most directional) to the highest (*i.e.* most convoluted) are shown in Figure 27. The behavior of *che-2* is markedly less directional than that of the wild-type. While 29% of wild-type trajectories display probabilities that are lower than 0.05, this fraction is reduced to 7% in *che-2* mutants. Overall, the distribution of the

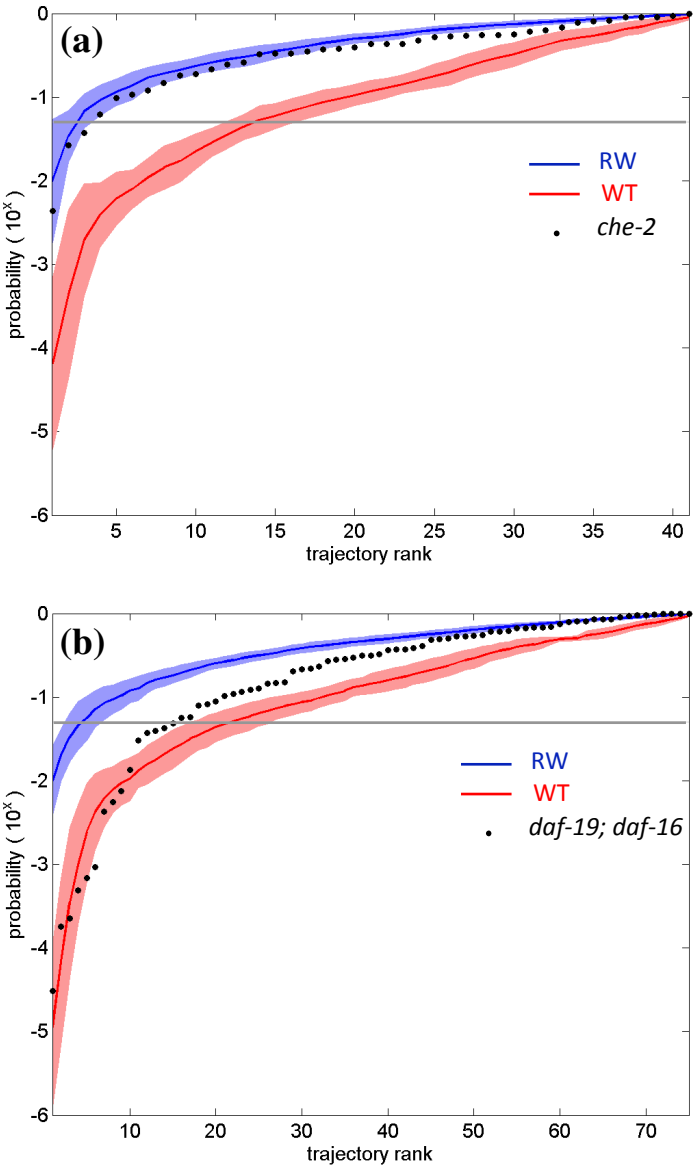

Fig. 27. Directionality indices of the ciliary mutants, *che-2* and *daf-19*. **(a)** Directionality indices *p* for a set of paths of *che-2* (*n* = 41). The index of a given path equals the probability of obtaining from the null model a larger net displacement than the experimental. On the y axis, in log scale: directionality indices of individual paths. On the x axis: trajectory rank of paths sorted from the most to the least directional. Black dots: *che-2*. Red curve: wild-type (WT). Red shading: average WT +/- one std. P-value (Kolmogorov-Smirnov test): 0.003. Blue curve: null model. Blue shading: average null model +/-one std. P-value (Kolmogorov-Smirnov test): 0.6. Gray line: p=0.05. 7% $p < 0.05$. **(b)** Directionality indices for *daf-19;daf-16* (*n* = 75). Black dots: *daf-19;daf-16*. Red curve: WT. Red shading: average WT +/- one std. P-value (Kolmogorov-Smirnov test): 0.02. Blue curve: null model. Blue shading: average null model +/-one std. P-value (Kolmogorov-Smirnov test): 0.04. Gray line: p=0.05. 20% $p < 0.05$.

directionality indices of *che-2* displays a significant divergence from that of wild-type, (p=0.003 by Kolmogorov-Smirnov), whereas by the same test it fails to show a significant divergence from our null-model of random walk.

An analysis of the fine features of *che-2* locomotion with the camera setup has not been performed; however, the paths of *che-2,* as acquired with the scanners, are conspicuously different from those of N2 (Fig. 28). Trajectories of *che-2* display overall net displacements ranging between 2 to 4 cm, as opposed to the 10+ cm characteristic of wild-type directional trajectories. In addition, *che-2* mutants move slower than N2 (mean speed = 0.08+/- 0.05 mm/s for *che-2*; mean speed = 0.13 +/- 0.05 mm/s for the wild-type); decreased speed, however, should not by itself account for diminished directionality, since our measure is computed with reference to a set of synthetic trajectories with analogous local properties as the experimental paths.

The *che-2* phenotype we observe is consistent with the "confined-tracks" phenotype previously established for this mutant by other researchers, both on- and off-food (Fujiwara et al., 2002; Gray et al., 2005). This has been interpreted as representing a constitutive "dwelling" state of the animal. In other words, animals with impaired sensory perception might display a "default" behavioral state that phenocopies the behavior of the wild-type on food. Following this interpretation, sensory function might be simply required to transition to a non-dwelling (*i.e.*, searching or dispersal) state. This is consistent with the known activation pattern of several sensory neurons, which display activity upon removal of a stimulus, rather than upon its presentation (Chalasani et al., 2010; Wakabayashi et al., 2004).

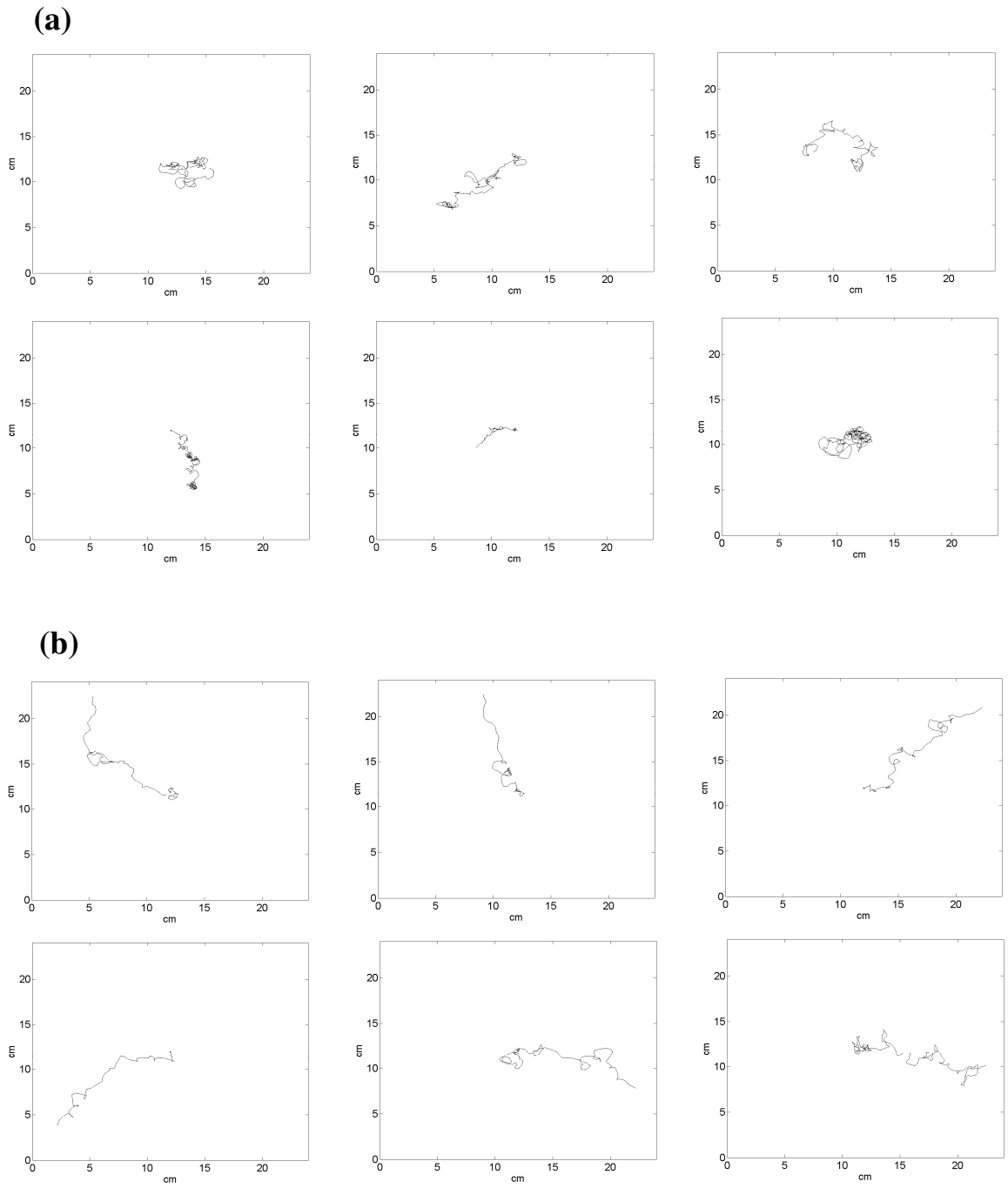

Fig. 28. Trajectories of *che-2* mutants. **(a)** Trajectories of *che-2* mutants, scanner-array setup. **(b)** Trajectories of the wild-type, scanner-array setup.

daf-19 mutants, which lack all cilia, display an incompletely penetrant phenotype

che-2 is a target of the RFX transcription factor *daf-19,* which transcriptionally activates a battery of genes involved in ciliary development. *daf-19* mutants generally display more severe phenotypes than mutants in any of its targets. In particular, mutations that affect a specific isoform of *daf-19* result in a complete absence of cilia (Perkins et al., 1986; Senti and Swoboda, 2008). The severity and penetrance of the morphological defect is also reflected at the behavioral level; in fact, mutations in *daf-19* result in complete suppression of chemotactic behavior (Cori Bargmann, pers. comm.).

daf-19 mutants are also dauer constitutive, displaying in that an opposite phenotype than that of *che-2,* or other cilia-defective genes. In order to perform assays on adult animals we utilized a strain double mutant for *daf-19* and for the FOXO transcription factor *daf-16*, which lies further downstream in the dauer formation pathway. Defects in *daf-16* by themselves are not expected to result in significant behavioral defects. The *daf-19* allele we employed in this study, *m86*, is a stop mutation within the protein's DNA binding domain.

We collected n=75 trajectories of *daf-19; daf-16* mutants. At a glance, most trajectories exhibit an obviously defective phenotype, reminiscent of that displayed by *che-2* mutants. Those trajectories are characterized by small overall displacements and tracks that are confined to a restricted area around the origin. Surprisingly, however, a subset of the population displayed markedly directional behavior. These outliers are enough in number to bias the distribution of the directionality indices, which we computed in the usual way. In fact, by the usual Kolmogorov-Smirnov statistics, the distribution for the

population appears to deviate significantly from both the wild-type one and our random one (Fig. 27).

It can be observed that the directional tail of the distribution (*i.e.* points ranked 1 to 10) overlaps with that of the wild-type; in contrast, the least directional points follow the distribution of the null model. At intermediate values of the directionality index, *daf-19; daf-16* animals display an intermediate phenotype between that of the wild-type and the null model. Overall, the mutant distribution exhibits residual directionality, and a less severe phenotype than that of its target gene *che-2* (20% $p<0.05$; *pKS* (vs. WT) = 0.02; *pKS* (vs. null model) = 0.04).

We reasoned that the directional and non-directional phenotypes displayed by distinct *daf-19* animals might correlate with the integrity of their neural architecture. In order to get an estimate of the penetrance of the ciliary defect for those animals, we performed a dye-filling assay. When nematodes are soaked in a lipophilic dye such as FITC or DiI, amphidial and phasmidial neurons fill with the dye and become visible under epi-fluorescence; dye-filling of sensory neurons is a good predictor of ciliary integrity (Perkins et al.,1986). Remarkably, no dye-filling animal was observed on the plate in a duplicate of the experiment (0%, WT = 100%, n~200 animals/assay).

To get further insight into the morphological integrity of the outliers, we performed transmission electron microscopy on two of these animals (Fig. 29, directionality indices $p = 0.04$, $p = 10^{-5}$ respectively) (EM performed by Yun Lu). Surprisingly, both animals displayed a complete lack of cilia in the amphidial region, suggesting the intriguing

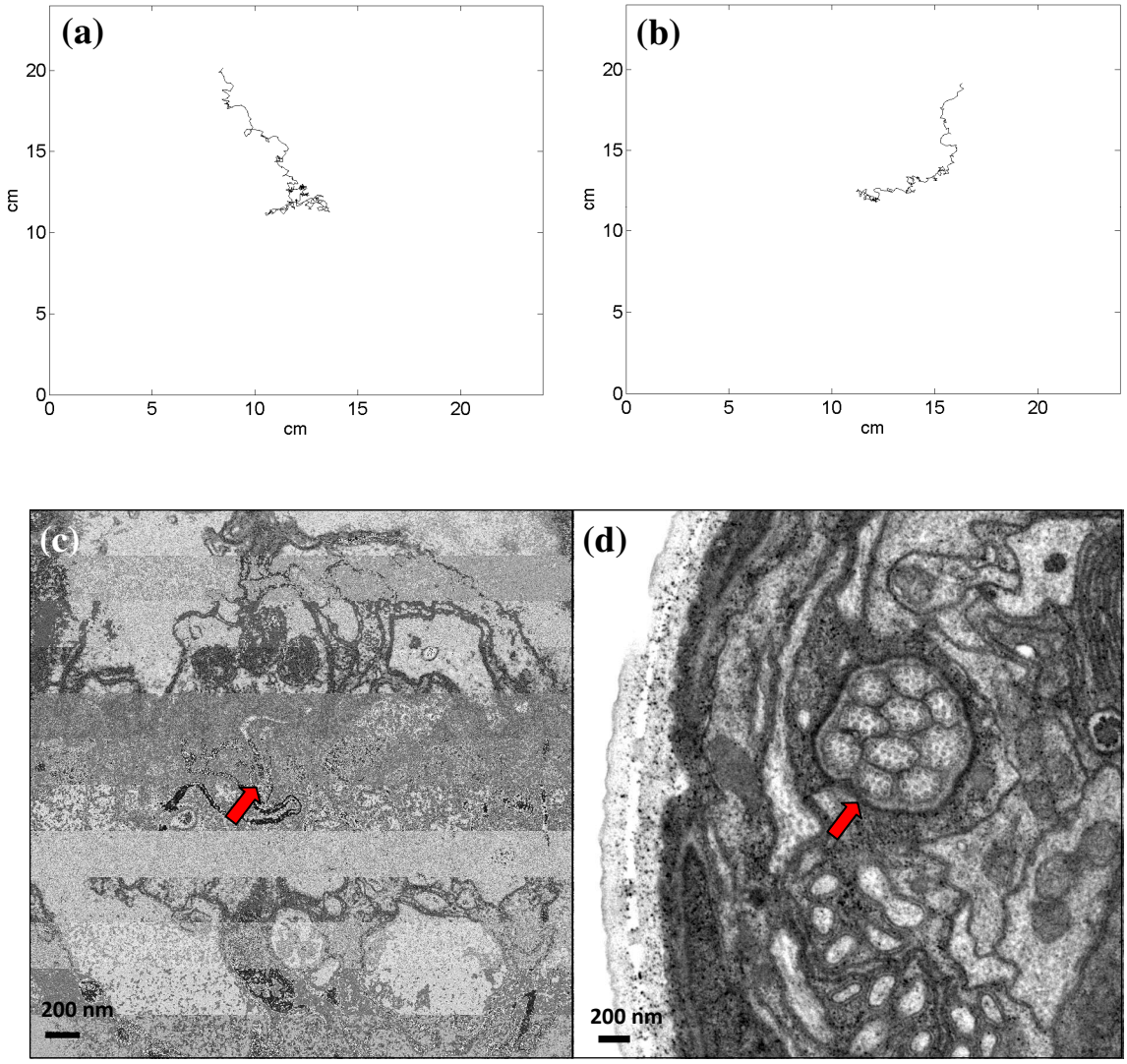

Fig. 29. EM micrograph of the amphid channel of *daf-19* mutants. **(a)**,**(b)** tracks of the two *daf-19;daf-16* mutants submitted for EM. Directionality index $p = 10^{-5}$, $p = 0.04$ respectively. **(c)** EM micrograph (detail) of a cross-section at the nose tip of the animal whose track is shown in **(a)**. Arrows point to the amphidial channel, which appears devoid of cilia. **(d)** EM micrograph (detail) of a cross-section at the nose tip of a wild-type adult animal (courtesy of Grigorios Oikonomou). Arrows point to the amphidial channel; cilia are visible within the channels. EM performed by Yun Lu.

possibility that, at least in this mutant background, ciliary function might be dispensable for directional behavior.

Specific mutations in signal transduction channels disrupt directional behavior

The cGMP channel *tax-4/tax-2* is required for directional behavior

As discussed before, the *che*-2 results are of difficult interpretation. We sought to gain further insight into the role of sensory function by investigating the behavior of the neural activity mutants, *tax-4*/*tax-2*, and *osm-9*. *tax-4* and *tax-2* are coexpressed in most amphidial neurons (with the exception of AWA, ADF, ADL, ASH), as well as in the oxygen-sensing cells BAG, URX, AQR and PQR; mutations in those genes result in impaired chemotaxis, thermotaxis, aerotaxis and phototaxis. We assayed the behavior of the reference allele of *tax-4*, *p678*, which results in premature truncation of the protein; concurrently, we investigated the behavior of the *ks28* allele, which results in more pronounced behavioral defects than the reference allele (Komatsu et al., 1996). For *tax-2*, the reference allele p691 was utilized. A dataset of $n = 43$ trajectories for *tax-4 (p678)* yields the following results (Fig. 30). The distribution of directionality indices cannot be distinguished, statistically, from that obtained from the null model, and displays a significant divergence from wild-type behavior (11% $p<0.05$, *pKS* (vs. WT) = 0.02; *pKS* (vs. null model) = 0.9). Similar results were obtained for *tax-4(ks28)* and *tax-2(p691)* (*tax-4(ks28)*: 8% $p<0.05$, *pKS* (vs. WT) = 0.006; *pKS* (vs. null model) = 0.9; *tax-2(p691)*: 0% $p<0.05$, *pKS* (vs. WT) = 0.01; *pKS* (vs. null model) = 0.3) (Fig. 30). An analysis of the tracks displayed by *tax-4(p678)* reveals that this mutant does not phenocopy the behavior of *che-2* mutants; in fact, the paths of *tax-4* mutants appear to display longer

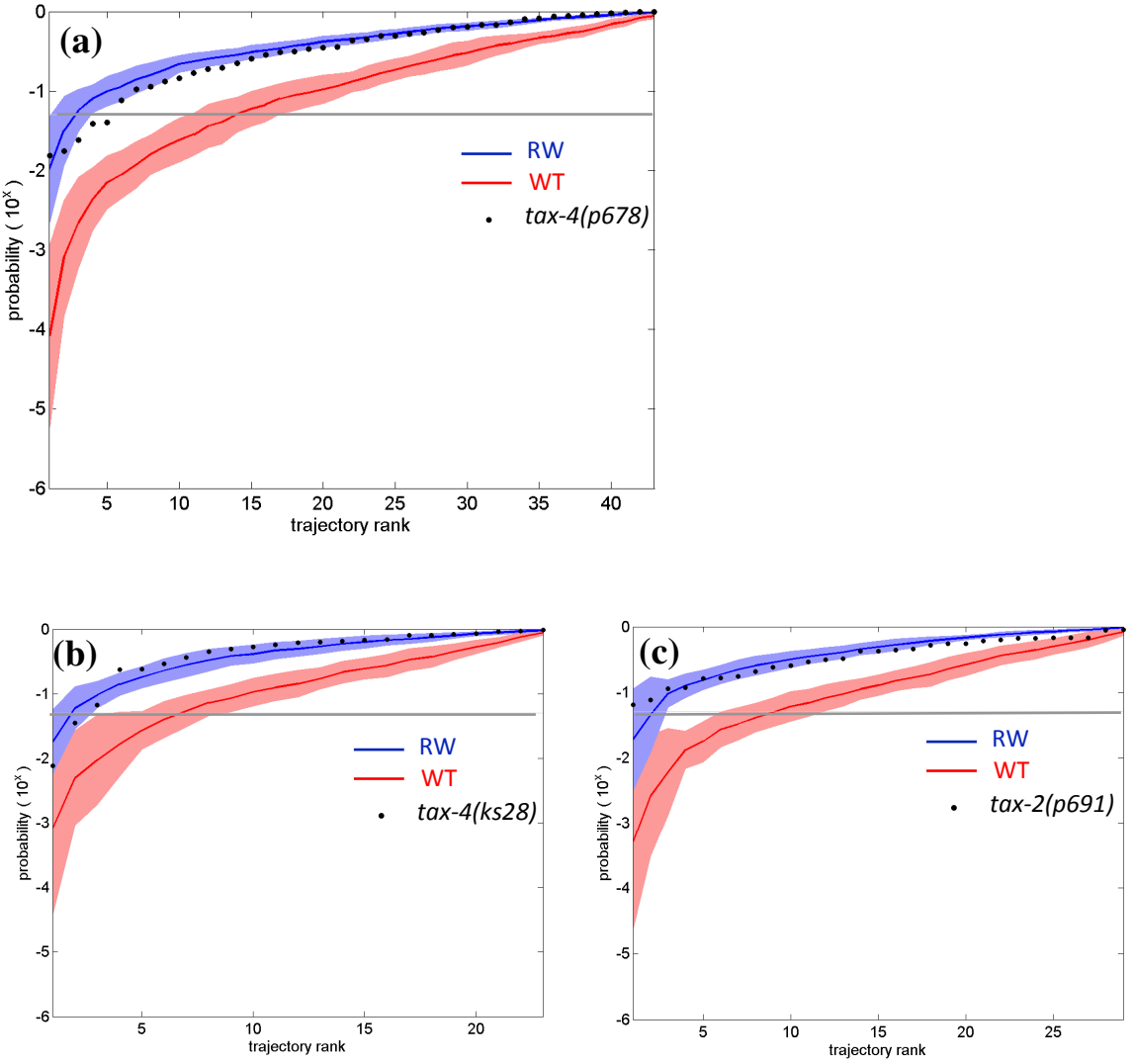

Fig. 30. Directionality indices of *tax-4/tax-2* mutants. **(a)** Black dots: *tax-4(p768)*. Red curve: wild-type (WT). Red shading: average WT +/- one std. P-value (Kolmogorov-Smirnov test): 0.02. Blue curve: null model. Blue shading: average null model +/-one std. P-value (Kolmogorov-Smirnov test): 0.9. Gray line: p=0.05. 11% $p < 0.05$ (n = 43). **(b)** Black dots: *tax-4(ks28)*. Red curve: WT. Red shading: average WT +/- one std. P-value (Kolmogorov-Smirnov test): 0.006. Blue curve: null model. Blue shading: average null model +/-one std. P-value (Kolmogorov-Smirnov test): 0.9. Gray line: p=0.05. 8% $p < 0.05$ (n = 23). **(c)** Black dots: *tax-2(p691)*. Red curve: WT. Red shading: average WT +/- one std. P-value (Kolmogorov-Smirnov test): 0.01. Blue curve: null model. Blue shading: average null model +/-one std. P-value (Kolmogorov-Smirnov test): 0.3. Gray line: p=0.05. 0% $p < 0.05$ (n = 29).

excursions than those of *che-2* (Fig. 31). As opposed to *che-2*, *tax-4* mutants also display a distribution of speed that resembles that of the wild-type (average speed = 0.1+/-0.1 mm/s). The non-directional behavior exhibited by *tax-4* mutants might then result from the more convoluted structure of those trajectories, as compared those of the wild-type, suggesting that TAX-4 loss-of-function might be targeting specifically the worm's mechanism for behavioral persistence.

Mutations in the TRPV channel *osm-9* do not affect directional behavior

The AWA, ADF, ADL and ASH neurons, in the amphids, and the PHA and PHB neurons of the phasmids signal through the opening of a different ion channel, a TRPV channel encoded by the gene *osm-9*. Mutations in *osm-9* target most of the animals' known responses to repulsive stimuli, with the exception of AWB-mediated avoidance to some odors, and of harsh body touch, which is sensed by mechanosensory neurons that innervate the animal's body (Colbert et al., 1997; Tobin et al., 2002). We sought to investigate whether the activity of OSM-9-expressing neurons was required for directional behavior. Assays were performed with the *ky10* allele of *osm-9* (Colbert et al., 1997). The results obtained for a dataset of n = 35 trajectories are shown Fig. 32. The distribution appears to taper off at smaller values of the directionality index than the wild-type; nonetheless, *osm-9* mutants do not exhibit a significant non-directional phenotype (25% $p<0.05$, *pKS* (vs. WT) = 0.9; *pKS* (vs. null model) = 0.0008). This result and the *tax-4/tax-2* results, taken together, suggest that non-AWB mediated nociception might be dispensable for the behavior, and point to a specific requirement for cyclic-GMP signaling in maintaining long-term directionality.

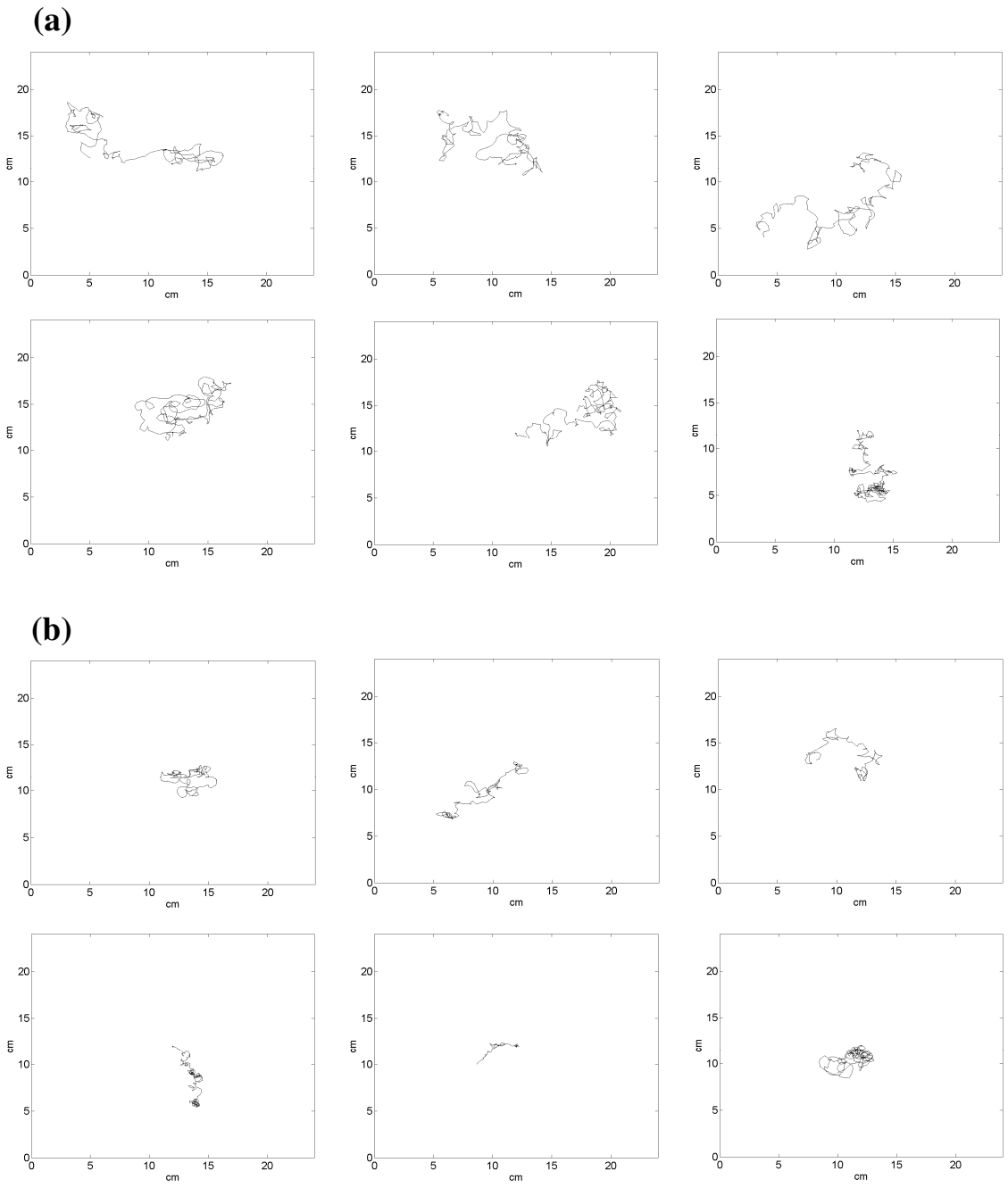

Fig. 31. Trajectories of *tax-4* and of *che-2* mutants. **(a)** Trajectories of *tax-4(p678)* mutants, scanner-array setup. **(b)** Trajectories of *che-2* mutants, scanner-array setup.

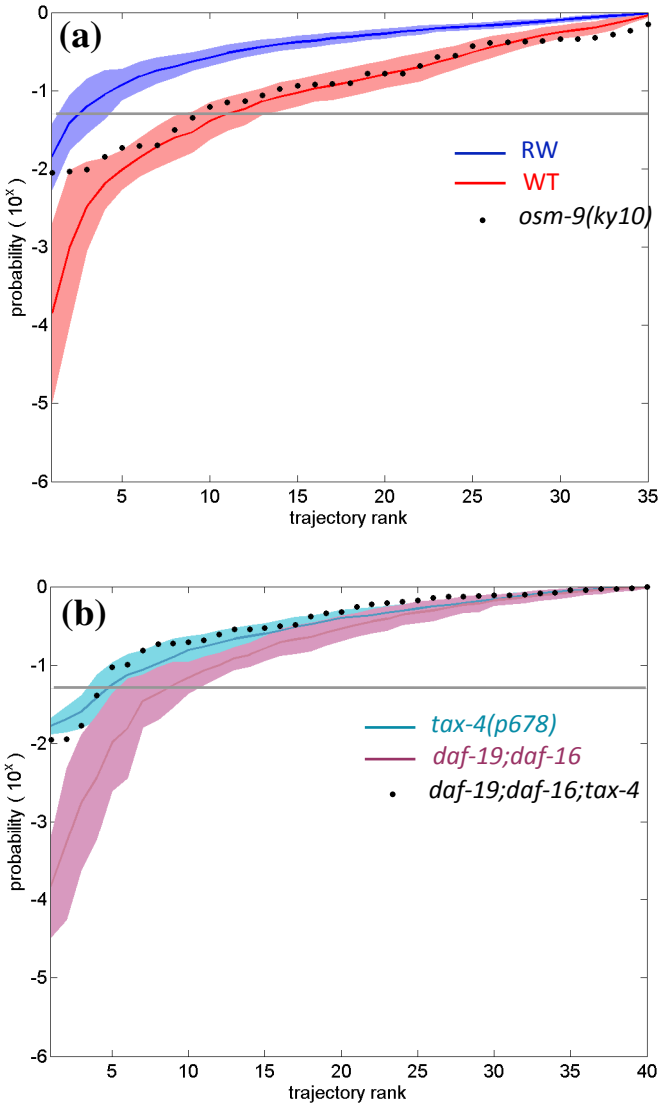

Fig. 32. Directionality indices of *osm-9* mutants and *daf-19;tax-4* mutants. **(a)** Black dots: *osm-9*. Red curve and shading: average wild-type +/- one std. P-value (Kolmogorov-Smirnov test): 0.9. Blue curve and shading: null model average +/-one std. P-value (Kolmogorov-Smirnov test): 0.0008. Gray line: p=0.05. 25% $p < 0.05$ ($n = 43$). **(b)** Black dots: triple mutant *daf-19;daf-16;tax-4*. Green curve and shading: *tax-4* average +/- one std. P-value (Kolmogorov-Smirnov test): 0.7. Purple curve: average directionality indices of a subsample of *daf-19;daf-16* trajectory. Purple shading: *daf-19;daf-16* average +/- one std. P-value (Kolmogorov-Smirnov test): 0.2. Gray line: p=0.05. 10% $p < 0.05$ ($n = 40$) (*tax-4(p678)*: 11% $p < 0.05$. *daf-19;daf-16*: 20% $p < 0.05$).

The residual directionality of *daf-19* mutants appears to require TAX-4 function

The phenotype of *tax-4* mutants indicates that directional behavior requires the activity of a specific subset of sensory neurons, and thus suggests that the behavior might be driven by sensorial inputs. This result is arguably at odds with the residual directionality displayed by *daf-19* mutants, which lack all sensory cilia and thus display severe sensory defects. To determine whether directional behavior, in this background, also required the function of TAX-4, we investigated the behavior of a triple mutant for *daf-19, daf-16*, and *tax-4*.

Shown in Figure (Fig. 32) is the behavior of the triple mutant (n = 40) compared to that of *tax-4* and of *daf-19; daf-16* alone. The trend of the distribution for the triple mutant suggests similar behavior to that displayed by *tax-4* mutants; in other words, the directionality of non-ciliated *daf-19* animals appears to require the function of the *tax-4/tax-2* cGMP channel (*pKS* (*daf-19;daf-16;tax-4* vs. *tax-4*) = 0.7). This result, however, does not constitute conclusive evidence for a TAX-4 requirement, as the distribution for *daf-19; daf-16*; *tax-4* does not display a significant divergence from the distribution for *daf-19; daf-16* alone (*pKS* (*daf-19;daf-16;tax-4* vs. *daf-19;daf-16*) = 0.2).

Targeting sensory transduction upstream of TAX-4 does not disrupt directionality

The signal transduction channel encoded by *tax-4* is required broadly for sensory perception; therefore, the finding that mutations in *tax-4* result in non-directional behavior eliminates only but a few sensory stimuli from the range of all possible biasing cues. However, it appears that the cGMP signal transduction pathway upstream of *tax-4*

employs different guanylate cyclases in different subset of cells. Taking advantage of previously-identified mutations in those genes, we therefore sought to characterize the behavior of animals specifically defective in thermosensation, oxygen sensation, chemosensation and sensation of light. The results of experiments performed on those sensory mutants are described below.

gcy-8; gcy-18; gcy-23 thermotaxis mutants display directional behavior

The phenotype of *gcy-8; gcy-18; gcy-23* triple mutants, a set of three guanylate cyclases that function in the AFD thermosensory neuron, recapitulates the athermotactic behavior displayed by animals in which AFD is ablated by laser microsurgery (Inada et al., 2006). We confirmed the athermotactic phenotype by assaying the behavior of *gcy-8; gcy-18; gcy-23* mutants in a linear temperature gradient (Fig. 33). We observe ~20% of the mutant population in the hot region of the gradient, compared to the ~80% obtained when assaying wild-type animals. The remainder of the mutant population disperses somewhat evenly across regions at intermediate and cold temperatures. We collected a set of $n = 39$ trajectories of *gcy-8; gcy-18; gcy-23* triple mutants, and proceeded to quantify behavior in the usual manner. As shown in Figure (Fig. 33), the mutant population displays wild-type behavior by our criterion (25% $p<0.05$, *pKS* (vs. WT) = 0.9; *pKS* (vs. null model) = 0.002). This result suggests that a thermotactic explanation for the long-range persistence in the animals' direction of motion is unlikely.

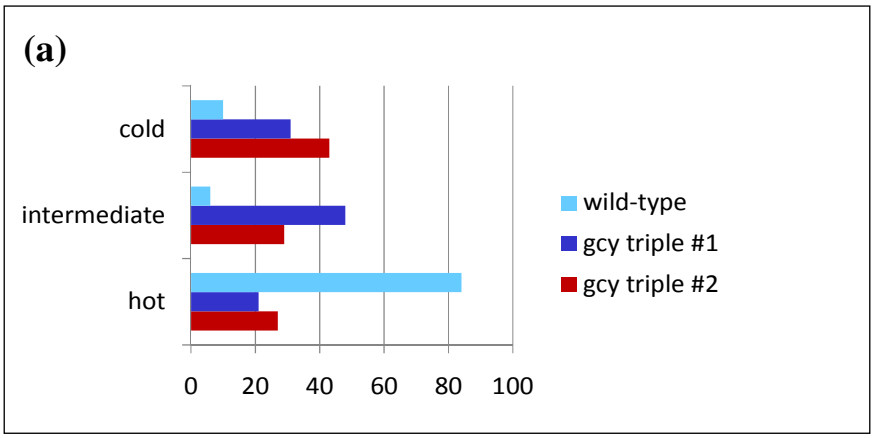

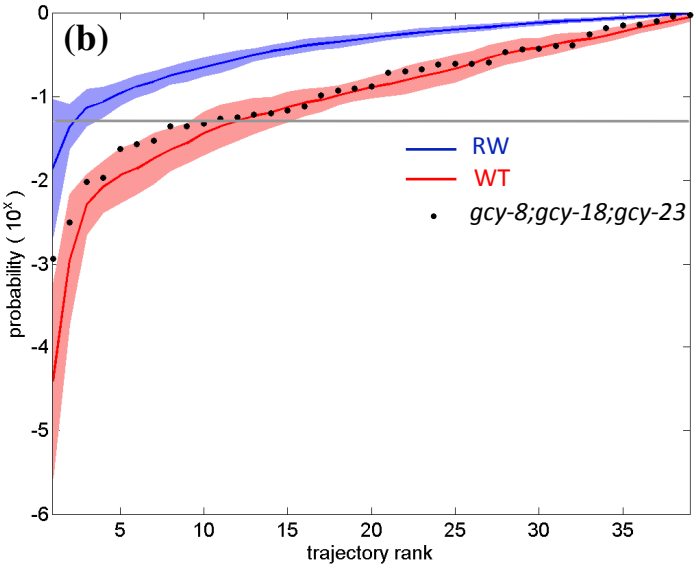

Fig. 33. Directionality indices of *gcy-8;gcy-18;gcy-23* mutants. **(a)** Thermotaxis behavior of *gcy-8;gcy-18;gcy-23* mutants vs. the wild-type. Animals were cultivated at 25 °C. *gcy-8;gcy-18;gcy-23* mutants fail to accumulate in the hot region of the plate. **(b)** Black dots: *gcy-8;gcy-18;gcy-23*. Red curve and shading: average wild-type +/- one std. P-value (Kolmogorov-Smirnov test): 0.9. Blue curve and shading: null model average +/-one std. P-value (Kolmogorov-Smirnov test): 0.002. Gray line: p=0.05. 25% $p < 0.05$ (n = 39).

gcy-31; gcy-33; gcy-35 aerotaxis mutants display directional behavior

Responses to oxygen concentrations have been shown to implicate a set of soluble guanylate cyclases which are differentially expressed by the sensory URX, AQR, PQR and BAG neurons. Although these cyclases might be redundant in function, a combination of calcium imaging and behavioral studies (Chang et al., 2006; Gray et al., 2004; Zimmer et al., 2009) has identified a requirement for the guanylate cyclase *gcy-35* together with *gcy-31* and *gcy-33* for proper aerotactic responses.

Our assays are carried out at equilibrium with the atmosphere; therefore, we do not expect oxygen concentrations to deviate from the atmospheric stably over the scale of our assays. However, as it will be shown in the next section, a different set of experiments suggests a role for one (or all) of URX, AQR and PQR in mediating directional behavior. Intriguingly, URX and the thermosensory AFD neuron are the only neurons that are known to both require cGMP signaling and to depend upon cilia for their sensory function. This makes them the ideal candidates to reconcile our *daf-19* and *tax-4* findings.

The behavioral phenotype of *gcy-31; gcy-33; gcy-35* triple mutants is displayed in Figure 34. As expected, the distribution does not deviate significantly from that of the wild-type (30% $p<0.05$, *pKS* (vs. WT) = 0.8; *pKS* (vs. null model) = 0.003). This result, however, does not rule out possibility that AFD, URX, AQR, PQR and BAG might be regulating directional behavior, possibly by signaling through a different set of guanylate cyclases.

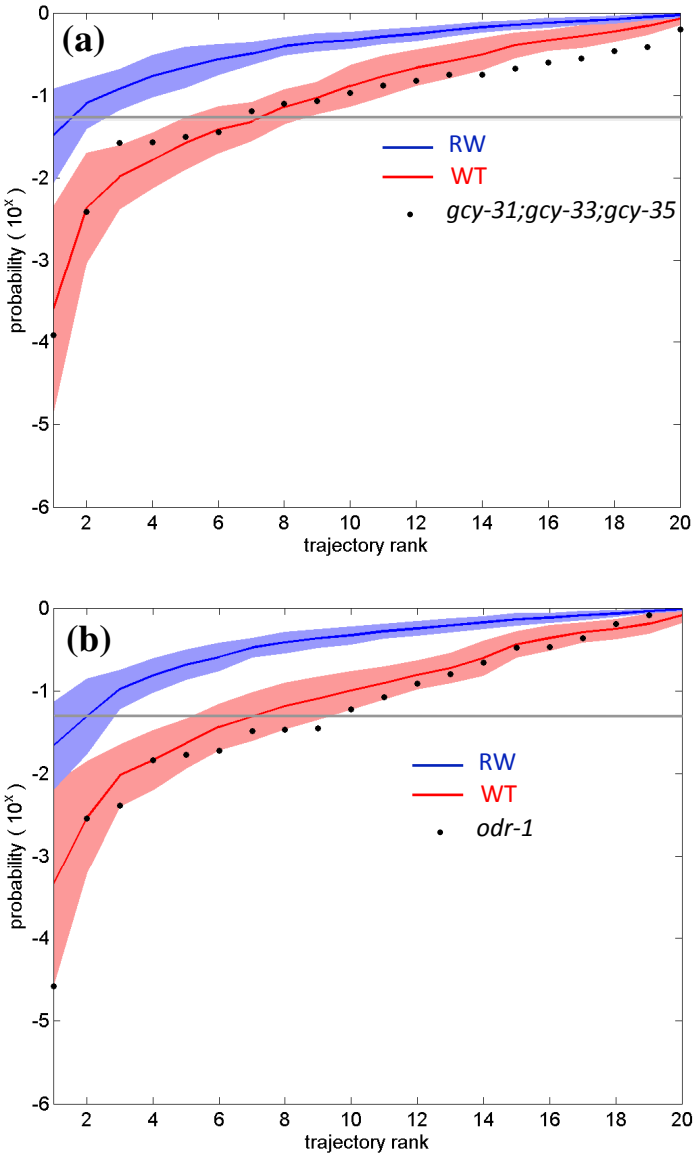

Fig. 34. Directionality indices of *gcy-31;gcy-33;gcy-35* mutants and of *odr-1* mutants. **(a)** Black dots: *gcy-31;gcy-33;gcy-35*. Red curve and shading: average wild-type +/- one std. P-value (Kolmogorov-Smirnov test): 0.8. Blue curve and shading: null model average +/- one std. P-value (Kolmogorov-Smirnov test): 0.003. Gray line: p=0.05. 30% $p < 0.05$ ($n = 20$). **(b)** Black dots: *odr-1*. Red curve and shading: average wild-type +/- one std. P-value (Kolmogorov-Smirnov test): 0.4. Blue curve and shading: null model average +/-one std. P-value (Kolmogorov-Smirnov test): 0.004. Gray line: p=0.05. 45% $p < 0.05$ ($n = 20$).

A chemosensory and photosensory *odr-1* mutant displays directional behavior

Transduction of odorant stimuli in the AWB and AWC neurons has been shown to require the guanylate cyclases *odr-1* and *daf-11* upstream of the cGMP-gated channel TAX-4 (Bargmann et al., 1993). Remarkably, *odr-1* is also required for proper avoidance responses to light (Liu et al., 2010). A dataset of n = 20 trajectories of *odr-1(n1936)* mutants displays wild-type behavior (Fig. 34) (45% $p<0.05$, *pKS* (vs. WT) = 0.4; *pKS* (vs. null model) = 0.004), which suggests that photosensation and olfaction do not contribute essentially to directionality.

Rescue of neural activity in specific sensory neurons

In order to establish which cells might direct the animals' behavior, and thus restrict the range of the possible sensory modalities implicated in the behavior, we sought to analyze the paths of animals in which TAX-4 function was rescued in a subset of sensory neurons.

Rescue of TAX-4 by its endogenous promoter partially restores wild-type directionality

First, we sought to verify the role of *tax-4* by characterizing the behavior of transgenic animals expressing TAX-4 under the control of its endogenous promoter. The distribution of directionality indices obtained for n=33 trajectories is shown in Figure 35. For comparison, the data is plotted together with the distributions of *tax-4* alone as well and of the wild-type (shown in blue and red, respectively; the shadings indicate standard

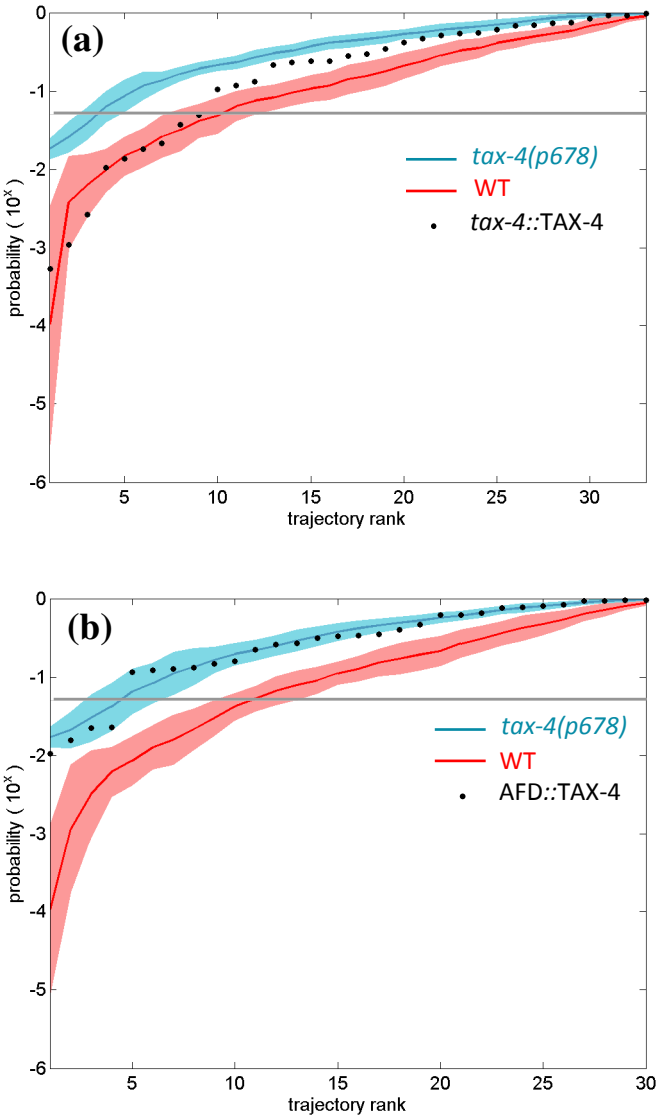

Fig. 35. Directionality indices of *tax-4*::TAX-4 and AFD::TAX-4 transgenic animals. **(a)** Black dots: *tax-4(ks28); tax-4::*TAX-4 + coelomocytes::GFP. Red curve and shading: average wild-type +/- one std. P-value (Kolmogorov-Smirnov test): 0.08. Green curve and shading: *tax-4* average +/-one std. P-value (Kolmogorov-Smirnov test): 0.6. Gray line: p=0.05. 27% $p < 0.05$ (n = 33). **(b)** Black dots: *tax-4(ks28); gcy-8::*TAX-4 + coelomocytes::GFP. *gcy-8::*TAX-4 is expressed in the AFD sensory neuron. Red curve and shading: average wild-type +/- one std. P-value (Kolmogorov-Smirnov test): 0.03. Blue curve and shading: *tax-4* average +/-one std. P-value (Kolmogorov-Smirnov test): 0.9. Gray line: p=0.05. 13% $p < 0.05$ (n = 30).

deviations, estimated over an ensemble of subsamples). The behavior of this rescued line appears somewhat bimodal: a subset of the trajectories displays mutant behavior, whereas the remaining (directional) subset exhibits wild-type directionality. This result indicates partial rescue of wild-type directionality. However, because of this dual behavior, the distribution fails to display a significant divergence from that of *tax-4* mutants alone by the Kolmogorov-Smirnov test (27% $p<0.05$, *pKS* (vs. WT) = 0.08; *pKS* (vs. *tax-4*) = 0.6).

TAX-4 rescue in the thermosensory AFD neuron does not restore wild-type directionality

We then proceeded to analyze the behavior of a line expressing TAX-4 under the control of the thermosensory neuron AFD. A dataset comprised of 30 trajectories displays a distribution of directional indices that is indistinguishable from that of *tax-4* mutants alone, suggesting that directional behavior is not a result of temperature sensing in the animals (Fig. 35) (13% $p<0.05$, *pKS* (vs. WT) = 0.03; *pKS* (vs. *tax-4*) = 0.9), a result also confirmed by the wild-type phenotype displayed by the thermotactic *gcy-8; gcy-18; gcy-23* mutant.

Restoring TAX-4 function in two olfactory neurons does not result in directional behavior

In order to investigate whether odorant-sensing neurons might be playing a role in directing the animals' locomotion, we examined the behavior of a line expressing TAX-4 under the control of the *odr-3* promoter, which directs expression in the winged neurons AWB, AWC and AWA as well as in the ASH and ADF neurons. Among those cells,

only AWB and AWC depend on TAX-4 for signal transduction. The functionality of this construct in rescuing AWC-mediated behaviors has been confirmed a distinct behavioral paradigm (Dirk Albrecht, *pers. comm.*). No significant rescue was obtained with this line (Fig. 36) (3% $p<0.05$, *pKS* (vs. WT) = 0.001; *pKS* (vs. *tax-4*) = 0.8). Likewise, a construct directing TAX-4 expression in AWB alone did not result in a significant deviation from mutant behavior (Fig. 36) (0% $p<0.05$, *pKS* (vs. WT) = 0.0005; *pKS* (vs. *tax-4*) = 0.4). Taken together with the wild-type phenotype displayed by the *osm-9* and *odr-1* olfactory mutants, these results indicate that odorant-sensing cells might not be playing a role in directional behavior.

Restoring TAX-4 function in a set of five sensory neurons rescues directional behavior

We then turned to the analysis of a different line, one in which neural activity was rescued in the oxygen-sensing cells URX**,** AQR and PQR, as well as in the ciliated amphidial neurons ASJ and ASK. ASJ and ASK have been implicated in dauer pheromone sensation, photosensation, electrosensation, and to a lesser extent in chemotaxis to soluble compounds. Expression of TAX-4 in this subset of cells resulted in good, albeit partial, rescue of directionality (25% $p<0.05$, *pKS* (vs. WT) = 0.4; *pKS* (vs. *tax-4*) = 0.03) (Fig. 37). We therefore sought to determine whether a narrower set of cells could direct wild-type behavior. Rescue of TAX-4 function in the ASJ and ASK neurons alone did not result in significant directional behavior (3% $p<0.05$, *pKS* (vs. WT) = 0.01; *pKS* (vs. *tax-4*) = 0.9) (Fig. 37). A line expressing TAX-4 in the URX, AQR and

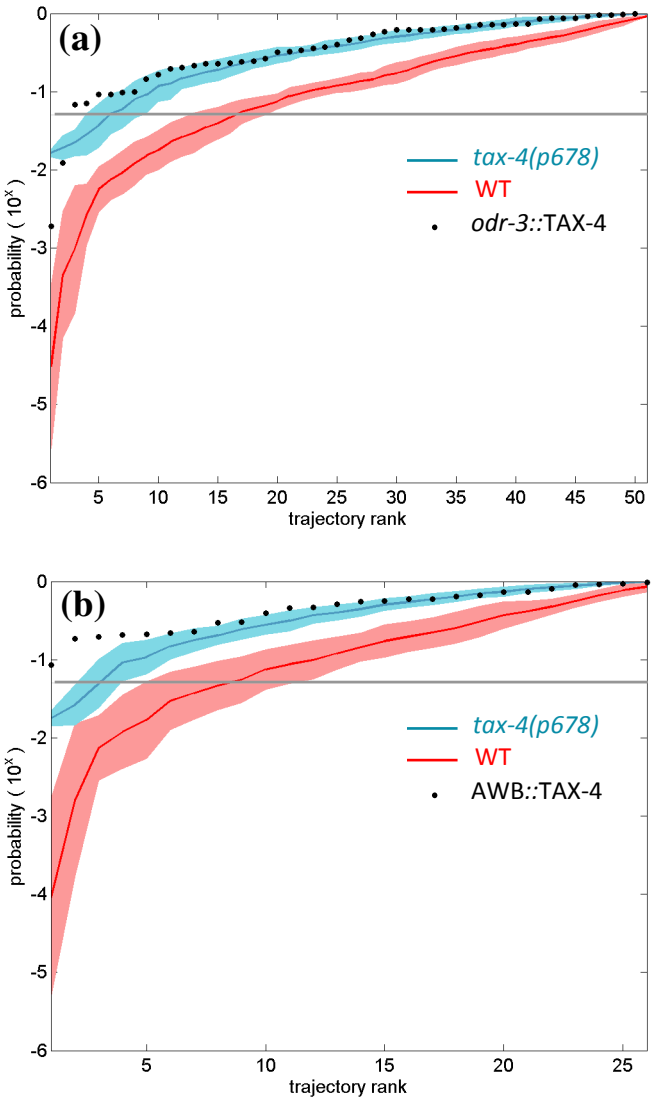

Fig. 36. Directionality indices of *odr-3*::TAX-4 and AWB::TAX-4 transgenic animals. **(a)** Black dots: *tax-4(ks28); odr-3::*TAX-4 + *elt-2*::GFP. *odr-3::*TAX-4 is expressed in the AWA, AWB, AWC, ADF, ASH sensory neurons. Red curve and shading: average wild-type +/- one std. P-value (Kolmogorov-Smirnov test): 0.001. Green curve and shading: *tax-4* average +/-one std. P-value (Kolmogorov-Smirnov test): 0.8. Gray line: p=0.05. 3% $p < 0.05$ ($n = 51$). **(b)** Black dots: *tax-4(ks28); str-1::*TAX-4 + coelomocytes::GFP. *str-1::*TAX-4 is expressed in the AWB sensory neuron. Red curve and shading: average wild-type +/- one std. P-value (Kolmogorov-Smirnov test): 0.0005. Blue curve and shading: *tax-4* average +/-one std. P-value (Kolmogorov-Smirnov test): 0.4. Gray line: p=0.05. 0% $p < 0.05$ ($n = 26$).

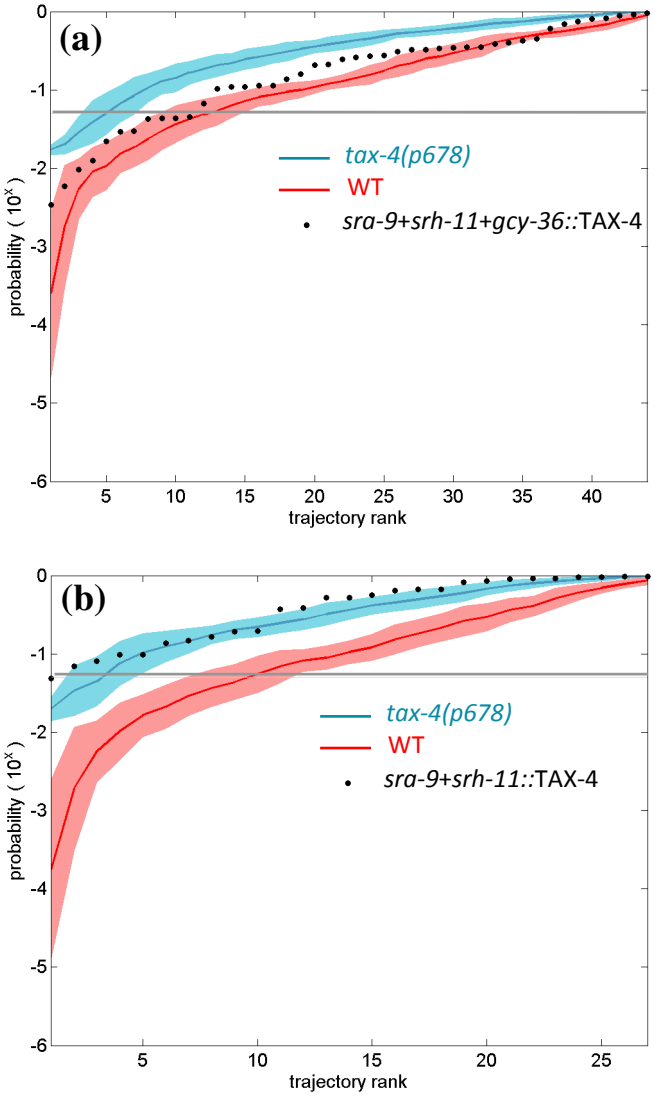

Fig. 37. Directionality indices of (*sra-9* + *srh-11* + *gcy-36*)::TAX-4 and of (*sra-9* + *srh-11*)::TAX-4 transgenic animals. **(a)** Black dots: *tax-4(p678);* (*sra-9* + *srh-11* + *gcy-36*)::TAX-4 + *elt-2*::GFP. The constructs drive expression in the ASJ, ASK, URX, AQR and PQR neurons. Red curve and shading: average wild-type +/- one std. P-value (Kolmogorov-Smirnov test): 0.4. Green curve and shading: *tax-4* average +/-one std. P-value (Kolmogorov-Smirnov test): 0.03. Gray line: p=0.05. 25% $p < 0.05$ (n = 44). **(b)** Black dots: *tax-4(p678);* (*sra-9* + *srh-11*)::TAX-4 + *elt-2*::GFP. *sra-9* + *srh-11* drive expression in the ASJ and ASK sensory neurons. Red curve and shading: average wild-type +/- one std. P-value (Kolmogorov-Smirnov test): 0.01. Blue curve and shading: *tax-4* average +/-one std. P-value (Kolmogorov-Smirnov test): 0.9. Gray line: p=0.05. 3% $p < 0.05$ (n = 27).

PQR neurons might display partial rescue (18% $p<0.05$, *pKS* (vs. WT) = 0.3; *pKS* (vs. *tax-4*) = 0.06) (Fig. 38). However, preliminary datasets of two lines expressing TAX-4 in the URX, AQR, PQR and ASJ neurons, and URX, AQR, PQR and ASK neurons, respectively, showed no rescue of directionality (ASJ + [URX]: 0% $p<0.05$, *pKS* (vs. WT) = 0.02; *pKS* (vs. *tax-4*) = 0.5) (ASK + [URX]: 0% $p<0.05$, *pKS* (vs. WT) = 0.003; *pKS* (vs. *tax-4*) = 0.3) (Fig. 38). Further experimental evidence (*i.e.* additional lines and cell-ablation experiments) will be needed to conclusively implicate ASJ, ASK, URX, AQR and PQR in the behavior, and to determine whether the neural basis of directionality is indeed distributed among all five cells.

Different paths within a plate do not display directional correlations

A different, phenomenological approach was sought in order to address whether the biasing cue might be specific to the particular plate employed. Such would be the case, for example, if the plates displayed fungal contamination at a particular spot, which we had failed to detect. To that end, we investigated the correlation between the path directions of animals that were assayed in close succession to each other on a same plate.

We performed a set of $n = 27$ assays on the scanners setup, by subsequent testing of a second animal on a given plate within minutes of collection of the first trajectory. Reassuringly, the distribution of relative orientations of the n pairs of paths acquired in this fashion, defined as the angle between respective end-to-end vectors, displayed no detectable correlation, suggesting that the directional bias does not result from chemotactic behavior to a specific spot within the plate (Fig. 39). This result is consistent with preliminary population assays ($N \sim 100$) performed with the camera setup, which

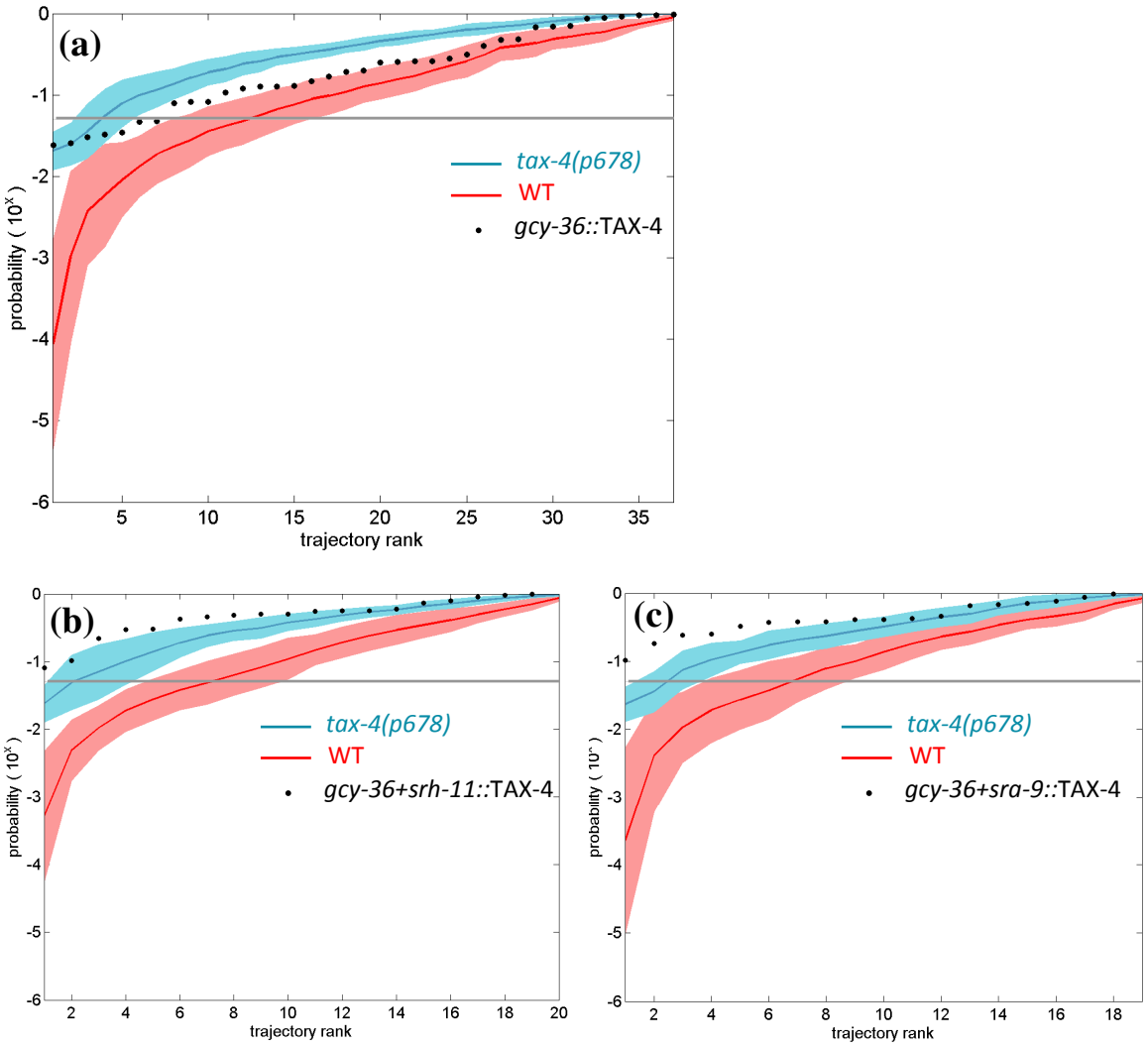

Fig. 38. Directionality indices of *gcy-36*::TAX-4, *gcy-36* + *srh-11*::TAX-4 and *gcy-36* + *sra-9* transgenic animals. **(a)** Black dots: *tax-4(p678); gcy-36*::TAX-4 + *elt-2*::GFP. *gcy-36* drives expression in the AQR, PQR and URX neurons. Red curve and shading: average wild-type +/- one std. P-value (Kolmogorov-Smirnov test): 0.3. Green curve and shading: *tax-4* average +/-one std. P-value (Kolmogorov-Smirnov test): 0.06. Gray line: p=0.05. 18% p<0.05 (n=37). **(b)** Black dots: *tax-4(p678);* (*gcy-36* + *srh-11*)::TAX-4 + *elt-2*::GFP. *srh-11* drives expression in the ASJ neuron. Red curve and shading: average wild-type +/- one std. P-value (Kolmogorov-Smirnov test): 0.02. Blue curve and shading: *tax-4* average +/-one std. P-value (Kolmogorov-Smirnov test): 0.5. Gray line: p=0.05. 0% $p < 0.05$ (n = 20). **(c)** Black dots: *tax-4(p678);* (*gcy-36* + *sra-9*)::TAX-4 + *elt-2*::GFP. *sra-9* drives expression in the ASK neuron. Red curve and shading: average wild-type +/- one std. P-value (Kolmogorov-Smirnov test): 0.003. Blue curve and shading: *tax-4* average +/-one std. P-value (Kolmogorov-Smirnov test): 0.3. Gray line: p=0.05. 0% $p < 0.05$ (n = 19).

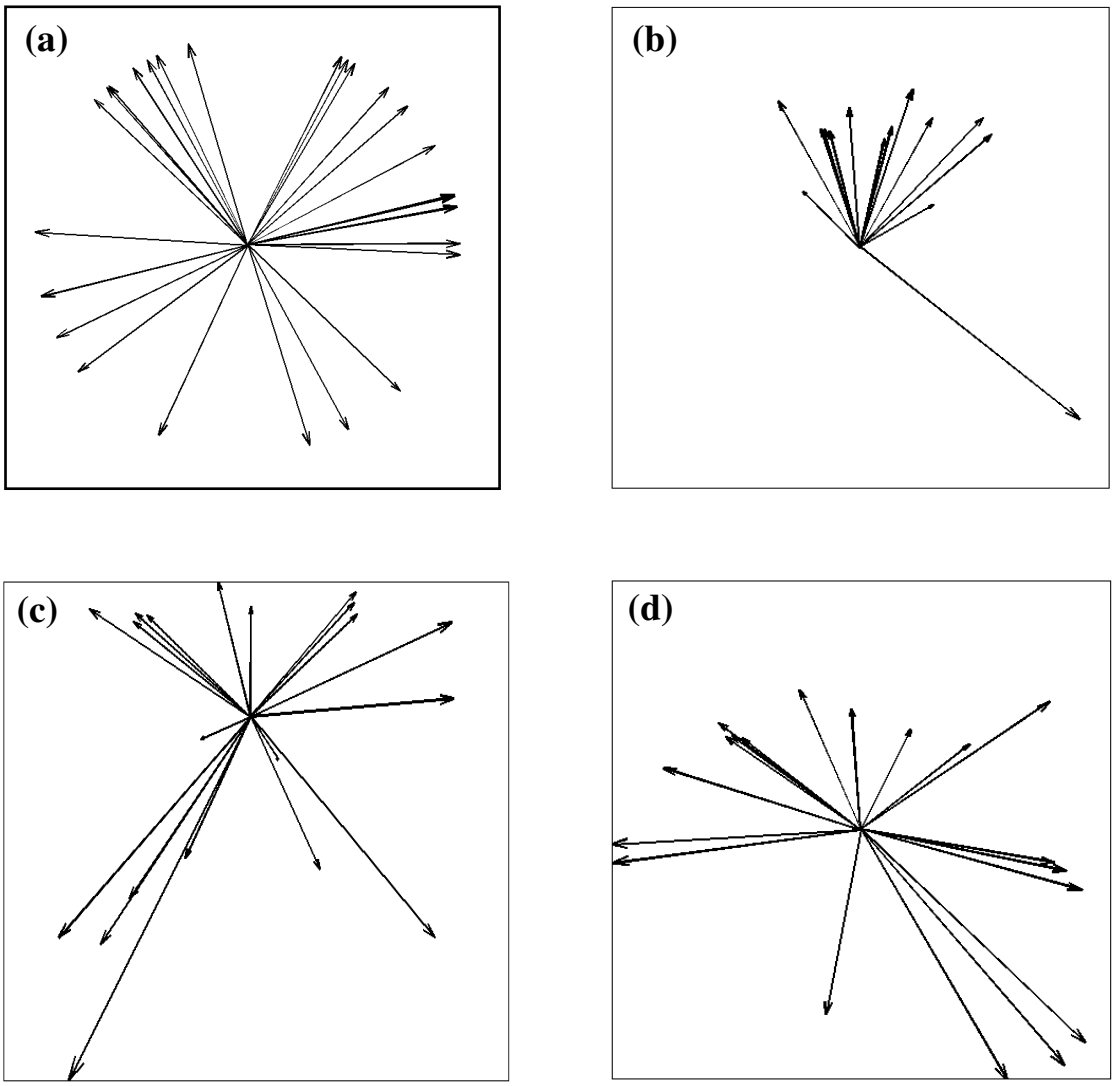

Fig. 39. Relative directions of trajectories on a same plate, and off-center trajectories. **(a)** Relative orientation of the end-to-end vectors of pairs of animals assayed consecutively on a same plate (*n*=27). **(b)** Plot of the end-to-end vectors of animals started midway between the center and the edge. The vector's orientation is plotted relative to its closest edge. ~3-weeks-old plates, *n*=16. **(c)** Plot of the end-to-end vectors of animals started midway between the center and the edge. The vector's orientation is plotted relative to its closest edge. Freshly-poured plates, *n*=21. **(d)** Plot of the end-to-end vectors of animals started midway between the center and the edge. The vector's orientation is plotted relative to its closest edge. 12-days-old plates, *n*=20.

show a roughly uniform distribution of path directions.

Lastly, we conducted a set of assays where individual animals were started mid-way between the center and the edge of the plate. This experimental design addresses the concern that *C. elegans* might be directing its motion towards a yet uncharacterized signal emanating from the edges of the plate, or from the surrounding environment. This experiment was performed in triplicate. In one of the triplicates we utilized plates that had been stored in air-tight containers at 4˚C for about 3 weeks; those assays revealed, unexpectedly, a significant preference among the animals' paths for outward-bound directions rather than inward-bound ones (Fig. 39). The observed bias suggests that the animals' behavior might be affected by a yet uncharacterized cue, such as medium inhomogeneities due to aging of the plates. This possibility calls for additional control experiments, which we outline and discuss in the following chapter.

However, we did not observe such a bias in a second and third replicate of the experiment, which we performed, respectively, on freshly poured plates and on 12-days-old plates. Furthermore, the set of trajectories we obtained in these replicates display, quantitatively, the same directional behavior as observed previously (Fig. 40). Therefore, the possible presence of a chemotactic cue does not by itself account for the animals' directional behavior.

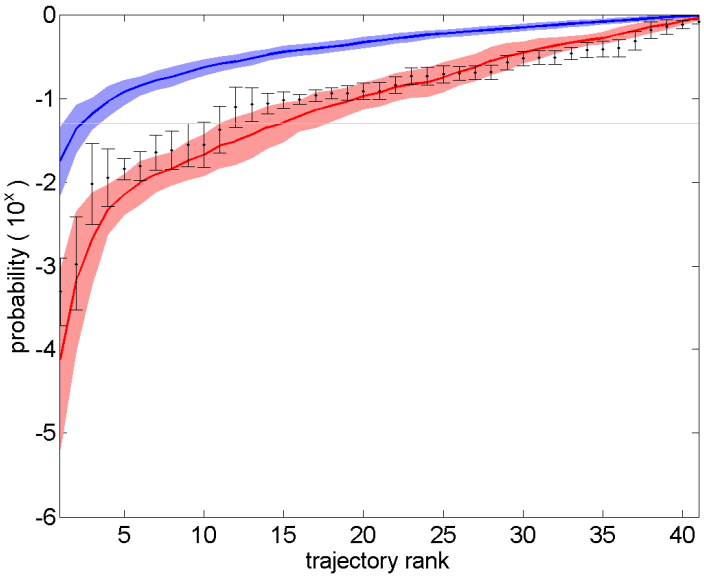

Fig. 40. Directionality indices of off-center trajectories. We pooled together the two sets of radially-unbiased trajectories (see Fig. 39, **(c)** and **(d)**) and computed their directionality indices as described previously. Black dots, black error bars: data. Red curve and shading: average of a set of subsamples of the previous (on-center) scanners dataset +/- one std. P-value (Kolmogorov-Smirnov test): 0.7. Blue curve and shading: null model average +/- one std. P-value (Kolmogorov-Smirnov test): 10^{-8}. Gray line: p=0.05. 26% $p < 0.05$ ($n = 41$).

Chapter 5. Discussion and future directions

Possible mechanisms of directional persistence

Our characterization of the paths of *C. elegans* on large agar surfaces in the absence of food reveals striking, long-range directional behavior. This behavior is unlikely to result from propagation of local directional correlations only, as it occurs over time scales that are much larger than the typical time scale of local persistence in the direction of motion. Furthermore, the paths exhibit, at intermediate times, motion that is less oriented than that displayed at large times, suggesting that directionality might be an emerging feature of the animals' behavior at large timescales.

What could be the mechanism by which *C. elegans* maintain an overall directional course, given what is known of its sensory and neural capabilities? First of all, is it possible to claim with any generality that the data cannot be accounted for by a stochastic, isotropic model of locomotion, unless it is also assumed that the animal remembers where it is going? Second, if the animals' motion is indeed biased, can we distinguish between orientation mechanisms based on external cues versus mechanisms that rely solely on self-generated cues?

1. Isotropic random-like walks with super-diffusive, directed behavior

In order to address the first point, we need to consider whether we may have overlooked features that, if incorporated into our null model of locomotion, would alter the

conclusions of our analysis. In this work, we have relied mainly on two approaches to quantify the long-range properties of the animals' locomotion. In the first approach, we compute the probability of obtaining, from random, a larger value of the net displacement than experimentally observed; this quantity is, obviously, model-dependent. The second approach we took consists in computing the scaling coefficient of the mean square displacements; this last method possesses larger generality, but its significance is again estimated by reference to the null model.

The physiology of the movement of *C. elegans* suggests some immediate refinements to the model. For example, a proper null model ought to account for correlations between speed and angular velocity, as animals will exhibit larger displacements between consecutive frames if their motion is uninterrupted by intervening changes in direction. Such correlations do not affect the asymptotic, diffusive properties of a walk; they will, however, result in ballistic motion over longer time scales than those characteristic of a random walk lacking such correlations. Therefore, the super-diffusive scaling we observe might be simply due to an observation time that is still within the time range of ballistic motion.

Similarly, our quantitative conclusions might be altered if the temporal statistics of turning events is taken into account. As observed in previous studies, in *C. elegans* sharp turns tend to happen in close succession to each other, and therefore ought to be considered as a single reorientation event. An analysis that disregards the clustered nature of the turning behavior of *C. elegans* results in redistribution of those turns along the trajectory, and, as a consequence, underestimates the degree of directionality of the random process. We reasoned that coarse-graining of the trajectories by increasing the

sampling rate experimentally (*i.e.* by acquiring at the scanners' frame rate) or by sampling the data *a posteriori* would average out the temporal structure of locomotion, and thereby minimize this source of artifactuality. However, we have yet to conclusively determine whether correlations in the timing of turns at the coarse-grained scales can be deemed irrelevant.

As discussed previously, Lévy-like processes represent yet another mechanism by which to obtain long-range directionality without violating the assumption of isotropic motion. Strictly speaking, if runs are taken to be equal to the animals' discrete displacements, we have to reject such a description, as the distribution of step lengths is bounded to the maximum distance the animal can travel at our acquisition rate, and therefore does not possess the defining characteristic of a Lévy walk – a slowly, power-law decaying tail.

However, runs are more appropriately defined in a looser way, by lumping together subsequent segments of the path when they do not display sharp changes in direction. It is unlikely that this definition will result in a power-law distribution of step lengths, since we do not observe bouts of long, unperturbed movement in the animals' paths. Nevertheless, a quantitative analysis of the runs' distribution is required in order to determine whether we have the grounds to conclusively reject that class of models.

Our null model could be refined to take into account the temporal structure of turning events, by clustering together turns that occur in close succession – assuming that the data allows unambiguous assignment of individual turns to clusters. These clusters would naturally parse the trajectory into a set of segments which we would identify as our new displacements vectors. In fact, variations of this segmentation procedure have

been employed in previous studies (Iino and Yoshida, 2009; Pierce-Shimomura et al., 1999; Stephens et al., 2010). However, in our experimental conditions, animals do not appear to alternate between clearly separated locomotory states; therefore, the segmentation procedure would have to rely on arbitrary simplifications and parameter choices.

Behavioral studies also suggest that the frequency of changes in direction depends on the absolute time elapsed since the animals were first removed from food. This is a general issue when attempting to model the animals' locomotion, as any parameter of the process can exhibit a complicated dependence on time, behavioral state, and on the total history of the process. Determining whether or not the animals occupy distinct behavioral states, or whether the basic properties of the motion depend on time or on history, and incorporating those features in a into a null model, is no trivial task considering the behavioral variability among individuals, and the statistical power afforded by the single trajectory. How, then, can we be certain that our conclusions are robust with respect to the set of simplifying assumptions made on the statistics of the movement?

One possibility is to quantify the behavior of the path in a model-independent way, by assessing, for instance, whether the data displays features that can only be explained by invoking a directional bias. An example of such features would be a self-correlation of the turning angles, a dependence of the turning angle on the heading, or correlations between the module of the displacement and the heading. Determining the deviation of the distribution of turning angles (or of their coarse-grained version) from uniform also does not rely on specific assumptions on the null model. In fact, the observation that increasing the coarse-graining scale results in narrowing of the distribution of turning

angles around the zero is a strong indication of anisotropy, and therefore difficult to reconcile with both Lévy walk models and intermittent, 'tumble-and-run'-like models.

The results obtained by comparing the data to synthetic "mirror" trajectories constitute further indication that the animals' motion is, in fact, anisotropic. Mirror trajectories are constructed from individual experimental trajectories by reversing, or not (with probability 1/2) the whole portion of the path associated with a turn, and by reassembling the segments of the path (runs and turns) so that the directions at the ends of the segments coincide. This procedure ensures, by definition, that the resulting paths will display the same local velocity correlations and same temporal distribution of turns as their corresponding experimental paths. Remarkably, the reversal of turn direction disrupts the directional bias displayed by the data**,** thus definitively indicating that directionality is the result of emerging longer range correlations in the trajectory.

2. Taxis-like scenarios

The analysis presented in this work contains strong indications that the behavior displayed by *C. elegans* might not be explained by unbiased models of locomotion. The simplest explanation for such directionality is, of course, that the animals' environment contains a biasing sensory cue. Indeed, the loss of directionality observed in *tax-4* mutants of *C. elegans* suggests that the activity of sensory neurons is required for directional behavior. The opposite conclusion might be drawn, however, from the observation that *daf-19* mutants display residual wild-type directionality. This foreshadows the intriguing hypothesis that ciliary function might not be required to maintain a directional course. To reconcile this result with a sensory explanation for the

behavior, this suggests that we look foremost into sensory modalities that involve non-ciliated neurons, such as AFD-mediated thermosensation or URX-mediated oxygen sensation. Alternatively, this result might imply that neural activity, but not sensory inputs, are required to achieve directed motion.

Cell-specific rescue of neural activity provides a means to gain further insight into the sensory modalities implicated in directional behavior. Expression of TAX-4 in the AWB and AWC olfactory neurons did not rescue directional behavior. Taken together with the wild-type directionality displayed by *odr-1* chemotactic mutants, this result suggests that the external cue, if any, is unlikely to be a volatile compound. Similarly, expression of TAX-4 in the thermosensory neuron AFD did not result in directional behavior, a result that is also consistent with the observation that targeting thermosensation by mutations in *gcy-8; gcy-18; gcy-23* does not disrupt directionality. These latter results address the concern that the animals' behavior might constitute a taxis response to the temperature gradient present in the scanners setup.

As discussed in the previous section, an explanation of directionality in terms of aerotaxis is most unlikely, given that all assays are carried out at equilibrium with the atmosphere. This is consistent with the result obtained for the aerotactic-defective mutant, *gcy-31; gcy-33; gcy-35*, which, by our directionality criterion, displays no significant defect. However, because of the redundancy in the signal transduction pathway downstream of oxygen sensation, the genetic lesion alone cannot be assumed to completely suppress oxygen sensation.

What can be argued about other sensory cues? The wild-type phenotype displayed by *odr-1* mutants suggests that we rule out phototaxis, since photosensation appears to share the same signal transduction pathway as olfaction. Further experimental evidence can be obtained by characterizing the behavior of mutants for the putative photoreceptor *lite-1*. Gravitational forces at the scale of the worm are ~100 times smaller than surface tension forces; preliminary data suggests that placing the animals in a gravitational potential by tilting the assay plates does not result in preferential upwards or downwards movement.

The molecular bases of electrosensory behavior have not yet been characterized, and indeed an electrical signal is detectable on both the scanners and the camera setup. However, the electric potential measured on the camera setup is three orders of magnitude smaller than the one typically applied in behavioral assays. Moreover, *C. elegans* displays an orientation response only in static or slowly rotating fields, while our measured fields oscillate at frequencies of ~60Hz for the camera setup, and ~50kHz for the scanners, a frequency range that is beyond the tracking capabilities of the animals. Because of the fast-varying nature of the signal, it is also unlikely that animals might be navigating by magnetotaxis.

Interestingly, rescue of directionality is observed when driving expression of TAX-4 in a set of five sensory neurons, which includes the oxygen-sensing cells URX, AQR and PQR in addition to the amphidial neurons ASJ and ASK. ASJ and ASK are known to mediate weak chemotactic responses to soluble attractants, as well as to transduce responses to the dauer pheromone. In light of the functional differences between those five cells, we reasoned that it would be possible to identify a role for the chemosensory neurons ASJ and ASK alone, or else for the oxygen-sensing cells URX, AQR and PQR

alone. However, expressing TAX-4 in the oxygen-sensing cells only weakly rescues wild-type directionality, whereas attempts to rescue in the ASJ and ASK cells have yielded negative results. Further experimental evidence (*i.e.* cell ablation experiments, chronic neuronal activation) will be needed to conclusively implicate ASJ, ASK, URX, AQR and PQR in the behavior, and to determine whether directionality indeed requires the joint contribution of all five cells.

Our rescue experiments have not yet addressed the role of the ASE neuron, which is the main sensory mediator of chemotaxis to soluble compounds, nor that of the ASI and ASG neurons, which have a minor role in chemotaxis besides their role in regulating the dauer developmental decision (in addition, the ASI neuron is also involved in modulation of turning frequency off food). We will, however, discuss below the hypothesis that the animals' might be chemotaxing in a gradient of a soluble substance based on the results of phenomenological experiments as well as on theoretical considerations.

The roughly uniform distribution of path headings among the population suggests that, if a gradient or other cue is present, its direction might vary from assay to assay, and possibly be specific to a given assay plate. Addressing this concern, no correlation between headings was observed when a second animal was assayed after a first on a same plate. This result suggests that the hypothesis of a fixed cue within the plate is unlikely; it does not, however, rule out the possibility that multiple cues might be present in the environment. In one possible scenario, animals might pick up on a faint sensory cue, just above the threshold of detection, and follow that direction to the edge of the plate. It may be possible to confirm this hypothesis by analyzing the tracks of animals assayed on a slowly rotating stage.

An alternative possibility is that the plates display a gradient possessing radial symmetry. Given that our agar medium is first autoclaved and then stirred for several hours before being poured, we thought it unlikely that animals might be chemotaxing to salt gradients within our assay plates, since that would require gradients in the animals' detectable (millimolar) range to extend over scales of several centimeters. To address this question experimentally, we modified our protocol by starting individual animals from a point mid-way between the center and the edge of the plate. Surprisingly, in one out of three triplicates of the experiment, animals displayed a significant directional bias towards the edges of the plate.

The different results obtained for the experimental triplicates urged us to re-examine the possible sources of variability in our experimental conditions. As it turns out, the inconsistency between triplicates might be traced to the age of the plates, since the set of assays displaying radial bias was obtained by utilizing plates that were poured ~3 weeks prior to the assays. In contrast, no significant bias was observed when animals were assayed on a set of freshly poured plates, or on plates that were 12-days-old.

How could the age of the medium affect the behavior of the worm? Our modified NGM recipe contains agar, water, and cholesterol in addition to millimolar concentrations of NaCl, $MgSO_4$, $CaCl_2$ and of a potassium-phosphate pH buffer. We hypothesize that the intervening time between the preparation of the medium and the actual assays might result in higher salt concentrations at the edges of the plate, because of differential evaporation. With a water diffusion constant of 10^{-5} cm^2/s, such a gradient would attain a length scale of the order of 10 cm in 10 days (the typical "resting time" of our plates), which is consistent with the behavioral scale of the observed directionality. More

difficult to account for is the magnitude of the gradient, as the known detection range of *C. elegans* would require millimolar differences in concentration, and thus differential loss of ~50% the water content at the edges versus at the center of the plate.

In future work, we plan to establish or reject the presence of a salt gradient by directly measuring salt concentrations on the plate at varying distances from its center. The hypothesis of the presence of a salt gradient can also be addressed by genetic means, by targeting the function of the ASE neurons, the main mediators of chemotaxis to salts. This can be accomplished by mutations in the *che-1* gene, which regulates specification of the ASE fate (Uchida et al., 2003), or in the *daf-11* gene, which is not expressed in the ASE pair but nevertheless results in impaired responses to the attractants cAMP, Cl^- and biotin, as well as in other behavioral and developmental phenotypes (Vowels and Thomas, 1994). A putative role of ASE could then be confirmed by cell-specific rescue of TAX-4.

However, it must be noted that the experimental conditions upon which we observe a radial bias lie at the extremes of those adopted in our work. In fact, with the exception of that particular experiment, all our studies were performed on plates that had rested for intermediate periods of time of 1 to 2 weeks prior to the assays. A replicate of the experiment on a set of 12-days-old plates suggests that the animals' behavior might not be affected at those intermediate aging times. More importantly, the trajectories obtained in the two radially-unbiased replicates display marked directional behavior, indicating that salt chemotaxis does not exhaustively account for directionality.

3. Self-based mechanisms of directionality

How could we explain directional persistence other than as a response to an external cue? It can be speculated that the worm's behavior results from a self-based, sensorial mechanism, in analogy to the chemical trails that drive ants along foraging paths. In this scenario, animals would secrete a repulsive substance along their path, which would then inform their direction at following times. Without making detailed assumptions about the specifics of the sensing mechanism, and how it would feed back into the animals' locomotion, it should nevertheless be possible to examine some of the qualitative predictions that result from this hypothesis.

For example, in order to keep up with the effective speed of *C. elegans*, which is of the order of the millimeter per minute, the repulsive substance would presumably have to diffuse through air rather than through water. This suggests that olfactory neurons would be implicated in the behavior, a prediction that is not in agreement with our experimental findings. We also expect that such sensory-based mechanism would fall apart if the animals' paths are laid over a number of other paths with different orientations. Preliminary investigations suggest that this is not the case, although the results we observe might be reconciled with a chemical trail hypothesis if the repulsive substance decays over time.

More refined predictions could be derived from a modeling effort, one which assumed, for instance, the secretion and subsequent diffusion of a decaying substance at every point of the path over time. By simulating this process for the trajectories obtained experimentally, we could investigate whether the animals' paths follow a direction that

leads them down the gradient of the repulsive substance. The local recrossings displayed by the animals' trajectories could possibly be reconciled with such an avoidance mechanism by assuming an imprecise, noisy sensing mechanism, or by assuming stochasticity in the implementation of direction.

Further insight into the underlying mechanism for directionality might be gleaned from the analysis of the fine-grained features of the animals' movement. For example, the presence of correlations between turning angles would likely suggest a memory mechanism; in contrast, correlations between displacements and heading, or between heading and turning angles, would by definition imply that direction is been encoded, and hence suggests that animals might be exploiting external inputs. A closer inspection of the animals' looping behavior might prove particularly informative, as the direction of motion is strongly perturbed during a loop; it will be interesting to determine to what extent the animals' direction, after a looping episode, is reset to the direction held before the loop was initiated, or whether instead loops result in randomization of direction, which is then subsequently readjusted.

More generally, an analysis of the local properties of the paths might help to identify a small set of parameters such that the animals' movement, in the space defined by those parameters, would segregate into distinct behavioral classes (both within a path and across the population). The scaling exponent of the mean square displacements, computed locally over a time window T, could constitute one such parameter, although, in practice, its application is limited by the requirement that the lagtime τ be much smaller than the time window T: $\tau << T$. Other potential candidates are the joint distribution of speed and angular velocity, computed over an interval T; the ratio of the

length travelled in *T* by the total path length in that same interval; and the path's radius of curvature.

Optogenetic techniques allow an experimental test of predictions resulting from the assumption of a chemical trail. It is possible to perturb an animal's heading while bypassing the sensory neuronal layer by stimulating specific command interneurons engineered to express channelrhodopsin (Guo et al., 2009; S. Ramanathan, *pers. comm.*). By steering animals with respect to their track, we could determine whether local perturbations do not affect behavior on the long term, which would be consistent with the animals' direction being informed by a signal emanating from the path.

In conclusion, our results hint at the possibility that animals might rely solely on proprioceptive mechanisms to maintain a directional course. How could such mechanism be implemented at the level of the worms' nervous system? Based on their morphology, several neurons in *C. elegans* have been postulated to possess a proprioceptive function. These are cells that project long processes which seem to be devoid of synapses (White et al., 1986). More recently, calcium imaging studies have confirmed that one such neuron (the DVA interneuron) responds to physiological stretch (Li et al., 2009); interestingly, this neuron synapses directly onto the AQR neuron (White et al., 1986), which is one of the five cells that TAX-4 rescue experiments implicate in directional behavior.

We can speculate that sensitivity to body stretch endows the animals with a sense of direction. Body curvature might convey information on the radius of curvature of the path; this could, in turn, translate into heading information, if time was also being monitored. Such mechanism, however, would not account for directional persistence

across sharp, discrete perturbations of body shape, such as those characterizing reversals and omega bends. In this latter case, we would have to assume that specific aspects of sharp turns (*i.e.* the turn's amplitude; its dorsal or ventral bias) are under neuronal control, and that this information feeds back into the circuit that ultimately controls locomotion.

Indeed, laser ablation studies suggest that head motor neurons might encode specific features of the omega bend (Gray et al., 2005). Calcium activity in *C. elegans* neurons can now be measured in moving animals (Guo et al., 2009; Ben Arous et al., 2010), opening the way to direct experimental investigation of the correlation between neuronal activity patterns and locomotory output. Remarkably, head motor neurons synapse backward onto the interneuronal layer, allowing for the possibility that those neurons might act as the node where control of locomotion is coupled to, and determined by past locomotory output. In this picture, TAX-4 sensory neurons would work not as transducers of external stimuli, but, rather, as a driving force in the circuit, activating the interneuronal layer that controls the execution of turns by means of their spontaneous patterns of activity.

Bibliography

Abramowitz, M., and Stegun, I.A., 1972. Handbook of Mathematical Functions with Formulas, Graphs, and Mathematical Tables. Dover Publications, New York.

Albert, P., Brown, S., and Riddle, D., 1981. Sensory control of dauer larva formation in *Caenorhabditis elegans*. J Comp Neurol. **198**, 435-451.

Aronovitz, J.A., and Nelson, D.R., 1986. Universal features of polymer shapes. J. Physique **47**, 1445-1456.

Bargmann, C., and Mori, I., Chemotaxis and Thermotaxis, in: Riddle DL, B. T., Meyer BJ, Priess JR, (Ed.), *C. elegans* II. 2nd edition, Cold Spring Harbor Laboratory Press, Cold Spring Harbor (NY) 1997.

Bargmann, C., Thomas, J., and Horvitz, H., 1990. Chemosensory cell function in the behavior and development of Caenorhabditis elegans. Cold Spring Harb Symp Quant Biol 55, 529-38.

Bargmann, C.I., Chemosensation in C. elegans, in: WormBook: The Online Review of *C. elegans* Biology, 2006.

Bargmann, C.I., and Horvitz, H.R., 1991a. Control of larval development by chemosensory neurons in *Caenorhabditis elegans*. Science **251**, 1243-1246.

Bargmann, C.I., and Horvitz, H.R., 1991b. Chemosensory neurons with overlapping functions direct chemotaxis to multiple chemicals in *C. elegans*. Neuron **7**, 729-742.

Bargmann, C.I., Hartwieg, E., and Horvitz, H.R., 1993. Odorant-selective genes and neurons mediate olfaction in C. elegans. Cell **74**, 515-527.

Bartumeus, F., Da Luz, M.G.E., Viswanathan, G.M., and Catalan, J., 2005. Animal search strategies: a quantitative, random-walk analysis. Ecology **86**, 3078-3087.

Bartumeus, F., Catalan, J., Viswanathan, G.M., Raposo, E.P., and da Luz, M.G.E., 2008. The influence of turning angles on the success of non-oriented animal searches. Journal of Theoretical Biology **252**, 43-55.

Ben Arous, J., Laffont, S., and Chatenay, D., 2009. Molecular and sensory basis of a food related two-state behavior in *C. elegans*. PLoS ONE **4**, e7584.

Ben Arous J., Tanizawa Y., Rabinowitch I., Chatenay D., and Schafer WR., 2010. Automated imaging of neuronal activity in freely behaving *Caenorhabditis elegans*. J Neurosci Methods **187,** 229-34

Benhamou, S., 2004. How to reliably estimate the tortuosity of an animal's path: straightness, sinuosity, or fractal dimension? Journal of Theoretical Biology **229**, 209-220.

Benhamou, S., 2006. Detecting an orientation component in animal paths when the preferred direction is individual-dependent. Ecology **87**, 518-528.

Benhamou, S., and Bovet, P., 1992. Distinguishing between elementary orientation mechanisms by means of path-analysis. Animal Behaviour **43**, 371-377.

Bénichou, O., Loverdo, C., Moreau, M., and Voituriez, R., 2006. Two-dimensional intermittent search processes: An alternative to Levy flight strategies. Physical Review E **74**, 4.

Bénichou, O., Coppey, M., Moreau, M., Suet, P.H., and Voituriez, R., 2005. Optimal search strategies for hidden targets. Physical Review Letters **94**, 198101.

Berg, H.C., 1988. A physicist looks at bacterial chemotaxis. Cold Spring Harb Symp Quant Biol. **53**, 1-9.

Berg, H.C., and Brown, D.A., 1972. Chemotaxis in *Escherichia coli* analysed by three-dimensional tracking. Nature **239**, 500-504.

Berg, H.C., and Anderson, R.A., 1973. Bacteria swim by rotating their flagellar filaments. Nature **245**, 380-2.

Berkolaiko, G., and Havlin, S., 1998. Number of distinct sites visited by Levy flights injected into a d-dimensional lattice. Physical Review E **57**, 2549-2552.

Birnby, D.A., Link, E.M., Vowels, J.J., Tian, H., Colacurcio, P.L., and Thomas, J.H., 2000. A transmembrane guanylyl cyclase (DAF-11) and Hsp90 (DAF-21) regulate a common set of chemosensory behaviors in *Caenorhabditis elegans*. Genetics **155**, 85-104.

Biro, D., Freeman, R., Meade, J., Roberts, S., and Guilford, T., 2007. Pigeons combine compass and landmark guidance in familiar route navigation. Proceedings of the National Academy of Sciences **104**, 7471-7476.

Biron, D., Wasserman, S., Thomas, J.H., Samuel, A.D.T., and Sengupta, P., 2008. An olfactory neuron responds stochastically to temperature and modulates *Caenorhabditis elegans* thermotactic behavior. Proceedings of the National Academy of Sciences **105**, 11002-11007.

Boyer, D., Miramontes, O., and Ramos-Fernandez, G., 2008. Evidence for biological Lévy flights stands. arXiv:08021762v1 [q-bioPE].

Brown, R., 1828. A brief account of microscopical observations made in the middle of June, July, and August, 1827, on the particles contained in the pollen of plants. Philosophical Magazine **4**, 162-163.

Budick, S.A., and Dickinson, M.H., 2006. Free-flight responses of *Drosophila melanogaster* to attractive odors. J Exp Biol **209**, 3001-3017.

Chalasani, S.H., Kato, S., Albrecht, D.R., Nakagawa, T., Abbott, L.F., and Bargmann, C.I., 2010. Neuropeptide feedback modifies odor-evoked dynamics in *Caenorhabditis elegans* olfactory neurons. Nat Neurosci **13**, 615-621.

Chalfie, M., Tu, Y., Euskirchen, G., Ward, W.W., and Prasher, D.C., 1994. Green fluorescent protein as a marker for gene expression. Science **263**, 802-805.

Chang, A.J., Chronis, N., Karow, D.S., Marletta, M.A., and Bargmann, C.I., 2006. A distributed chemosensory circuit for oxygen preference in *C. elegans* PLoS Biol **4**, e274.

Cheung, A., Zhang, S., Stricker, C., and Srinivasan, M., 2007. Animal navigation: the difficulty of moving in a straight line. Biological Cybernetics **97**, 47-61.

Cheung, B.H.H., Cohen, M., Rogers, C., Albayram, O., and de Bono, M., 2005. Experience-dependent modulation of *C. elegans* behavior by ambient oxygen. Current Biology **15**, 905-917.

Coates, J.C., and de Bono, M., 2002. Antagonistic pathways in neurons exposed to body fluid regulate social feeding in *Caenorhabditis elegans*. Nature **419**, 925-929.

Coburn, C.M., and Bargmann, C.I., 1996. A putative cyclic nucleotide-gated channel is required for sensory development and function in *C. elegans*. Neuron **17**, 695-706.

Codling, E.A., and Hill, N.A., 2005. Sampling rate effects on measurements of correlated and biased random walks. Journal of Theoretical Biology **233**, 573-588.

Colbert, H.A., and Bargmann, C.I., 1995. Odorant-specific adaptation pathways generate olfactory plasticity in *C. elegans*. Neuron **14**, 803-812.

Colbert, H.A., Smith, T.L., and Bargmann, C.I., 1997. OSM-9, A novel protein with structural similarity to channels, is required for olfaction, mechanosensation, and olfactory adaptation in *Caenorhabditis elegans*. The Journal of Neuroscience **17**, 8259-8269.

Collett, M., Collett, T.S., and Srinivasan, M.V., 2006. Insect navigation: measuring travel distance across ground and through air. Current Biology **16**, R887-R890.

Collett, T.S., and Collett, M., 2002. Memory use in insect visual navigation. Nat Rev Neurosci **3**, 542-552.

Croll, N.A., 1975. Components and patterns in the behaviour of the nematode *Caenorhabditis elegans*. Journal of Zoology **176**, 159-176.

Culotti, J.G., and Russell, R.L., 1978. Osmotic avoidance defective mutants of the nematode *Caenorhabditis elegans*. Genetics **90**, 243-256.

Dacke, M., and Srinivasan, M.V., 2008. Two odometers in honeybees? J Exp Biol **211**, 3281-3286.

Darwin, C., 1873. Origin of certain instincts. Nature **7**, 417-418.

de Bono, M., and Bargmann, C.I., 1998. Natural variation in a neuropeptide Y receptor homolog modifies social behavior and food response in *C. elegans*. Cell **94**, 679-689.

Dusenbery, D.B., 1980a. Responses of the nematode *Caenorhabditis elegans* to controlled chemical stimulation. Journal of Comparative Physiology A: Neuroethology, Sensory, Neural, and Behavioral Physiology **136**, 327-331.

Dusenbery, D.B., 1980b. Appetitive response of the nematode *Caenorhabditis elegans* to oxygen. J. Comp. Physiol **136**, 333-336.

Dusenbery, D.B., Sheridan, R.E., and Russell, R.L., 1975. Chemotaxis-defective mutants of the nematode *Caenorhabditis elegans*. Genetics **80**, 297-309.

Edwards, A.M., Phillips, R.A., Watkins, N.W., Freeman, M.P., Murphy, E.J., Afanasyev, V., Buldyrev, S.V., da Luz, M.G.E., Raposo, E.P., Stanley, H.E., and Viswanathan, G.M., 2007. Revisiting Lévy flight search patterns of wandering albatrosses, bumblebees and deer. Nature **449**, 1044-1048.

Edwards, S.L., Charlie, N.K., Milfort, M.C., Brown, B.S., Gravlin, C.N., Knecht, J.E., and Miller, K.G., 2008. A novel molecular solution for ultraviolet light detection in *Caenorhabditis elegans*. PLoS Biol **6**, e198.

Einstein, A., 1905. Über die von der molekularkinetischen Theorie der Wärme geforderte Bewegung von in ruhenden Flüssigkeiten suspendierten Teilchen. Ann. d. Phys. **322**, 549–560.

Esch, H.E., Zhang, S., Srinivasan, M.V., and Tautz, J., 2001. Honeybee dances communicate distances measured by optic flow. Nature **411**, 581-583.

Etienne, A.S., Maurer, R., and Seguinot, V., 1996. Path integration in mammals and its interaction with visual landmarks. J Exp Biol **199**, 201-209.

Firle, S., Bommarco, R., Ekbom, B., and Natiello, M., 1998. The influence of movement and resting behavior on the range of three carabid beetles. Ecology **79**, 2113-2122.

Flory, P.J., 1953. Principles of polymer chemistry. Cornell University Press.

Frisch, K. von, 1967. The dance language and orientation of bees. Belknap Press of Harvard University Press, Cambridge, MA.

Fujiwara, M., Sengupta, P., and McIntire, S.L., 2002. Regulation of body size and behavioral state of *C. elegans* by sensory perception and the EGL-4 cGMP-dependent protein kinase. Neuron **36**, 1091-1102.

Gabel, C.V., Gabel, H., Pavlichin, D., Kao, A., Clark, D.A., and Samuel, A.D.T., 2007. Neural circuits mediate electrosensory behavior in *Caenorhabditis elegans*. The Journal of Neuroscience **27**, 7586-7596.

Görner, P., and Claas, B., Homing behavior and orientation in the funnel-web spider *Agelena labyrinthica Clerck*, in: Barth, F. G., (Ed.), Neurobiology of Arachnids, Springer-Verlag, Berlin, Heidelberg, New York. 1985, pp. 275–297.

Gould, J.L., 1998. Sensory bases of navigation. Current Biology **8**, R731-R738.

Gray, J.M., Hill, J.J., and Bargmann, C.I., 2005. A circuit for navigation in *Caenorhabditis elegans*. Proc. Nat. Acad. Sci. USA **102**, 3184-3191.

Gray, J.M., Karow, D.S., Lu, H., Chang, A.J., Chang, J.S., Ellis, R.E., Marletta, M.A., and Bargmann, C.I., 2004. Oxygen sensation and social feeding mediated by a *C. elegans* guanylate cyclase homologue. Nature **430**, 317-322.

Grima, R., 2005. Strong-coupling dynamics of a multicellular chemotactic system. Physical Review Letters **95**, 128103.

Guo, Z.V., Hart, A.C., and Ramanathan, S., 2009. Optical interrogation of neural circuits in *Caenorhabditis elegans*. Nature Methods **6,** 891-896

Hafting, T., Fyhn, M., Molden, S., Moser, M.-B., and Moser, E.I., 2005. Microstructure of a spatial map in the entorhinal cortex. Nature **436**, 801-806.

Hart, A.C., Sims, S., and Kaplan, J.M., 1995. Synaptic code for sensory modalities revealed by *C. elegans* GLR-1 glutamate receptor. Nature **378,** 82-85

Hedgecock, E.M., and Russell, R.L., 1975. Normal and mutant thermotaxis in the nematode *Caenorhabditis elegans*. Proc. Nat. Acad. Sci. USA **72**, 4061-4065.

Heinze, S., and Homberg, U., 2007. Maplike representation of celestial E-vector orientations in the brain of an insect. Science **315**, 995-997.

Heinze, S., and Reppert, S.M., 2011. Sun compass integration of skylight cues in migratory monarch butterflies. Neuron **69**, 345-358.

Herbers, J.M., 1981. Time resources and laziness in animals. Oecologia **49**, 252-262.

Hill, N.A., and Hader, D.P., 1997. A biased random walk model for the trajectories of swimming micro-organisms. Journal of Theoretical Biology **186**, 503-526.

Hodgkin, J., and Doniach, T., 1997. Natural variation and copulatory plug formation in *Caenorhabditis elegans*. Genetics **146**, 149-164.

Hoffmann, G., 1983. The random elements in the systematic search behavior of the desert isopod *Hemilepistus-Reaumuri*. Behavioral Ecology and Sociobiology **13**, 81-92.

Hölldobler, B., and Wilson, E.O., 1990. The ants. Belknap Press, Harvard University, Cambridge, Massachusetts.

Iino, Y., and Yoshida, K., 2009. Parallel use of two behavioral mechanisms for chemotaxis in *Caenorhabditis elegans*. The Journal of Neuroscience **29**, 5370-5380.

Inada, H., Ito, H., Satterlee, J., Sengupta, P., Matsumoto, K., and Mori, I., 2006. Identification of guanylyl cyclases that function in thermosensory neurons of *Caenorhabditis elegans*. Genetics **172**, 2239-2252.

Kareiva, P., and Shigesada, N., 1983. Analyzing insect movement as a correlated random walk. Oecologia **56**, 234-238.

Katz, M., and George, E., 1985. Fractals and the analysis of growth paths. Bull Math Biol. **47**, 273-86

Kennedy, J.S., 1983. Zigzagging and casting as a programmed response to wind-borne odor - a review. Physiological Entomology **8**, 109-120.

Kimchi, T., and Terkel, J., 2002. Seeing and not seeing. Current Opinion in Neurobiology **12**, 728-734.

Komatsu, H., Mori, I., Rhee, J.-S., Akaike, N., and Ohshima, Y., 1996. Mutations in a cyclic nucleotide-gated channel lead to abnormal thermosensation and chemosensation in *C. elegans*. Neuron **17**, 707-718.

Komatsu, H., Jin, Y.-H., L'Etoile, N., Mori, I., Bargmann, C.I., Akaike, N., and Ohshima, Y., 1999. Functional reconstitution of a heteromeric cyclic nucleotide-gated channel of *Caenorhabditis elegans* in cultured cells. Brain Research **821**, 160-168.

Kramer, D., and McLaughlin, R., 2001. The behavioral ecology of intermittent locomotion. Am. Zool. **41**, 137-153.

L'Etoile, N.D., and Bargmann, C.I., 2000. Olfaction and odor discrimination are mediated by the *C. elegans* guanylyl cyclase ODR-1. Neuron **25**, 575-586.

Larralde, H., Trunfio, P., Havlin, S., Stanley, H.E., and Weiss, G.H., 1992. Territory covered by N diffusing particles. Nature **355**, 423-426.

Levandowsky, M., Klafter, J., and White, B.S., 1988. Swimming behavior and chemosensory responses in the protistan microzooplankton as a function of the hydrodynamic regime. Bulletin of Marine Science **43**, 758-763.

Lewis, J., and Hodgkin, J., 1977. Specific neuroanatomical changes in chemosensory mutants of the nematode *Caenorhabditis elegans*. J Comp Neurol. **172**, 489-510.

Li, W., Feng, Z., Sternberg, P.W., Xu, X.Z., 2009. A *C. elegans* stretch receptor neuron revealed by a mechanosensitive TRP channel homologue. Nature **440,** 684-687.

Li, L., Nørrelykke, S.F., and Cox, E.C., 2008. Persistent cell motion in the absence of external signals: a search strategy for eukaryotic cells. PLoS ONE **3**, e2093.

Lipp, H.-P., Vyssotski, A.L., Wolfer, D.P., Renaudineau, S., Savini, M., Tröster, G., and Dell'Omo, G., 2004. Pigeon homing along highways and exits. Current Biology **14**, 1239-1249.

Liu, J., Ward, A., Gao, J., Dong, Y., Nishio, N., Inada, H., Kang, L., Yu, Y., Ma, D., Xu, T., Mori, I., Xie, Z., and Xu, X.Z.S., 2010. *C. elegans* phototransduction requires a G protein-dependent cGMP pathway and a taste receptor homolog. Nat Neurosci **13**, 715-722.

Lohmann, K.J., Lohmann, C.M.F., Ehrhart, L.M., Bagley, D.A., and Swing, T., 2004. Animal behaviour: geomagnetic map used in sea-turtle navigation. Nature **428**, 909-910.

Lundquist, E.A., Reddien, P.W., Hartwieg, E., Horvitz, H.R., and Bargmann, C.I., 2001. Development. 2001. **128,** 4475-4488.

Macnab, R.M., 1977. Bacterial flagella rotating in bundles: a study in helical geometry. Proc. Nat. Acad. Sci. USA **74**, 221–225.

Macnab, R.M., and Koshland, D.E.J., 1972. The gradient-sensing mechanism in bacterial chemotaxis. Proc. Nat. Acad. Sci. USA **69**, 2509-2512.

Macosko, E.Z., Pokala, N., Feinberg, E.H., Chalasani, S.H., Butcher, R.A., Clardy, J., and Bargmann, C.I., 2009. A hub-and-spoke circuit drives pheromone attraction and social behaviour in *C. elegans*. Nature **458**, 1171-1175.

Mandelbrot, B., 1967. How long is the coast of Britain? Statistical self-similarity and fractional dimension. Science **156**, 636-638.

Marsh, L.M., and Jones, R.E., 1988. The form and consequences of random-walk movement models. Journal of Theoretical Biology **133**, 113-131.

McNamara, J., and Houston, A., 1980. The application of statistical decision-theory to animal behavior. Journal of Theoretical Biology **85**, 673-690.

Merkle, T., and Wehner, R., 2008. Landmark guidance and vector navigation in outbound desert ants. J Exp Biol. **211**, 3370–3377.

Michel, J.-B., Yeh, P.J., Chait, R., Moellering, R.C., and Kishony, R., 2008. Drug interactions modulate the potential for evolution of resistance. Proc. Nat. Acad. Sci. USA **105**, 14918-14923.

Mises, R.von, 1964. Mathematical Theory of Probability and Statistics. Academic Press, London.

Mittelstaedt, M.L., and Mittelstaedt, H., 1980. Homing by path integration in a mammal. Naturwissenschaften **67**, 566-567.

Montague, P.R., and Berns, G.S., 2002. Neural economics and the biological substrates of valuation. Neuron **36**, 265-284.

Mori, I., and Ohshima, Y., 1995. Neural regulation of thermotaxis in *Caenorhabditis elegans*. Nature **376**, 344-348.

O'Brien, W.J., Browman, H.I., and Evans, B.I., 1990. Search strategies of foraging animals. American Scientist **78**, 152-160.

Ortiz, C.O., Etchberger, J.F., Posy, S.L., Frokjaer-Jensen, C., Lockery, S., Honig, B., and Hobert, O., 2006. Searching for neuronal left/right asymmetry: genomewide analysis of nematode receptor-type guanylyl cyclases. Genetics **173**, 131-149.

Papi, F., 1992. Animal homing. Chapman & Hall, London.

Pearson, K., 1905. The problem of the random walk. Nature **72**, 294-294.

Perkins, L.A., Hedgecock, E.M., Thomson, J.N., and Culotti, J.G., 1986. Mutant sensory cilia in the nematode *Caenorhabditis elegans*. Developmental Biology **117**, 456-487.

Pierce-Shimomura, J.T., Morse, T.M., and Lockery, S.R., 1999. The fundamental role of pirouettes in *Caenorhabditis elegans* chemotaxis. The Journal of Neuroscience **19**, 9557-9569.

Qian, H., Sheetz, M.P., and Elson, E.L., 1991. Single particle tracking. Analysis of diffusion and flow in two-dimensional systems. Biophysical Journal **60**, 910-921.

Ramot, D., Johnson, B.E., Berry, T.L., Jr., Carnell, L., and Goodman, M.B., 2008. The Parallel worm tracker: a platform for measuring average speed and drug-induced paralysis in nematodes. PLoS ONE **3**, e2208.

Raposo, E.P., Buldyrev, S.V., da Luz, M.G.E., Santos, M.C., Stanley, H.E., and Viswanathan, G.M., 2003. Dynamical robustness of Lévy search strategies. Phys Rev Lett **91**, 240601.

Rayleigh, L., 1905. The problem of the random walk. Nature **72**, 318-318.

Rossel, S., and Wehner, R., 1982. The bee's map of the E-vector pattern in the sky. Proc. Nat. Acad. Sci. USA **79**, 4451-4455.

Rudnick, J., and Gaspari, G., 1986. The asphericity of random-walks. Journal of Physics A-Mathematical and General **19**, L191-L193.

Ryu, W.S., and Samuel, A.D.T., 2002. Thermotaxis in *Caenorhabditis elegans* analyzed by measuring responses to defined thermal stimuli. The Journal of Neuroscience **22**, 5727-5733.

Samu, F., Sziranyi, A., and Kiss, B., 2003. Foraging in agricultural fields: local 'sit-and-move' strategy scales up to risk-averse habitat use in a wolf spider. Animal Behaviour **66**, 939-947.

Scholey, J., Ou, G., Snow, J., and Gunnarson, A., 2004. Intraflagellar transport motors in *Caenorhabditis elegans* neurons. Biochem Soc Trans. **32**, 682-684.

Segall, J.E., Block, S.M., and Berg, H.C., 1986. Temporal comparisons in bacterial chemotaxis. Proc. Nat. Acad. Sci. USA **83**, 8987-8991.

Sengupta, A., van Teeffelen, S., and Löwen, H., 2009. Dynamics of a microorganism moving by chemotaxis in its own secretion. Physical Review E **80**, 031122.

Senti, G., and Swoboda, P., 2008. Distinct isoforms of the RFX transcription factor DAF-19 regulate ciliogenesis and maintenance of synaptic activity. Mol. Biol. Cell **19**, 5517-5528.

Senti, G., Ezcurra, M., Lobner, J., Schafer, W.R., and Swoboda, P., 2009. Worms with a single functional sensory cilium generate proper neuron-specific behavioral output. Genetics **183**, 595-605.

Seyfarth, E.-A., Hergenröder, R., Ebbes, H., and Barth, F.G., 1982. Idiothetic orientation of a wandering spider: compensation of detours and estimates of goal distance. Behavioral Ecology and Sociobiology **11**, 139-148.

Shtonda, B.B., and Avery, L., 2006. Dietary choice behavior in *Caenorhabditis elegans*. J Exp Biol **209**, 89-102.

Sokolowski, M., 1980. Foraging strategies of *Drosophila melanogaster*: a chromosomal analysis. Behav Genet **10**, 291-302.

Sommer, S., and Wehner, R., 2004. The ant's estimation of distance travelled: experiments with desert ants, *Cataglyphis fortis*. Journal of Comparative Physiology A: Neuroethology, Sensory, Neural, and Behavioral Physiology **190**, 1-6.

Starich, T.A., Herman, R.K., Kari, C.K., Yeh, W.H., Schackwitz, W.S., Schuyler, M.W., Collet, J., Thomas, J.H., and Riddle, D.L., 1995. Mutations affecting the chemosensory neurons of *Caenorhabditis elegans*. Genetics **139**, 171-188.

Stephens, G.J., Johnson-Kerner, B., Bialek, W., and Ryu, W.S., 2010. From modes to movement in the behavior of *Caenorhabditis elegans*. PLoS ONE **5**, e13914.

Sukul, N., and Croll, N., 1978. Influence of potential difference and current on the electrotaxis of Caenorhaditis elegans. J Nematol. **10**, 314-7.

Sulston, J., and Hodgkin, J., Methods, in: Wood, W. B., (Ed.), The Nematode *Caenorhabditis elegans*, Cold Spring Harbor Laboratory Press, Cold Spring Harbor, NY 1988, pp. 587–606.

Swoboda, P., Adler, H.T., and Thomas, J.H., 2000. The RFX-type transcription factor DAF-19 regulates sensory neuron cilium formation in *C. elegans*. Molecular Cell **5**, 411-421.

Taube, J.S., 2007. The head direction signal: origins and sensory-motor integration. Annual Review of Neuroscience **30**, 181-207.

Tobin, D.M., Madsen, D.M., Kahn-Kirby, A., Peckol, E.L., Moulder, G., Barstead, R., Maricq, A.V., and Bargmann, C.I., 2002. Combinatorial expression of TRPV channel proteins defines their sensory functions and subcellular localization in *C. elegans* neurons. Neuron **35,** 307-318.

Uchida, O., Nakano, H., Koga, M., and Ohshima, Y., 2003. The *C. elegans che-1* gene encodes a zinc finger transcription factor required for specification of the ASE chemosensory neurons. Development **130**, 1215-1224.

Uhlenbeck, G.E., and Ornstein, L.S., 1930. On the theory of brownian motion. Phys. Rev. **36,** 823–841.

Vergassola, M., Villermaux, E., and Shraiman, B.I., 2007. `Infotaxis' as a strategy for searching without gradients. Nature **445**, 406-409.

Viswanathan, G.M., Buldyrev, S.V., Havlin, S., da Luz, M.G.E., Raposo, E.P., and Stanley, H.E., 1999. Optimizing the success of random searches. Nature **401**, 911-914.

Vowels, J., and Thomas, J., 1994. Multiple chemosensory defects in daf-11 and daf-21 mutants of *Caenorhabditis elegans*. Genetics **138**, 303-316.

Wakabayashi, T., Kitagawa, I., and Shingai, R., 2004. Neurons regulating the duration of forward locomotion in *Caenorhabditis elegans*. Neuroscience Research **50**, 103-111.

Walker, M.M., 1997. Structure and function of the vertebrate magnetic sense. Nature **390**, 371-376.

Wallraff, H., 1996. Seven theses on pigeon homing deduced from empirical findings. J Exp Biol **199**, 105-111.

Walls, M.L., and Layne, J.E., 2009a. Fiddler crabs accurately measure two-dimensional distance over three-dimensional terrain. J Exp Biol **212**, 3236-3240.

Walls, M.L., and Layne, J.E., 2009b. Direct evidence for distance measurement via flexible stride integration in the fiddler crab. Current Biology **19**, 25-29.

Wang, Y., Apicella, A., Lee, S.-K., Ezcurra, M., Slone, R.D., Goldmit, M., Schafer, W.R., Shaham, S., Driscoll, M., and Bianchi, L., 2008. A glial DEG/ENaC channel functions with neuronal channel DEG-1 to mediate specific sensory functions in *C. elegans*. EMBO J **27**, 2388-2399.

Ward, A., Liu, J., Feng, Z., and Xu, X.Z.S., 2008. Light-sensitive neurons and channels mediate phototaxis in *C. elegans*. Nat Neurosci **11**, 916-922.

Ward, S., 1973. Chemotaxis by the nematode *Caenorhabditis elegans*: identification of attractants and analysis of the response by use of mutants. Proc. Nat. Acad. Sci. USA. **70**, 817-21.

Wehner, R., 2003. Desert ant navigation: how miniature brains solve complex tasks. Journal of Comparative Physiology A: Neuroethology, Sensory, Neural, and Behavioral Physiology **189**, 579-588.

Wehner, R., and Srinivasan, M.V., 1981. Searching behavior of desert ants, genus *Cataglyphis* (Formicidae, Hymenoptera). Journal of Comparative Physiology **142**, 315-338.

White, J.G., Southgate, E., Thomson, J.N. and Brenner, S. 1986. The structure of the nervous system of the nematode *C. elegans*. Philos. Trans. R. Soc. Lond. Series B. Biol. Sci. **314,** 1-340

Wiltschko, W., and Wiltschko, R., 2005. Magnetic orientation and magnetoreception in birds and other animals. Journal of Comparative Physiology A: Neuroethology, Sensory, Neural, and Behavioral Physiology **191**, 675-693.

Wittlinger, M., Wehner, R., and Wolf, H., 2006. The ant odometer: stepping on stilts and stumps. Science **312**, 1965-1967.

Wolf, H., and Wehner, R., 2000. Pinpointing food sources: olfactory and anemotactic orientation in desert ants, *Cataglyphis fortis*. J Exp Biol. **203**, 857-868.

Zimmer, M., Gray, J.M., Pokala, N., Chang, A.J., Karow, D.S., Marletta, M.A., Hudson, M.L., Morton, D.B., Chronis, N., and Bargmann, C.I., 2009. Neurons detect increases and decreases in oxygen levels using distinct guanylate cyclases. Neuron **61**, 865-879.